ANALYSIS OF RATCHETING BY USING DIFFERENT YIELD CRITERIA AND KINEMATIC HARDENING MODELS FOR UNIAXIAL AND BIAXIAL LOADING

A THESIS SUBMITTED TO
THE GRADUATE SCHOOL OF NATURAL AND APPLIED SCIENCES
OF
MIDDLE EAST TECHNICAL UNIVERSITY

BY

MERT İŞLER

IN PARTIAL FULFILLMENT OF THE REQUIREMENTS
FOR
THE DEGREE OF MASTER OF SCIENCE
IN
MECHANICAL ENGINEERING

AUGUST 2018

Approval of the thesis:

ANALYSIS OF RATCHETING BY USING DIFFERENT YIELD CRITERIA AND KINEMATIC HARDENING MODELS FOR UNIAXIAL AND BIAXIAL LOADING

submitted by **MERT İŞLER** in partial fulfillment of the requirements for the degree of **Master of Science in Mechanical Engineering Department, Middle East Technical University** by,

Prof. Dr. Halil Kalıpçılar _____
Dean, Graduate School of **Natural and Applied Sciences**

Prof. Dr. M.A. Sahir Arıkan _____
Head of Department, **Mechanical Engineering**

Prof. Dr. Haluk Darendeliler _____
Supervisor, **Mechanical Engineering Department, METU**

Examining Committee Members:

Prof. Dr. Süha Oral
Mechanical Engineering Department, METU _____

Prof. Dr. Haluk Darendeliler
Mechanical Engineering Department, METU _____

Prof. Dr. Suat Kadıoğlu
Mechanical Engineering Department, METU _____

Assist. Prof. Dr. Ulaş Yaman
Mechanical Engineering Department, METU _____

Prof. Dr. Can Çoğun
Mechatronics Engineering Department, Çankaya University _____

Date: _____

I hereby declare that all information in this document has been obtained and presented in accordance with academic rules and ethical conduct. I also declare that, as required by these rules and conduct, I have fully cited and referenced all material and results that are not original to this work.

Name, Last Name: MERT İŞLER

Signature :

ABSTRACT

ANALYSIS OF RATCHETING BY USING DIFFERENT YIELD CRITERIA AND KINEMATIC HARDENING MODELS FOR UNIAXIAL AND BIAXIAL LOADING

İşler, Mert
M.S., Department of Mechanical Engineering
Supervisor : Prof. Dr. Haluk Darendeliler

August 2018, 130 pages

Ratcheting is defined as accumulation of plastic strain under cyclic loading. It affects the fatigue failure time of materials as well as the length of service life. To predict this behavior, many models have been proposed to simulate ratcheting responses of materials. However, it is a general problem that these models are close to simulate one type of ratcheting, but fails to simulate one another. For this reason, uniaxial and biaxial models are proposed by adding terms to the formulations. On the other hand, most of the models are able to simulate ratcheting behavior to limited number of cycles. Some models predict shakedown (stabilization) for further cycles while some models give ovepredicted results. In this aspect, kinematic hardening models are worth to be investigated. In this thesis, six of most common kinematic hardening models (Armstrong-Frederick, Bari-Hassan, Burlet-Cailletaud, Chaboche, Ohno-Wang and Prager) are used to simulate the ratcheting behavior of isotropic materials in both uniaxial and biaxial aspect. For uniaxial loading, Ohno-Wang model gave the least amount of ratcheting, while Prager model gave no accumulation. As for biaxial loading, Chaboche model predicted the least amount of accumulation. Prager

model could not simulate ratcheting for biaxial loading too. In this study, anisotropic material assumption, whose yield criteria are given by Hill and Aretz, is also used for Armstrong-Frederick, Ohno-Wang, Chaboche and Prager models to investigate the ratcheting effect. Models with Aretz yield criterion predicted excessive ratcheting compared to Hill and von-Mises. Constitutive models with Hill's yield criterion simulated ratcheting slightly greater than the models with von-Mises yield criterion. When the kinematic hardening models are compared for each yield criterion separately, their order of estimated ratcheting amounts remained the same.

Keywords: Ratchetting, Cyclic Plasticity, Kinematic Hardening

ÖZ

BİR VE İKİ EKSENLİ YÜKLEMELERDE PLASTİK DEFORMASYON BİRİKİMİNİN FARKLI AKMA KRİTERLERİ VE KİNEMATİK SERTLEŞME MODELLERİ KULLANILARAK İNCELENMESİ

İşler, Mert
Yüksek Lisans, Makina Mühendisliği Bölümü
Tez Yöneticisi : Prof. Dr. Haluk Darendeliler

Ağustos 2018 , 130 sayfa

Plastik gerinim birikimi ya da plastic deformasyon birikimi döngüsel yüklemeler altında gelişir. Bu, malzemelerin yorulma zamanları ve servis ömürlerini etkiler. Bu davranışı tahmin edebilmek için, plastic gerinim birikimini simule eden birçok model önerilmiştir. Ancak, modellerin bazı tip birikimleri tahmin edip bazılarını tahmin edememeleri genel bir problemdir. Bu sebepten, önceki formüllere terimler eklenmek suretiyle tek eksenli ve iki eksenli modeller oluşturulmuştur. Diğer taraftan, modellerin çoğu yalnızca belli bir yükleme döngüsü sayısına kadar gerinim yığılımını tahmin edebilmektedir. Daha sonraki döngüler için bazı modeller yığılmanın kaybolması (stabilizasyon) tahminini yapabilirken, bazıları ise fazla gerinim vermektedir. Bu açıdan, kinematik sertleşme modelleri araştırılmalıdır. Bu tezde, en bilinen kinematik sertleşme modellerinden altı tanesi (Armstrong-Frederick, Bari-Hassan, Burlet-Cailletaud, Chaboche, Ohno-Wang ve Prager), tek eksenli ve iki eksenli yüklemeler altındaki izotropik malzemelerin deformasyon birikimi davranışını incelemek için kullanılmıştır. Tek eksenli yüklemede Ohno-Wang modeli en az birikimi verirken,

Prager modeli hiç deformasyon yığılması tahmin edememiştir. İki yönlü yüklemede ise, Chaboche modeli en az miktarı vermiştir. Çok eksenli yüklemede de Prager modeli hiç bir yığılma tahmin edememiştir. Akma kriterleri Hill ve Aretz tarafından belirlenmiş olan anizotropik malzeme kabulleri de Armstrong-Frederick, Ohno-Wang, Chaboche ve Prager modelleri için yapılmıştır. Aretz akma kriterinin olduğu modeller, Hill ve von-Mises akma kriterlerinin olduğu modellere göre daha fazla yığılma birikimi tahmin etmiştir. Hill akma kriterinin olduğu modeller ise, von-Mises akma kriterinin olduğu modellerden çok küçük farklarla daha fazla yığılma birikimi simule etmiştir. Kinematik sertleşme modelleri kendi içlerinde ayrı ayrı değerlendirildiğinde, modellerin tahmin ettiği yığılma değerlerinin sırası değişmemiştir.

Anahtar Kelimeler: Deformasyon Birikimi, Döngüsel Plastisite, Kinematik Sertleşme

To my family

ACKNOWLEDGMENTS

First, I would like to thank Prof. Dr. Haluk Darendeliler for his supervision of thesis and guidance.

I would like to appreciate kind help of Prof. Dr. Süha Oral with his knowledge on finite element analysis.

I would appreciate the help of Dr. Shahram A. Dizaji. The contribution to my vision and knowledge with his strong competence on coding and finite element analysis is invaluable.

My family has been very helpful to me for all times as well as in thesis process. They deserve many more than this few sentences of this chapter. Every time I got stuck with the subjects or the burden I got, they just made me relax and work harder. They were always with me whatever I did.

A really important person in this process is my first room mate Serhat Bilyaz. I really thank him for sharing his experiences on doing researches and analyzing the literature. Beyond this, his friendly, sometimes as an older brother, attitude was always making me get happy and relax. I also want to declare my gratitude to Eylül Şimşek who is another warm friend at the beginning of my graduate years.

Bilal Atar's and Muhammed Çakır's companionship were also valuable for me. I got very useful helps on finite element analysis and modeling. Also, their kind friendship was encouraging me all the time. My another room mate Metin Biçer was also effective on me to get eager to work harder. Hence, I am also grateful to him.

TABLE OF CONTENTS

LIST OF FIGURES

FIGURES

LIST OF ABBREVIATIONS

A-F	Armostrong-Frederick Kinematic Hardening
A-O	AbdelKarim-Ohno Kinematic Hardening
B-C	Burlet-Cailletaud Kinematic Hardening
B-H	Bari-Hassan Kinematic Hardening
D-P	Dafalias-Popov Two Surface
O-W	Ohno-Wang Kinematic Hardening
OW-TANA	A different version of Ohno-Wang model modified by Tanaka

CHAPTER 1

INTRODUCTION

Materials exhibit irreversible deformation after yield point. Upon this yield limit, stress states can be calculated using Hooke's Law. However, after the initial yield, the stress increases nonlinearly. Therefore, several constitutive relations were established to predict the stress values on each corresponding strain in the plastic region.

Materials are generally not loaded for once in their service life. Many of them are exposed to cyclic loading. Therefore, their response under cyclic load should be analyzed for failure. There are two failure modes resulted from cyclic loading.

The first and most commonly known mode is fatigue. Internal cracks occur in the materials as they get deformed. The material suddenly fails as soon as the crack reaches to the surface. This is a catastrophic failure. Therefore, internal structure must be examined in order to know how these cracks are propagating and to estimate the fatigue failure time. There are two types of fatigue analyses. The first one is high cycle fatigue in which the number of load cycles is greater than 10^5 and magnitude of the loads are small such that deformations are in elastic region. The second one is low cycle fatigue in which magnitude of the loads are high and number of cycles is less than 10^5. The deformations are in plastic region for low cycle fatigue. In this type of loading, there exist a second failure mode which is called ratcheting. In this mode, plastic strain accumulates in each cycle. Either the material gets out of service or it directly fractures when deformation reaches to fracture strain. This failure can be detected by naked eye (e.g. bulging of a pipe). Many models have been developed to predict this behavior. These models are mostly based on kinematic hardening.

1.1 Motivation

Ratcheting is observed in cyclic loading around a non zero mean stress. It causes failure in different ways. Direct collapse can be encountered causing material to be out of usage. Another way of failure is shortening the time of fatigue failure, which devastates the material with initiation of internal cracks. Yet another failure mode is excessive deformation.

Crucial components are subjected to cyclic loading with non-zero mean stress such as piping components in nuclear power plants, landing gears of airplanes or suspension of the automobiles. Therefore, it is important to predict the ratcheting behavior before the failure.

Back then, various kinematic hardening models were proposed to predict stresses in the materials through the plastic range. There are limited number of researches done on ratcheting behavior considering the seriousness of the phenomena. Commercial finite element packages provide predictions based on kinematic hardening. However, they are inadequate to simulate the ratcheting phenomena. Hence, researches on accumulation of strain should be carried out to improve the prediction of failure.

1.2 Research Objectives

The improvement of the kinematic hardening models used in ratcheting analysis are obtained by incremental development. In other words, researchers have used the previous formulae to propose new kinematic hardening models by changing or adding new parameters. For instance, Armstrong-Frederick model was established by introducing radial evanescence term to the linear model. Capability of new models had become closer to simulate ratcheting. On the other hand, there are different proposals not by adding terms, but starting from scratch. They distinguished from the others with the calculation of plastic modulus.

To the best knowledge of the author, all of the models included in the studies done on ratcheting analysis used von-Mises yield criterion. As a result, the modifications other than the plastic modulus calculation mostly arose in backstress tensor. Adding

new terms to the hardening parameters in the backstress tensor has improved the ratcheting predictions. These additions or alterations had different effects in uniaxial and biaxial models. In the literature, there are two types of models. The first type, coupled models, comprehends plastic modulus calculation to kinematic hardening rule through consistency condition. The second type is uncoupled models in which plastic modulus calculation is completely independent from the kinematic hardening rule.

The objective of this study is to compare capability of different hardening models in simulating ratcheting. Another objective is to examine the differences of results between various yield functions. Lacking features of these models will be detected. Therefore, following this thesis, new models that completes these features can be developed to enhance the possibility of predicting the exact amount of ratcheting.

1.3 Scope of the Research

In this thesis, aforementioned models will be analyzed to determine ratcheting behavior of materials in both uniaxial and biaxial loading. Different yield criteria will be used such as von-Mises, Hill and Aretz yield criteria.

Simulation capabilities of the existing kinematic hardening models will be tested by a commercial finite element package. Although the commercial packages have a limited built-in models to analyze cyclic loading of materials, subroutines can be implemented for applying kinematic hardening rules that are not available by default. Starting from the linear kinematic hardening model which is proposed by Prager, five other non-linear models are applied to evaluate cyclic modeling which are Armstrong-Frederick, Burlet-Cailletaud, Bari-Hassan, Chaboche, and Ohno-Wang models. These models will be used with von-Mises, Hill, and Aretz yield critera. Evaluation will be done considering uniaxial and biaxial response. Simulations will cover unsymmetric stress and strain cycling.

1.4 Outline of the Thesis

This work consists of seven chapters. In chapter 1, a brief introduction is given about the subject of thesis. Motivation with research objectives are present. Finally, in this chapter, scope of the thesis can be found.

In chapter 2, literature survey is written. In the first part, the past researches and studies that are made to improve ratcheting simulations are explained very briefly. In the second part, papers which are exploited to improve finite element modeling's accuracy and time optimization are summarized.

In chapter 3, theoretical formulation of constitutive models are given. General constitutive equations and yield functions are explained. Kinematic hardening rules are explained.

In chapter 4, details of finite element modeling are explained. After a general information, elements, integration method, scaling, and mesh dependency issues are considered. Results of analyses for searching an optimum analysis are presented.

In chapter 5, results of finite element simulations are given.

In chapter 6, discussion and conclusion of the results are included. Also, future work that can be done to improve the models are discussed briefly.

Finally, references are provided.

CHAPTER 2

LITERATURE SURVEY

This chapter is divided into two parts. In the first part, past studies about ratcheting are explained. These papers generally do not give information about finite element techniques that the authors adopted while analyzing suggested kinematic hardening models. Hence, a second part of this chapter, which involves studies and papers about different features of finite element analyses techniques are included.

2.1 Studies about Ratcheting

In this part, previous studies about ratcheting are summarized.

The first linear kinematic hardening model was proposed by Prager [33]. Although this model can be used in plasticity calculations with acceptable error for isotropic materials with von Mises yield criterion, ratcheting behavior cannot be observed since it brings about closed hysteresis loops. Therefore, modifications on the model has been done. Except for Mroz's and Besseling's multilinear models, all of the improvements are done by converting the hardening rule from linear to nonlinear.

The very first one of the nonlinear kinematic hardening rules which is able to predict some amount of ratcheting has been derived by Armstrong and Frederick [2]. They introduced a dynamic recovery term to incremental linear backstress formula. However, this model overpredicted both uniaxial and multiaxial ratcheting. Therefore, modifications have been done on this model. Many of them, as explained in this chapter, exist in dynamic recovery term.

Tseng and Lee, performed a study on general plasticity model including two surfaces

named yield surface or inner surface and memory surface or the boundary surface [38]. Although the study is not merely about ratcheting, there are useful information which can be beneficial when modeling a cyclic behavior to consider when coding the constitutive equations to simulate strain accumulation. Memory surface has been defined in the paper as the surface that passes through the maximum historical stress. The inner surface always keeps in touch with the outer one or memory surface. In their proposed plasticity model, memory surface is expanding in isotropic way. On the other hand, since the inner surface keeps the touch with the outer one, it exhibits kinematic hardening behavior. It can both rotate and translate, but the size remains unchanged. Numerical examples are given in the study. These are about monotonic loading, cyclic loading, cyclic creep, cyclic stress relaxation and generalized cyclic loading. Plastic modulus calculation is different from the other models. In the results, the new proposed model, was investigated and it was decided that model is simulating the loading cases well.

In 1984, Yoshida et al. looked for the effect of maximum stress, stress ratio, steady stress and cycle number on biaxial ratcheting using a thin walled tube specimen [41]. They concluded that direction of ratcheting in biaxial case was independent from cycle number and maximum stress. For the same stress occasions, biaxial and uniaxial ratcheting amounts were observed to be the same. Direction of ratcheting in biaxial loading was investigated in this study also.

Ruggles and Krempl's study was about the influence of test temperature on the ratchetting behavior of type 304 stainless steel. They conducted experiments at 550°C, 600°C, and 650°C [35]. Two kinds of loading histories were applied. One of them was to a virgin material and the other one was the material that is exposed to stress relaxation. Throughout the history, the stress and strain controlled loading were mixed. For the prior history, in which the material was virgin, the prominent factor that cause ratcheting was said to be the viscous effects although it was not expected for low temperatures. For higher temperatures, strain aging was effective for prohibition of inelastic deformation accumulation.

Chaboche et al. have partitioned the back stress components of the nonlinear kinematic hardening rule of Armstrong and Frederick [7]. Model proposed in the study

was tested on both uniaxial and multiaxial conditions. One of the important conclusion they came up with is the fact that there is a correspondence between uniaxial and multiaxial ratcheting and for plastically equivalent conditions, multiaxial ratcheting is smaller than the uniaxial ratcheting. The proposed model in their study was a time independent one in which viscous effects were not included. Results showed that the model predicted ratcheting in uniaxial experiments approximately. However, it needs to be improved for the other types of experiments on ratcheting especially for multiaxial conditions.

Hassan and Kyriakides has tested two materials which exhibits cyclic softening and cyclic hardening [19]. In uniaxial part, stainless steel 304, which undergoes cyclic hardening, and carbon steel 1018, which undergoes cyclic softening, are used. In the modeling, J2 type plasticity was used with von-Mises yield criterion. Plastic modulus was calculated using Dafalias-Popov model. After numerous experiments, it was concluded that cyclic softening and hardening were greatly impressive on ratcheting behavior. For CS 1018, ratcheting after some amount of plastic strain increases exponentially. When some modifications done considering this cyclic hardening with the usage of D-P model, prediction of ratcheting has improved. D-P model is a two surface model in which there exists a bounding surface and elastic region's surface. In stress-strain curve, the memory surface or bounding surface represents two straight lines limiting the tensile yield point on the top and compressive yield point on the bottom. Position of these two surface determines the plastic modulus [13].

Delobelle did a research on phenomenological modeling of ratcheting under uniaxial and biaxial loading of austenitic steel [14]. The tests for ratcheting under uniaxial loading, nonsymmetrical stress control, tension torsion tests and axial cycles under internal pressure were done. Objective of the research was to implement suitable models for simulating the rate and amount of ratcheting under different loading conditions. The viscoplastic modeling was described in a rather detailed way in the paper. Both for uniaxial and biaxial ratcheting, different constitutive models were used. In the results part, it was stated that for uniaxial case, ratcheting occurs after maximum stress exceeds 210 MPa and for 25 MPa mean stress, the amount gets maximum. The axial loading with internal pressure tests agreed with the predictions. However, if a second alternating load has advanced, then the phase difference between these two

loads became important. In the paper, introduction of radial evanescence term has also improved the estimation of ratcheting well. All in all, according to the authors, modeling given in the paper simulated ratcheting in both uniaxial and multiaxial loading quite well.

Jiang et al. proposed a hardening rule which is again based on A-F kinematic hardening rule [23]. In their study, memory surface concept, which brings the maximum stress from the loading history was used. Backstress was divided into partitions. However, the formula that describes the each partition was different from Chaboche's model. Also, different material constants were introduced. In the conclusion, model is said to be able to predict the prior loading history effect on the ratcheting and the change in the ratcheting direction for multiple step loading.

Ohno and Wang suggested a different model based on the cricitical state of dynamic recovery term [28]. Tests were done on uniaxial and multiaxial loadings. Model consisted of two versions. The first version modified Armstrong-Frederick model by adding a threshold to dynamic recovery term. This was done by a Heaviside step function. With this enhancement, the model became superior to Armstrong-Frederick's model but as for ratcheting, it was still poor. Therefore, the second version of Ohno-Wang model was proposed. Heaviside step function in the first version of this model was replaced with a power term in the second version. Therefore, more material constants were introduced to the formulation. In the conclusion, second version got closer to simulation of ratcheting.

Potsberg et al. have compared the Ohno-Wang model's predictions with the experimental results [32]. They went up to 400 load cycles claiming that there existed no significant ratcheting beyond this number of cycles. As a result, to the 150th load cycle, all the simulation results were parallel to the experimental results. However, after 150th load cycle, two kinds of results were obtained. In experiments in which increasing mean stress was present, after hundred cycle, ratcheting was underpredicted. After further cycles, ratcheting rate became constant. On the other hand, in experiments containing decreasing stress amplitude, amount of ratcheting was well predicted. Moreover, negative ratcheting could also be predicted with the Ohno and Wang model.

Corona et al. made comparison among models including two flow rules and four kinematic hardening rules on five different loading paths [12]. Cases that are investigated were different than uniaxial loading. In the experiments, specimens were tubular. They were subjected to constant internal pressure together with axial strain. With the presence of these, tubular specimens were cycled in the way that there would be biaxial ratcheting. Paths were strain symmetric cycling at constant pressure, inclined load path with and negative slopes, bowtie and reverse bowtie paths, and hourglass path. Two different calculations for plastic modulus were adopted which are named as Drucker-Palgen model and D-P model. For both models, one can decouple flow rule and kinematic hardening rule. In this study, Prager-Ziegler rule, A-F rule, Mroz rule and stress increment rule were used as kinematic hardening models. After experiments and analyses that were done using these models and rules, predictions were acceptable for loading paths of strain-symmetric cycling at constant pressure, positive and negative sloped inclined loading paths and hourglass path. However, for loading histories of bowtie paths predictions are not good.

Hassan et al. have worked on improved ratcheting analysis of piping components [21]. In their study, the primary mode of failure in piping components subjected to seismic loading were investigated. Two assumptions were questioned. The first primary mode of failure was collapse while second primary mode was fatigue failure. Another concern was the effect of ratcheting on fatigue life. Improvement made by the researchers of this study was the modification on the calculation of plastic modulus. Drucker-Palgen plastic modulus equation was implemented to the overall modeling. In conclusion, the new model was able to simulate ratcheting more efficiently than the previous ones. However, for complex loading histories, the model has failed.

Yoshida studied on the cyclic plasticity models and proposed a new viscoplastic constitutive model [40]. Four types of experiments were done. They are uniaxial tension, cyclic straining, stress controlled ratcheting and strain controlled ratcheting. The difference that distinguish this study from the others is that the emphasis is on the yield-point phenomena. Therefore, all the calculations were done considering the slip systems and dislocations. The microstructure of the materials was considered. Also the study included viscoplasticity. Hence, rate equations appeared in the formulation. Stress rate was found to be effective on ratcheting. Proposed model simulated

the shakedown in all the experiments on ratcheting after finite amount of cycles.

Portier et al. stuied on a group of cyclic plasticity models to compare simulation results and experimental results [31]. They used 316 austenitic stainless steel for the experiments. The loading was both uniaxial and biaxial in this study. The first model used for simulations was the base model for most of the applications which is A-F hardening rule. However, this model overestimated the ratcheting in biaxial loading. Different than this, Burlet-Cailletaud model, Ohno and Wang model, and Tanaka model which modifies the Ohno-Wang model were used. As a conclusion of this study, it was observed that the model which has been obtained by modifying Ohno-Wang model (mentioned as OW-TANA model in the paper) was better than the other tried models in predicting ratcheting behavior.

Another study was done by Abdel-Karim and Ohno on kinematic hardening model suitable for ratcheting with steady state [1]. The model contained two kinds of dynamic recovery terms. One was included in all values while the other activates after a threshold value. Experiments include ratcheting in multiaxial, uniaxial loading as well as cyclic stress relaxation and nonproportional cyclic straining. The conclusions that the authors come up with are the kinematic hardening model obtained was successful in predicting multiaxial ratcheting as well as the uniaxial ratcheting and dynamic recovery term which occurs all times is less effective than the one appears only after a critical state of back stress.

Bari and Hassan studied on anatomy of coupled constitutive models for ratcheting simulation [3]. They investigated the performance of simulating ability to predict ratcheting of five plastic constitutive models. Included models in this research were Prager, A-F, Chaboche, Ohno-Wang and Guionnet models. The term "coupled" was used because the models mentioned in the study have their plastic modulus calculation coupled with its kinematic hardening rules using consistency condition. They found out Prager and A-F models fail to simulate ratcheting. Chaboche and Ohno-Wang models predict uniaxial ratcheting well but overpredict the biaxial ratcheting. Guionnet model also failed to predict the true amount of biaxial and uniaxial ratcheting. However, it was eligible at one of the loading path of biaxial experiment. After all, they suggested uncoupling of the plastic modulus calculation and kinematic

hardening rule. Another suggestion of the study was that in multiaxial ratcheting simulation, the material parameters should be found from the multiaxial experiments.

In 2001, Bari and Hassan tested the ability of uncoupled models to predict multiaxial ratcheting [4]. In the paper, coupled models were defined as the models in which plastic modulus calculations were related to kinematic hardening rule using consistency condition. However, in the uncoupled models, kinematic hardening rule and plastic modulus calculation is separated. Therefore, multiaxial ratcheting investigations by using coupled model may not reflect the cases appropriately. In this research, rules proposed by Armstrong-Frederick, Voyiadjis-Sivakumar, Philips-Tang, Philips-Lee, Philips-Lu, Tseng-Lee, Kaneko and Xia-Ellyin were analyzed first. After that, a new model constructed using modified Dafalias-Popov model and kinematic hardening rule of Chaboche, which partitions the Armstrong-Frederick rule was investigated. Moreover, Ohno-Wang model's predictions are also included. The most interesting part of the results was that Kaneko kinematic hardening rule with Dafalias-Popov model was found to produce negative ratcheting. Among the tried models, modified Dafialas-Popov was found to be very close to experimental values. Other models were also seemed good to predict but there were different loading types. Not all of the models gave good results for all type of loadings. The different loadings were uniaxial cycle, axial strain cycle with constant internal pressure, bowtie and reverse bowtie cycle.

In 2002, a new study of Bari and Hassan was published which is focused on improvement of the cyclic plasticity modeling to predict multiaxial ratcheting [5]. In this study, several cyclic plasticity models were investigated in their capacity of simulating uniaxial and biaxial ratcheting responses. These models are derived by Chaboche, Ohno-Wang, McDowell, Jiang-Sehitohlu, Vojiadjis-Basuroychowdhury and Abdel Karim-Ohno. The assumption made in the research was the shape of yield surface does not change during loading. As a result, for uniaxial ratcheting, response was only affected by the calculation of plastic modulus. On the other hand, in multiaxial ratcheting, kinematic hardening rule used in the cyclic plasticity model was found dominant on the prediction. It was concluded that when the parameters were calculated considering only uniaxial loading case, models failed to predict ratcheting in multiaxial case. In this paper, a new rule introducing a parameter which is dependent

on the multiaxial experiment was involved. At the end, adequacy of estimation of ratcheting had improved.

Mahbadi and Eslami has considered Prager and Armstrong-Frederick models to simulate ratcheting for both isotropic and anisotropic materials with axial loading, bending and thermal variation [26]. In the paper, the curves for strain hardening in compressive and tensile loading were assumed to be the same. Reverse plasticity was defined in this paper as zero accumulation of plastic deformation after each cycle. This is what the authors reached for simulation of ratcheting of isotropic materials using Prager model. On the other hand, for anisotropic materials, the model came up some amount of ratcheting. As for Armstrong-Frederick model, non-zero mean stress gives ratcheting but zero mean stressed and strain controlled experiments advances no ratcheting, i.e., reversed plasticity is reached.

Chen et al. have worked on uniaxial ratcheting. This time, the focus was on the high number of cycles [9]. The model proposed by Burlet-Cailletaud predicted shake down and model proposed by Ohno-Wang overpredicted the ratcheting. In this study, a new parameter, namely Delobelle parameter, was added on cyclic plasticity model to make a balance of shakedown and overprediction of the two mentioned models. In the conclusion, the new model proposed was found to give better results for high number of loading cycles.

After the study of uniaxial ratcheting response, Chen and Jiao had worked on application of a modified kinematic hardening rule for multiaxial ratcheting prediction [8]. In their study, as in uniaxial ratcheting response research, the parameter that gives a compromise between Burlet-Cailletaud and Ohno-Wang model, namely the Delobelle parameter, was used. With the addition of the new term, predictions were quite well for all loading paths.

Kulkarni et al. have made a study on uniaxial and biaxial ratcheting study using SA333 Gr.6 steel [25]. In the study, other than implementing different cyclic plasticity models, effect of amplitude of loading was examined. Influence of frequency of the loading cycles were another concern for the authors in this research. In the conclusion, it was found that uniaxial racheting response depends stress history, value of mean stress and amplitude of the cycle. Shakedown was also observed in the exper-

iments. The frequency was not effective on the ratcheting rate. Ratcheting rate only depended on stress history and stress amplitude. In the biaxial case, ratcheting was observed in circumferential direction and no ratcheting was observed on longitudinal direction.

Gupta et al. looked for the ratcheting behavior of SA333 Gr.6 steel used for piping components [15]. The focus was not on the different models' ability to predict ratcheting. After the experiments, it was found that softening occurs during the strain cycling. Stress rate and stress ratio were effective on the ratcheting. Also, Lüders bands influences the cyclic deformation behavior of the material.

Kang and Kan studied on time dependent ratcheting using three kind of constitutive models [24]. These were unified viscoplastic model of AbdelKarim-Ohno, creep plasticity model and creep viscoplasticity model. As a result of the experiments, it was observed that unified viscoplastic model of AbdelKarim-Ohno was not able to predict time dependent ratcheting. With the creep plasticity model, with a proper creep law, time dependent ratcheting might be predicted well for the cases in which creep was dominated by deformation. For the weak creep behavior, the ratcheting estimations were poor in this model. The third model mentioned namely the viscoplasticty creep superposition model was able to simulate time dependent ratcheting behavior in various stress rates with various hold times.

Yaguchi and Takahashi's research included ratcheting of viscoplastic materials with cyclic softening using 9Cr-1Mo steel [39]. The material showed viscoplastic behavior as well as cyclic softening. Both uniaxial and biaxial experiments were included in the study. Experiments were done on temperatures between 200°C and 600°C. In the stress controlled uniaxial ratcheting tests, the material response of ratcheting was unexpectedly high. Accumulation has been observed around zero mean stress. Also, under a slightly negative mean stress, ratcheting occurred in the opposite direction. This was another unexpected result. Under uniaxial loading, ratcheting depended on the loading rate and cyclic softening behavior as well as the maximum stress and the stress ratio. When stress rate was smaller or the hold time is longer, material exhibited larger ratcheting at high temperatures. Stress history was also effective. For multiaxial loading, increase in mean stress and alternating strain increases the rate of

ratcheting. It proposed in the paper that the reason of unexpected ratcheting result might be the tension-compression asymmetry of the material.

Chen et al. did experiments on multiaxial ratcheting using four types of constitutive models which are Ohno-Wang model, McDowell model, Jiang-Sehitoglu model and AbdelKarim-Ohno model [10]. As a result of the experiments, researchers have reported that Ohno-Wang and McDowell models overpredicted multiaxial ratcheting. Jiang-Sehitoglu model was found more adequate than these former two. In AbdelKarim-Ohno Model, when the parameter used for calculation of backstress was calculated using multiaxial experiments, predictions were found well. However, for uniaxial cases, this parameter made model failed in predicting uniaxial ratcheting. In this study, an alteration of dynamic recovery term in the classical nonlinear model was done and with this way, predictions improved significantly. A new multiplier was attached to the formula. Whether the parameters were determined from uniaxial or multiaxial experiments had a significant effect on results as in AbdelKarim-Ohno model.

Mahbadi and Eslami did a research whose goal is to decide the type and level of stresses that cause to ratcheting or shakedown [27]. Thick spherical vessels and cylindrical vessels were the specimens. As in the first study published by these two authors, Armstrong-Frederick and Prager models are used. The conclusion reached is kinematic hardening rule dependent on Prager model gives shakedown for isotropic thick sphere of cylindrical vessels. As for anisotropic materials with the same specimens, ratcheting occurs. Armstrong-Frederick model brings an amount of ratcheting and it is close to obtained experimental results.

Rahman et al. followed an experimental procedure of cyclic bending of pressurized pipes for investigating the availability of cyclic plasticity models in predicting ratcheting behavior. Prager, Besseling, Chaboche, Ohno-Wang, Abdel Karim-Ohno, Bari-Hassan, and Chen-Jiao models were implemented in their study [34]. It has been reported that models were inadequate to predict ratcheting for the loading case in the study when parameters had been calculated from material response. Modified Chaboche model (also known as Bari-Hassan model) was the one specializes on the parameter determination. With the improvement of this, estimation of ratcheting

behavior was enhanced. However, for the authors, this improvement was not sufficient. Therefore, it was suggested that the models should be enhanced and structural characteristics such as residual stress, anisotropy needed to be added to the models.

Hassan et al. pointed out the effect of non-proportionality of loading on ratcheting behavior in both uniaxial and multiaxial cases [20]. As a result of this, all the models considered in the paper were rate insensitive and temperature independent ones. Four different load paths were investigated. The first one was uniaxial and the others were all multiaxial loading paths. Cyclic plasticity models adopted in this study were modified Chaboche and multi-mechanism models. Chaboche's first model gave good predictions only for proportional loading. Therefore, modified version of it was used in the study. The multi-mechanism model has not been frequently used in the earlier studies. In that model, plastic strain was divided. After the experiments, it was concluded that Chaboche model's predictions were well for uniaxial loading, shear ratcheting, axial and shear strain ratcheting of square-two square paths. Multi-mechanism model simulated uniaxial ratcheting good but overpredicted the other two mentioned. Therefore, for low cycle analyses, improvement in the modeling should be enhanced especially for non-proportional loadings.

Halama and his coworkers has a study of general cyclic plasticity [16]. In that, ratcheting is also included. Some of embedded models in commercial finite element packages were tried. In the paper, ratcheting was defined as "cylic creep". Throughout the thesis, this term refers to ratcheting. However, in this work, radius of yield surface was also changed and calculations were done considering this.

2.2 Studies on Finite Element Modeling

In this part, past studies about finite element methods that contribute to this thesis are involved. In the light of these studies, accuracy of the results are enhanced and time of analyses are decreased.

Chung and Cho worked on determining the error using energy concept [11]. They conducted a research to detect whether an analysis gives the correct result or not, using the relation between kinetic energy and internal energy of the system. Their

experiments were on drawing process. Tool velocity was very slow. Hence, their investigation was for quasi static processes. In conclusion of their study, it could be seen that when ratio of kinetic to internal energy is one tenth, analysis is reliable for quasi static case.

Harewood and McHugh focused on comparison of implicit and explicit analyses [17]. They used crystal plasticity by implementing user subroutines on ABAQUS. Other than their comments on implicit and explicit analyses, their main conclusions were that explicit method is much more preferable than implicit method in complex loading. Implicit method's ability to get results in cases which requires small time increments is limited.

Sun, K.H. Lee and H.P. Lee published a paper about explicit and implicit analyses comparison, too [37]. Their investigations was on crash of an elastic bar and a cylindrical disk to a rigid wall. Their conclusion was that for small time problems, explicit method was better and for problems in which stress waves were not too big, implicit method should be preferred.

Hughes and Liu tried to develop a stability rule for both implicit and explicit analyses [22]. They used several algorithms namely Newmark algorithms and predictor-corrector algorithms. Applying some methods and conducting experiments, they concluded that implicit analysis is unconditionally stable while explicit analysis has always require some conditions to be stable.

Other than implicit-explicit analyses papers, there are some other studies for mass scaling. Olovsson, Unosson and Simonsson's method for a different type of mass scaling increased the crtical time step [30]. With this way, analysis time was decreased. Their key point on modification of mass scaling was detecting some rigid body motions and subtracting them from scaling. With a new formulation for density increment, they reached a better and faster way of explicit finite element analysis.

In another study a different type of mass scaling to increase the critical time step was adopted [29]. Their method was adding some terms to mass matrix. By doing this, largest eigenvalues were lessened meaning that critical time step was bigger. This resulted in greater time incrementation and time elapsed was smaller.

Sun did a research on shear locking and hourglass effects with reduced integration elements using MSC Nastran, ABAQUS and ANSYS [36]. His study was done by using a single material beam and a composite beam. It recommends users to avoid using first order elements for no shear locking. Another important recommendation of this paper is to avoid using coarse meshes because of possible hourglass effect.

CHAPTER 3

THEORETICAL BACKGROUND

3.1 Introduction

In forming the constitutive equations for a plastic deformation, three typical properties that must be defined; yield function, flow rule and hardening rule. One of the key points of constitutive equation is selection of the hardening type

Yield criterion determines the loading level on which material passes to plastic region. Boundary between elastic and plastic regions is represented with a surface in stress space. This surface is defined for each criterion differently. In this thesis, von-Mises, Hill and Aretz yield criteria will be used. When plastic deformation starts, the yield surface either translates or enlarges or both translates and enlarges to include current state within the yield surface, as defined by the consistency condition. A yield criterion can be defined as

$$f(\boldsymbol{\sigma}, \boldsymbol{\alpha}) = \kappa \tag{3.1}$$

where $\boldsymbol{\sigma}$ is the stress tensor, $\boldsymbol{\alpha}$ is the backstress tensor and κ is the hardening parameter.

Flow rule relates increments of plastic deformation to increment of stresses. Generic form of the flow rule is

$$d\epsilon_{ij}^{p} = d\lambda \frac{\partial Q}{\partial \sigma_{ij}} \tag{3.2}$$

where $d\lambda$ is called plastic multiplier. In associated flow rule, function Q is the same as yield criteria. If it is different from the yield function, the flow rule is called non associated flow rule. In this thesis, associated flow rule is adopted. Further, kinematic

hardening formulation is effective on flow rules.

Hardening rules determine the behavior of yield surface. Isotropic, kinematic and combined hardening types were developed to predict the material behavior in plastic range. In isotropic hardening, the yield surface's shape and size in the stress space changes. Its radius enlarges with additional loading after yield point. However, center of the yield surface remains in its original position. This means after a loading which is beyond yielding limit, yield stress is proportionally increased in reverse direction. In another type of hardening, yielding occurs in a smaller amount of stress in the reverse direction because center of the yield surface shifts. Forward and backward paths do not intercept the yield surface on the same absolute value of stress. This is called as Bauschinger effect. The behavior inspired by this effect is called kinematic hardening. In kinematic hardening, size and shape of the yield surface do not change. The situation in which both the location of center and size of yield surfaces changes is combined hardening. Schematic representation of three approaches is given in Figure 3.1.

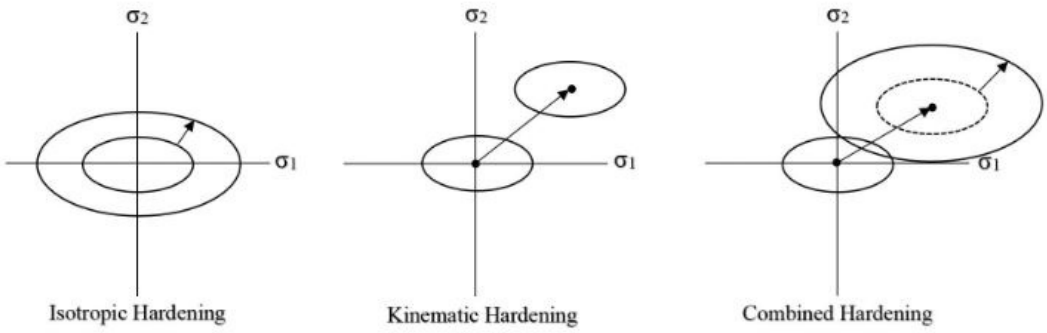

Figure 3.1: Schematic of three approaches to hardening

In this thesis, elastoplastic analysis with kinematic hardening will be used. All of the models in this study are rate independent. Therefore, incremental plasticity is used. Elastic calculations are held at first. Assuming the material as purely elastic, a trial stress will be determined. Using different yield criteria, it will be detected that whether the material exceeded the yield limit. In case the yield limit is not exceeded, next increment will start with further loading. After passing the yield point, radial return algorithm will be activated. In this algorithm, plastic multiplier $d\lambda$ will be

determined. After that, plastic stresses, strains and shift tensor will be found. Shift tensor, $\boldsymbol{\alpha}$ is zero at the beginning. It is updated in further steps.

First of all, additive decomposition is valid in incremental approach. Therefore,

$$d\boldsymbol{\epsilon} = d\boldsymbol{\epsilon}^p + d\boldsymbol{\epsilon}^e \tag{3.3}$$

where $d\boldsymbol{\epsilon}$ is the total strain increment, $d\boldsymbol{\epsilon}^p$ is the plastic strain increment and $d\boldsymbol{\epsilon}^e$ is the elastic strain increment.

In elastic calculation part, Hooke's Law with Lame constants is used. The increment of the elastic strain is:

$$d\boldsymbol{\epsilon}^e = \frac{1+\nu}{E} d\boldsymbol{\sigma} - \frac{\nu}{E} tr(d\boldsymbol{\sigma})\mathbf{I} \tag{3.4}$$

Or inversely, the stress increment is defined as:

$$d\boldsymbol{\sigma} = \lambda \boldsymbol{\delta} tr(d\boldsymbol{\epsilon}^e) + 2\mu d\boldsymbol{\epsilon}^e \tag{3.5}$$

where in last two equations, $\mathbf{I}$ is unit tensor, $\boldsymbol{\delta}$ is Kronecker delta tensor. Lame constants λ and μ are defined as

$$\lambda = \frac{\nu E}{(1+\nu)(1-2\nu)} \tag{3.6}$$

$$\mu = \frac{E}{2(1+\nu)} \tag{3.7}$$

In plastic part, associated flow rule is used:

$$d\boldsymbol{\epsilon}^p = d\lambda \frac{\partial F}{\partial \boldsymbol{\sigma}} \tag{3.8}$$

where F is the yield function. After determining plastic multiplier, plastic strain is found by using the flow rule. Then the stress increment can be written as:

$$d\boldsymbol{\sigma}' = 2\mu d\boldsymbol{\epsilon}' - d\lambda \frac{\boldsymbol{\sigma}'_{tr} - \boldsymbol{\alpha}'}{||\boldsymbol{\sigma}'_{tr} - \boldsymbol{\alpha}'||} \tag{3.9}$$

It is obtained by subtracting "plastic stress" from the initial trial stress. The plastic stress is

$$d\boldsymbol{\sigma}'_p = d\lambda \frac{\boldsymbol{\sigma}'_{tr} - \boldsymbol{\alpha}'}{||\boldsymbol{\sigma}'_{tr} - \boldsymbol{\alpha}'||} \tag{3.10}$$

and the trial stress is

$$d\boldsymbol{\sigma}'_{tr} = 2\mu d\boldsymbol{\epsilon}' \tag{3.11}$$

$$\boldsymbol{\sigma}'_{tr} = \boldsymbol{\sigma}'_{old} + d\boldsymbol{\sigma}'_{tr} \tag{3.12}$$

3.2 Yield Functions

Up to now, most researches have assumed materials as fully isotropic. Therefore, von-Mises is the common yield criterion for almost all of the studies. However, microstructure of materials may also has an effect on behavior during cyclic loading since there can be significant differences in mechanical responses on certain directions. Therefore, an anisotropic yield criterion should also be used in analyses. Therefore, three different yield criteria were used namely von-Mises, Hill and Aretz.

3.2.1 Von-Mises Yield Function

Von-Mises yield function can be written as:

$$J_2 - \sigma_Y^2 = 0 \tag{3.13}$$

where $J2$ is the second stress invariant. This function can be explicitly given for kinematic hardening as:

$$f = \sqrt{\frac{3}{2}(\sigma'_{ij} - \alpha'_{ij}) : (\sigma'_{ij} - \alpha'_{ij})} - \sigma_Y = 0 \tag{3.14}$$

where σ'_{ij} is the stress in deviatoric space, α'_{ij} is backstress tensor in the deviatoric space, and σ_Y is the initial yield stress.

3.2.2 Hill48 Yield Function

Hill48 yield function is:

$$2f = F(\sigma_{22} - \sigma_{33})^2 + G(\sigma_{33} - \sigma_{11})^2 + H(\sigma_{11} - \sigma_{22})^2 + 2L\sigma_{23}^2 + 2M\sigma_{31}^2 + 2N\sigma_{12}^2 - 1 \tag{3.15}$$

where the constants F, G, H, L, M, and N are:

$$F = \frac{1}{2}\left(\frac{1}{Y^2} + \frac{1}{Z^2} - \frac{1}{X^2}\right) \tag{3.16}$$

$$G = \frac{1}{2}\left(\frac{1}{Z^2} + \frac{1}{X^2} - \frac{1}{Y^2}\right) \tag{3.17}$$

$$H = \frac{1}{2}\left(\frac{1}{X^2} + \frac{1}{Y^2} - \frac{1}{Z^2}\right) \tag{3.18}$$

$$L = \frac{1}{2R^2} \tag{3.19}$$

$$M = \frac{1}{2S^2} \tag{3.20}$$

$$N = \frac{1}{2T^2} \tag{3.21}$$

where X, Y and Z are yield stresses in x, y and z direction, respectively. R, S and T are yield stresses for pure shear in yz, xy and xz planes. For the case $L = M = N = 3F = 3G = 3H$, this rule reduces to von-Mises yield criterion.

Hill's yield function can be written in terms of Lankford parameters. A Lankford parameter is denoted with r and is defined as the ratio of width strain to thickness strain.

$$r = \frac{d\epsilon_w^p}{d\epsilon_t^p} \tag{3.22}$$

r in any direction can be written as:

$$r_\theta = \frac{\frac{\partial F(\sigma_{ij})\sin^2\theta}{\partial \sigma_{xx}} + \frac{\partial F(\sigma_{ij})\cos^2\theta}{\partial \sigma_{yy}} - 2\frac{\partial F(\sigma_{ij})\sin\theta\cos\theta}{\partial \sigma_{xy}}}{\frac{\partial F(\sigma_{ij})}{\partial \sigma_{xx}} + \frac{\partial F(\sigma_{ij})}{\partial \sigma_{yy}}} \tag{3.23}$$

Using anisotropy coefficients in 0°, 45°and 90°, anisotropic behavior of the materials is defined and yield criterion can be written as

$$\sigma_{xx}^2 - \frac{2r_0}{1+r_0}\sigma_{xx}\sigma_{yy} + \frac{r_0(1+r_{90})}{r_{90}(1+r_0)}\sigma_{yy} + \frac{(r_0+r_{90})}{r_{90}(1+r_{90})}(2r_{45}+1)\sigma_{xy}^2 = \sigma_Y^2 \tag{3.24}$$

where σ_Y is the yield stress in x direction.

3.2.3 Aretz Yield Function

Aretz yield function is proposed for anisotropic materials as:

$$|\sigma_1|^m + |\sigma_2|^m + |\sigma_1 - \sigma_2|^m = 2Y_{ref}^m \tag{3.25}$$

where σ_1 and σ_2 are principal stresses and Y_{ref} is the yield stresses of the material and m is a constant.

Equation (3.25) was rearranged and written in a more general form as:

$$|\sigma_1'|^m + |\sigma_2'|^m + |\sigma_1'' - \sigma_2''|^m = 2Y_{ref}^m \tag{3.26}$$

The transformation equations for $\sigma_1', \sigma_2', \sigma_1''$ and σ_2'' are:

$$\sigma_1' = \frac{a_8\sigma_{11} + a_1\sigma_{22}}{2} + \sqrt{\left(\frac{a_2\sigma_{11} - a_3\sigma_{22}}{2}\right)^2 + (a_4)^2\sigma_{12}\sigma_{21}} \tag{3.27}$$

$$\sigma_2' = \frac{a_8\sigma_{11} + a_1\sigma_{22}}{2} - \sqrt{\left(\frac{a_2\sigma_{11} - a_3\sigma_{22}}{2}\right)^2 + (a_4)^2\sigma_{12}\sigma_{21}} \tag{3.28}$$

$$\sigma_1'' = \frac{\sigma_{11} + \sigma_{22}}{2} + \sqrt{\left(\frac{a_5\sigma_{11} - a_6\sigma_{22}}{2}\right)^2 + (a_7)^2\sigma_{12}\sigma_{21}} \tag{3.29}$$

$$\sigma_2'' = \frac{\sigma_{11} + \sigma_{22}}{2} - \sqrt{\left(\frac{a_5\sigma_{11} - a_6\sigma_{22}}{2}\right)^2 + (a_7)^2\sigma_{12}\sigma_{21}} \tag{3.30}$$

where the parameters $a_1, a_2, ..., a_8$ are anisotropy parameters.

The yield function can be represented as:

$$F(a_i, \sigma) = \bar{\sigma}(a_i, \sigma) - Y_{ref} \leq 0 \tag{3.31}$$

where the equivalent stress $\bar{\sigma}$ is

$$\bar{\sigma} = \left[\frac{1}{2}(|\sigma_1'|^m + |\sigma_2'|^m + |\sigma_1'' - \sigma_2''|^m)\right]^{1/m} \tag{3.32}$$

Although this model was created for plane stress problems, it can be applied to biaxial analyses in this thesis since the specimen is a hollow tube with a small thickness and the finite element model is full symmetric.

3.3 Kinematic Hardening Rules

In this section, six of these models will be defined. The backstress tensor is included in the yield functions. Since associated flow rule is used, hardening rules is effective on plastic strain prediction. In this thesis, the incremental hardening is defined as a function of several parameters.

$$d\boldsymbol{\alpha} = f(\boldsymbol{\sigma}, d\bar{\epsilon}, d\boldsymbol{\epsilon}^p, \boldsymbol{\alpha}', \mathbf{n}) \tag{3.33}$$

3.3.1 Prager Kinematic Hardening Rule

Prager introduced the kinematic hardening and proposed the following model.

$$d\boldsymbol{\alpha} = C d\boldsymbol{\epsilon}^p \tag{3.34}$$

where $d\boldsymbol{\alpha}$ is the backstress and C is a constant. It is a general and simple approach. Almost no material shows linear hardening. However, this model is a good starting point to improve simulations by modifying or adding terms. In fact, it can be used to predict stresses and loads in non-cyclic loading with not significant errors. The material constant C in Equation 3.34 is determined by using simple tension test experiments. Also in this model, the plastic modulus E_p is always constant. E_p can be determined from the following equation:

$$\frac{1}{E_t} = \frac{1}{E} + \frac{1}{E_p} \tag{3.35}$$

where E_t represents the tangential modulus on the plastic side during the elastoplastic analyses. Figure 3.2 shows how the modulus values are defined where E is elastic modulus and σ_Y is the initial yield stress.

3.3.2 Armstrong-Frederick Kinematic Hardening Rule

A-F rule is the ancestor of nonlinear kinematic hardening models that are currently being used for ratcheting simulations [2]. It has a dynamic recovery term which makes the model nonlinear. Translation of yield surface is defined as:

$$d\boldsymbol{\alpha} = C d\boldsymbol{\epsilon}^p - \gamma \boldsymbol{\alpha}' d\bar{\epsilon} \tag{3.36}$$

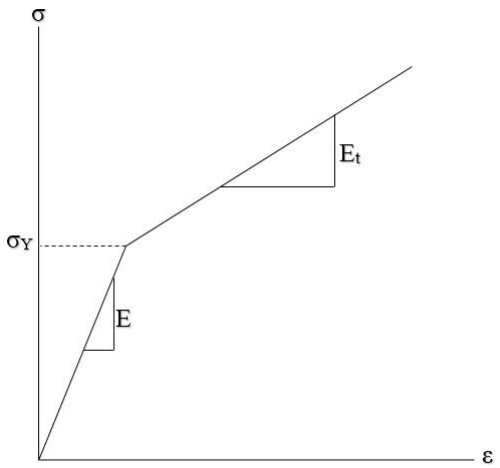

Figure 3.2: Representation of linear plastic behavior

where $\boldsymbol{\alpha}'$ is deviatoric backstress, γ is a material constant and $d\bar{\epsilon}$ is equivalent plastic strain which is defined as:

$$d\bar{\epsilon} = \sqrt{\frac{2}{3} d\boldsymbol{\epsilon}^p : d\boldsymbol{\epsilon}^p} \tag{3.37}$$

Addition of second term in the backstress tensor increment formula as well as non-constant plastic modulus makes the model possible to create open loops with cyclic loading. Therefore, this can model ratcheting in both uniaxial and multiaxial loading.

Plastic modulus calculation is derived from hardening rule through consistency condition. Implementing the condition, plastic modulus is obtained as:

$$E_p = C \pm \gamma \alpha_{(ii)} \tag{3.38}$$

where $\alpha_{(ii)}$ is the backstress in the direction of loading. Minus sign in Equation 3.38 indicates forward loading, which is the analyzed direction of ratcheting to where plastic strain accumulation is expected to occur. Plus sign implies the direction is the reversed.

3.3.3 Burlet-Cailletaud Kinematic Hardening Rule

Burlet-Cailletaud rule is another type of nonlinear kinematic hardening model [6]. It is obtained by modifying the second term of A-F hardening rule. Dynamic recovery term becomes radial return or radial evanescence term with this alteration. The model

is given as

$$d\boldsymbol{\alpha} = Cd\boldsymbol{\epsilon}^p - \gamma\left(\boldsymbol{\alpha}' : \mathbf{n}\right)\mathbf{n}d\bar{\epsilon} \tag{3.39}$$

where $\mathbf{n}$ is the direction of plastic strain. In uniaxial ratcheting experiments, the evanescence term has no difference with the second term of A-F rule since direction of loading is unique. Its effect can only be observed in multiaxial case.

3.3.4 Chaboche Kinematic Hardening Rule

This is a partitioned nonlinear kinematic hardening rule [7]. Backstress tensor is obtained by adding terms to each other. There are two versions of this model. The first one consists of three partitions. The second is obtained by adding a threshold term and includes four partitions.

First version of the model is written as

$$d\boldsymbol{\alpha} = \sum_{i=1}^{3} d\boldsymbol{\alpha}_i \tag{3.40}$$

$$d\boldsymbol{\alpha}_i = C_i d\boldsymbol{\epsilon}^p - \gamma_i \boldsymbol{\alpha}_i' d\bar{\epsilon} \tag{3.41}$$

where $i = 1, 2, 3$ and constants C_i, γ_i are determined from experiments.

Plastic modulus is found as

$$E_p = (C_1 \pm \gamma_1) + (C_2 \pm \gamma_2) + (C_3 \pm \gamma_3) \tag{3.42}$$

again minus sign indicates forward loading and plus sign indicates reverse loading.

All of the partitions are in the same form with A-F kinematic hardening rule. First partition has a large modulus and shakes down rapidly. Second one represents a nonlinear portion which acts as a transition between this large modulus portion and third nonlinear portion. At last, third portion simulates the linear part when $\gamma_3 = 0$. However, when it is a non-zero term, term becomes nonlinear. Ratcheting continues to occur and shake down is retarded from where shake down occurs on zero value of γ_3.

Second version of Chaboche model includes a threshold term as the fourth partition which is

$$d\boldsymbol{\alpha}_i = C_i d\boldsymbol{\epsilon}^p - \gamma_i \boldsymbol{\alpha}_i' \left\langle 1 - \frac{\bar{\boldsymbol{\alpha}}_i'}{f(\boldsymbol{\alpha}_i)} \right\rangle d\bar{\epsilon} \tag{3.43}$$

for $i = 4$. In Equation 3.43, $<>$ is McCauley's bracket in which $< a >= a$ for $a > 0$ and $< a >= 0$ for $a \leq 0$. In the bracket, function f is defined as:

$$f(\boldsymbol{\alpha}_i) = \left[\frac{3}{2}\boldsymbol{\alpha}_i' : \boldsymbol{\alpha}_i'\right]^{\frac{1}{2}} \tag{3.44}$$

3.3.5 Bari-Hassan Kinematic Hardening Rule

Bari-Hassan kinematic hardening model has also two versions as partitioned and not partitioned [5]. The first version is defined as

$$d\boldsymbol{\alpha} = Cd\boldsymbol{\epsilon}^p - \gamma\left[\delta\boldsymbol{\alpha}' + (1-\delta)(\boldsymbol{\alpha}' : \mathbf{n})\mathbf{n}\right] d\bar{\epsilon} \tag{3.45}$$

where δ is "Delobelle paratemer". In plastic modulus calculation, Delobelle parameter is not included for this proposed model. When Delobelle parameter $\delta = 0$, Equation 3.45 turns out to be B-C model and for $\delta = 1$, it is exactly the same as A-F model.

The second version is proposed as partitioned model.

$$d\boldsymbol{\alpha} = \sum_{i=1}^{M} d\boldsymbol{\alpha}_i \tag{3.46}$$

$$d\boldsymbol{\alpha}_i = C_i d\boldsymbol{\epsilon}^p - \gamma_i\left[\delta\boldsymbol{\alpha}_i' + (1-\delta)(\boldsymbol{\alpha}_i' : \mathbf{n})\mathbf{n}\right] d\bar{\epsilon} \tag{3.47}$$

for $i = 1, 2, 3$ and

$$d\boldsymbol{\alpha}_i = C_i d\boldsymbol{\epsilon}^p - \gamma_i\left[\delta\boldsymbol{\alpha}_i' + (1-\delta)(\boldsymbol{\alpha}_i' : \mathbf{n})\mathbf{n}\right]\left\langle 1 - \frac{\bar{\boldsymbol{\alpha}_i'}}{f(\boldsymbol{\alpha}_i)}\right\rangle d\bar{\epsilon} \tag{3.48}$$

for $i = 4$.

As can be seen, this model becomes Chaboche hardening rule when $\delta = 1$. Plastic modulus calculation for this part does not include Delobelle parameter too. Therefore, one can determine the plastic modulus by just using Chaboche rule's formula. The Delobelle parameter is expected to give a compromise between over prediction of A-F model and lower prediction of Chaboche model.

3.3.6 Ohno-Wang Kinematic Hardening Rule

Ohno-Wang model has also two different versions [28]. The first version of this model is:

$$d\boldsymbol{\alpha} = \sum_{i=1}^{M} d\boldsymbol{\alpha}_i \tag{3.49}$$

$$d\boldsymbol{\alpha}_i = C_i d\boldsymbol{\epsilon}^p - \gamma_i \boldsymbol{\alpha}_i' \left\langle d\boldsymbol{\epsilon}^p : \frac{\boldsymbol{\alpha}_i'}{f(\boldsymbol{\alpha}_i)} \right\rangle H \left[{\boldsymbol{\alpha}_i}^2 - \left(\frac{C_i}{\gamma_i} \right)^2 \right] \tag{3.50}$$

where H is the Heaviside step function. Input in the Heaviside step function shows that when hardening or backstress tensor reaches the value of $\dfrac{C_i}{\gamma_i}$, second term ceases and model becomes linear again. This prevents the formula from creating ratcheting strain after a certain point. Therefore, a second version, which replaces a power term instead of this Heaviside step function is written.

$$d\boldsymbol{\alpha}_i = C_i d\boldsymbol{\epsilon}^p - \gamma_i \boldsymbol{\alpha}_i' \left\langle d\boldsymbol{\epsilon}^p : \frac{\boldsymbol{\alpha}_i}{f(\boldsymbol{\alpha}_i)} \right\rangle \left(\frac{f(\boldsymbol{\alpha}_i)}{C_i/\gamma_i} \right)^{m_i} \tag{3.51}$$

where m_i is another material constant. With this second version, the cessation of ratcheting is avoided. For uniaxial loading, this model creates reasonable results.

Plastic modulus calculation is complicated for this model. It is also obtained by adding the partitions one by one. Also, Delobelle parameter is again not included in the calculation.

$$E_p = \sum_{i=1}^{M} H_i \tag{3.52}$$

$$(E_p)_i = \gamma_i \left[C_i d\boldsymbol{\epsilon}^p - \left(\frac{\bar{\alpha}_i}{C_i} \right)^{m_i} (\boldsymbol{\alpha}_i : \mathbf{n}) \left\langle \frac{d\boldsymbol{\epsilon}^p : \boldsymbol{\alpha}_i}{\bar{a}_i d\bar{\epsilon}} \right\rangle \right] \tag{3.53}$$

There are studies using this model by eight decomposition and twelve decomposition. There is no significant difference between them. Hence, for the sake of simplicity in subroutine coding, eight decomposition of second version is used in this study.

CHAPTER 4

FINITE ELEMENT ANALYSES

In solid mechanics, there are numerous analytic solutions to the problems. For simple loading cases and geometries, the displacements and resultants can be evaluated analytically. However, when the case is complicated, exact analytic solutions cannot always be found. As a result, specific numerical solution techniques are developed.

One of the recent techniques is the Finite Element Method. In this method the material is divided into smaller domains or elements that have simpler geometries and smaller dimensions. All of the elements are connected next to each other. For each of these elements, simpler trial solutions can be assumed for getting approximate solution. Also, coefficients of these trial solutions have some correspondence with the physics of the problem in finite element method.

Finite element method is widely used in the solution of mechanics problems as a result of its simplicity and strength in solving complicated problems. In this thesis, although the geometry is simple, the loading conditions and material behavior are complicated. Hence, a package that should give a flexibility on implementing different material behaviors and loading types is necessary. Finite element package Abaqus is used for all of the analysis for this reason. It gives opportunity to imply different plastic models through its own subroutines. These subroutines can be run by connecting a Fortran compiler to Abaqus.

Several features are considered during finite element analyses to obtain reliable results in the shortest time possible. First of all, analyses should be performed in such a way that the most trustworthy results can be get. Therefore, optimum method, either explicit analysis or implicit analysis should be determined. Then, appropriate element

type should be specified. Either 3D or 2D elements can be used and correct element type should be selected. Number of meshes or elements should be optimized because as the element number increases, time consumption of analyses also increases. On the other hand, correct results may not be obtained by using few number of elements. There are some other methods to decrease time consumption of analyses such as mass scaling and time scaling.

VUMAT user subroutines are written for implementing different kinematic hardening rules to the package. A complete constitutive model can be introduced in the coding. Therefore, both elastic and inelastic parts are considered in the subroutines. Radial return algorithm, which is also known as predictor method is used to get stress values in each increment.

4.1 Implicit and Explicit Analysis

In the solutions, dynamic analysis module of Abaqus is utilized. The case for this study is nonlinear analysis since materials exhibits nonlinear hardening behavior. For ratcheting, there is cyclic loading causing material to deform plastically in each cycle by small amounts such that the deformation cannot be simulated efficiently by static analysis.

In dynamic analysis, there two ways of integration. These are implicit methods and explicit methods. Explicit analysis determines the variables on time $t + \Delta t$ using the values of t. This method is always conditionally stable. Stability limit for increment is the time that an elastic stress wave propagates the smallest element dimension. On the contrary, implicit analysis has no limit for time increment. This method determines the variables of time $t + \Delta t$ by using the values of both t and $t + \Delta t$. As a result, a system of nonlinear equations arise. Therefore, solution of a problem using implicit method takes more time. The number of increments are far greater in explicit analysis.

4.1.1 Formulation of Implicit Analysis

Generic equations of implicit method for dynamic problems are well described in [37].

For implicit dynamic analysis

$$\boldsymbol{M}\ddot{\boldsymbol{u}}^{(i+1)} + (1+\alpha)\boldsymbol{K}\boldsymbol{u}^{(i+1)} - \alpha\boldsymbol{K}\boldsymbol{u}^{(i)} = \boldsymbol{F}^{(i+1)} \tag{4.1}$$

where $\boldsymbol{M}$ is mass matrix, $\boldsymbol{K}$ is stiffness matrix, $\boldsymbol{F}$ is the force matrix and $\boldsymbol{u}$ is displacement vector. Once $\ddot{\boldsymbol{u}}$ is determined from Equation 4.1, the velocity vector is found as:

$$\dot{\boldsymbol{u}}^{(i+1)} = \dot{\boldsymbol{u}}^{(i)} + \Delta t((1-\gamma)\ddot{\boldsymbol{u}}^{(i)} + \gamma\ddot{\boldsymbol{u}}^{(i+1)} \tag{4.2}$$

and the displacement vector is:

$$\boldsymbol{u}^{(i+1)} = \boldsymbol{u}^{(i)} + \Delta t\dot{\boldsymbol{u}}^{(i)} + \Delta t^2((\frac{1}{2}-\beta)\ddot{\boldsymbol{u}}^{(i)} + \beta\ddot{\boldsymbol{u}}^{(i+1)}) \tag{4.3}$$

where the constants are $\beta = \frac{1}{4}(1-\alpha^2)$, $\gamma = \frac{1}{2} - \alpha$, and $\frac{1}{3} \leq \alpha \leq 0$. These values are automatically chosen by Abaqus unless another value is specified by the user.

For problems that necessitate small time increments such as ratcheting cases, implicit analysis is unable to give results. Therefore, for analyses of all nonlinear kinematic hardening rules, explicit scheme is used throughout the analysis.

4.1.2 Formulation of Explicit Analysis

The governing equation of the explicit analysis is:

$$\boldsymbol{M}\ddot{\boldsymbol{u}}^{(i)} = \boldsymbol{F}^{(i)} - \boldsymbol{I}^{(i)} \tag{4.4}$$

where $\boldsymbol{M}$ is mass matrix, $\boldsymbol{F}$ is load vector and $\boldsymbol{I}$ is internal force vector. After $\ddot{\boldsymbol{u}}$ is solved by above equation, $\dot{\boldsymbol{u}}$ can be found as:

$$\dot{\boldsymbol{u}}^{(i+1)} = \dot{\boldsymbol{u}}^{(i+\frac{1}{2})} + \frac{1}{2}\Delta t^{(i+1)}\ddot{\boldsymbol{u}}^{(i+1)} \tag{4.5}$$

The displacement vector equations are as follows:

$$\dot{\boldsymbol{u}}^{(i+\frac{1}{2})} = \dot{\boldsymbol{u}}^{(i-\frac{1}{2})} + \frac{\Delta t^{(i+1)} + \Delta t^{(i)}}{2}\ddot{\boldsymbol{u}}^{(i)} \tag{4.6}$$

$$\boldsymbol{u}^{(i+1)} = \boldsymbol{u}^{(i)} + \Delta t^{(i+1)} \dot{\boldsymbol{u}}^{(i+\frac{1}{2})} \tag{4.7}$$

where the superscripts $i - \frac{1}{2}$ and $i + \frac{1}{2}$ represents the values at the midpoint times of increments. For the first increment, if not specified, velocities and accelerations are zero at the beginning.

In explicit method, small time increments are needed. Since the results of previous increments are used for calculating the values at the next increment, divergence can easily occur. To avoid divergence, there are some stability conditions. The maximum increment time should satisfy the condition:

$$\Delta t \leq \frac{2}{\omega_{max}} \tag{4.8}$$

where ω_{max} is the maximum eigenvalue of the system. When there is damping, the inequality turns out to be

$$\Delta t \leq \frac{2}{\omega_{max}} (\sqrt{1 + \eta^2} - \eta) \tag{4.9}$$

where η is the fraction of critical damping in the highest mode.

In Abaqus Explicit, time increments are determined automatically. The stability condition in (4.8) can also be explained as:

$$\Delta t = min \left(\frac{L_e}{c_d} \right) \tag{4.10}$$

where L_e is characteristic length of an element which can be defined as the smallest length in the meshing and c_d is the wave speed throughout the body whose formula is:

$$c_d = \sqrt{\frac{\lambda + 2\mu}{\rho}} \tag{4.11}$$

where λ and μ are Lame constants, ρ is the density of material.

4.2 Radial Return Algorithm

In the subroutines, radial return algorithm is used to determine stresses and elastic-plastic strains in plastic region. Total strains are known from finite element solution.

First, material is assumed to be purely elastic and elastic predictor stress is calculated using total strain. After that, using an algorithm, plastic strains are found and stress increments are obtained. By subtracting the plastic strain and stress from the trial state, all of the required values can be found.

4.2.1 Return Algorithm for Linear Plasticity

In this algorithm, plastic multiplier is derived from linear plasticity. It can be shown that $d\lambda = d\bar{\epsilon}$. Therefore, flow rule can be obtained as:

$$d\boldsymbol{\epsilon}^p = \frac{3}{2}(\mathbf{S}^{pr} - \boldsymbol{\alpha}^0)d\bar{\epsilon}/\sigma^{pr} \tag{4.12}$$

where $\mathbf{S}^{pr}$ is the trial stress, that is, the value of stress assuming the material is purely elastic at the beginning, in deviatoric space. Using several steps of manipulation, equivalent plastic strain is found as:

$$d\lambda = d\bar{\epsilon} = \frac{\sigma^{pr} - \sigma_y}{h + 3\mu} \tag{4.13}$$

Using this algorithm, new stress and strain (both elastic and plastic) values can be found. The linear plasticity model for determining plastic multiplier gives reasonable results. Therefore, it can be used in the analyses.

4.2.2 Return Algorithm for Nonlinear Plasticity

Equation 4.12 also holds for nonlinear plasticity. However, calculation of equivalent plastic strain is different. Using Newton-Raphson method starting with $d\lambda = 0$ and $\bar{\epsilon}^{n+1} = \bar{\epsilon}^n$, where $\bar{\epsilon}^{n+1}$ and $\bar{\epsilon}^n$ are plastic strains in next and previous steps, respectively. Then the series of equations are

$$f = ||\boldsymbol{\eta}^{tr}|| - (2\mu + h(\bar{\epsilon}^{n+1}))d\lambda - \kappa(\bar{\epsilon}^{n+1}) \tag{4.14}$$

$$\frac{\partial f}{\partial d\lambda} = -(2\mu + h) - \frac{\partial h}{\partial \boldsymbol{\epsilon}_p}d\lambda - \frac{\partial \kappa}{\partial \epsilon_p} \tag{4.15}$$

$$d\lambda = d\lambda - \frac{f}{\partial f/\partial d\lambda} \tag{4.16}$$

$$\bar{\epsilon}^{n+1} = \bar{\epsilon}^n + d\lambda \tag{4.17}$$

where $||\boldsymbol{\eta}^{tr}|| = ||\mathbf{S}^{pr} - \boldsymbol{\alpha}^0||$. Procedure is stopped when $f \approx 0$.

4.3 Methods for Decreasing the Time Consumption

Since the time increments are small and high number of loading cycles are to be utilized, methods for decreasing the analysis time without deviating the results are required. For this purpose, mass scaling is used. Mass scaling is suitable for the analysis of the current thesis since the dynamic analyses are being performed at slow speeds that can be considered as quasi-static and all of the tried models are rate-independent. Also, different from time scaling, mass scaling does not change the natural time schedule.

Mass scaling can be used to change the mass of a whole body or portion of it. It may be defined for one step of the analysis or for total time steps, called "fixed mass scaling". Moreover, it can be changed during the step, called "variable mass scaling".

Scaling can be done in several ways.

1. A factor that increases the masses of specified elements may be given as input by user.
2. A minimum time increment may be given. ABAQUS will arrange the mass scaling values accordingly. However in this method, all of the elements' masses will be scaled until the minimum time increment becomes equal to a specified value. Therefore while doing this, some of the elements' time scales may get too large. This is avoided by defining a scaling provided in third way.
3. Unlike in second method only the elements whose increments are less than specified value are modified. By this way, time increments for all elements get close to each other.

In this study, second method has been adopted for applicability of mass scaling.

Mass scaling artificially increases the densities of the elements. In equation (4.11) wave speed of the element was given. It contains density in the denominator having a square root function. Therefore, if the mass of an element is scaled by a factor c^2, wave speed of the element is decreased by c. This means the stable time increment limit is increased by factor c, speeding up the analyses.

Although mass scaling seems to be greatly advantageous method, it may have some adverse effects. Since the masses of bodies increase, dynamic effects should be carefully considered. If the mass of the material is increased so much, inertial forces may become dominant in the model and may cause results to be deteriorated especially for quasi static analyses. Also, program may miss some important values through enlarged time steps.

An optimum mass scaling analysis was done. Internal and kinetic energies and strains for mass scaling values of 0 to 2500 have been observed. After the analyses, it was seen that mass scaling can not be used for this model. Maximum strain reached by last cycle became higher than the model with no mass scaling. Strain values deviated from the original analysis starting from low mass scaling. Although energy values got higher by increasing mass scaling factor, condition of quasi-static analysis was protected (Figure 4.1 and Figure 4.2). High mass scale distorted the strain. Total accumulated strains were close to each other, that is, the overall predicted ratcheting was the same at different mass scaling factors which is not reliable for all of the models since there occurred a huge amount of strain at the end. Therefore, analysis for ratcheting frequency can be performed only for scaling factor of 10.

Another method for decreasing time consumption is increasing the load rate. One way of defining cyclic loading is using periodic option which involves Fourier series to define the loading as shown in Equation (4.18).

$$f(x) = C_0 + \sum A_0 sin(\omega x) + B_0 cos(\omega x) \tag{4.18}$$

where ω is frequency of the function. Load function may be given as sinusoidal wave in which $B_0 = 0$. C_0 represents the mean load or displacement around which the variable load or displacement will be given.

Rate of loading is changed by arranging ω value. However, if ω is too large, stress waves becomes high and quasi static analysis cannot be carried on because of dominant dynamic effects. To avoid this dynamic effect, kinetic energy to internal energy ratio should be kept lower than 0.1. Therefore, a compromise between low loading rate that makes analysis time so large and high loading rate that makes dynamic effects dominant should be found. For this purpose, a series of analyses at different load frequencies was performed. Analyses of high load frequency can deviate from

quasi static analysis. Unexpected dynamic effects are also prone to affect the results. This can be avoided by using lower frequencies in the loading. However, then analysis time increases. It can speed up by increasing the frequency. Therefore, series of analyses having a frequency spectrum of π to 20π has been run. It was observed that the model is quasi-static for all of the cycle speeds as kinetic energy to internal energy ratio is low enough in Figure 4.4 and Figure 4.5. Moreover, under 5π, kinetic energy was almost zero. Kinetic energy increases with increasing frequency. Internal energy also gets higher while processing 3.14 to 62.80. Still analysis is confined to use a loading frequency of 15.70 due to increasing strain values.

4.4 Mesh Dependency

Numbers and type of these meshes are important for analyses to give correct results. Therefore, a mesh dependency analysis should be done for validation of obtained results. If elements are too many, the analysis will run too long. On the contrary, if the number of elements is so small, then necessary number of integration points cannot be reached and obtained values may differ from the actual case.

To find optimum element number, analyses of ratcheting with A-F model by using different runs starting from 27 element to 10,800 element were done. Internal and kinetic energies and strain values were monitored. Since all of the models have been written in rate independent form, dynamic effects are avoided. Therefore, a quasi static analyses was followed. It is observed in Figure 4.7 and Figure 4.8 that this condition is satisfied for all number of meshes since kinetic energy values are at acceptable degree compared to internal energy. Another important data is the strain values since the main concern of the subject is accumulation of the strain. For mesh numbers smaller than 1200-1400, there existed deviations. However, when mesh number increases further, stable results were obtained. As Figure 4.9 shows, analyses can be done by using about 1200 element since the values are stabilized after that point.

4.5 The Used Model

Due to axisymmetry of the part, axisymmetric element "CAX4R" is used in the analyses. This is a 4-node continuum element for explicit method. It uses reduced integration. Mesh number is concluded as 1200. Frequency value has come out to be lower than 15.70 and mass scaling factor can at most be 10. For all of different kinematic hardening models with different yield criteria, the finite element analyses are performed using this model.

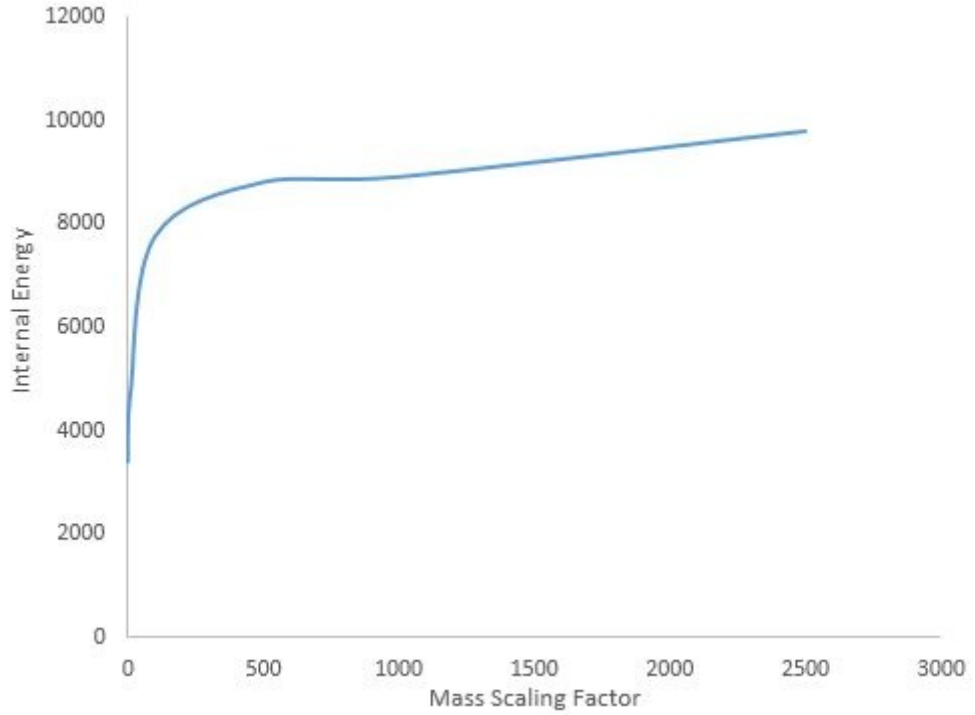

Figure 4.1: Internal energy vs mass scale factor

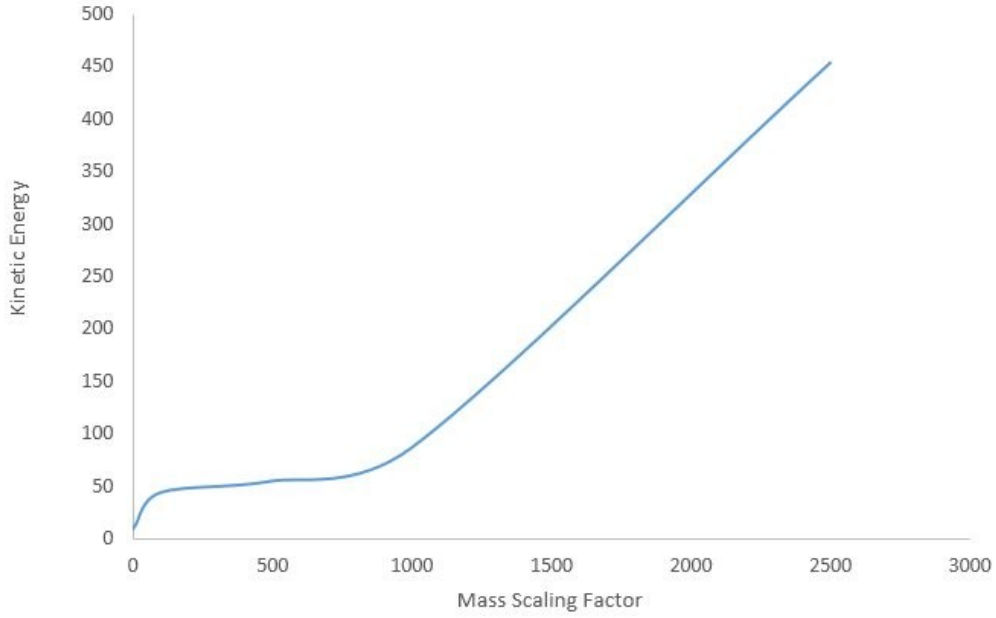

Figure 4.2: Kinetic energy vs mass scale factor

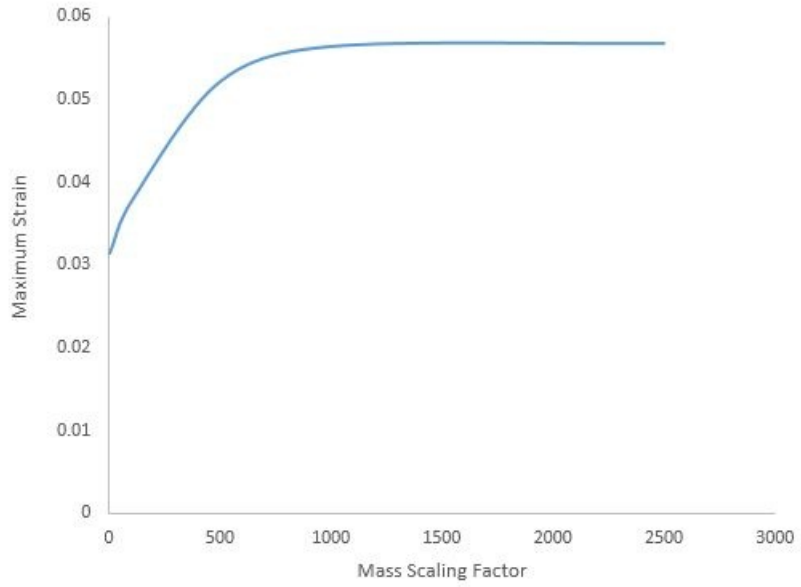

Figure 4.3: Maximum strain vs mass scale factor

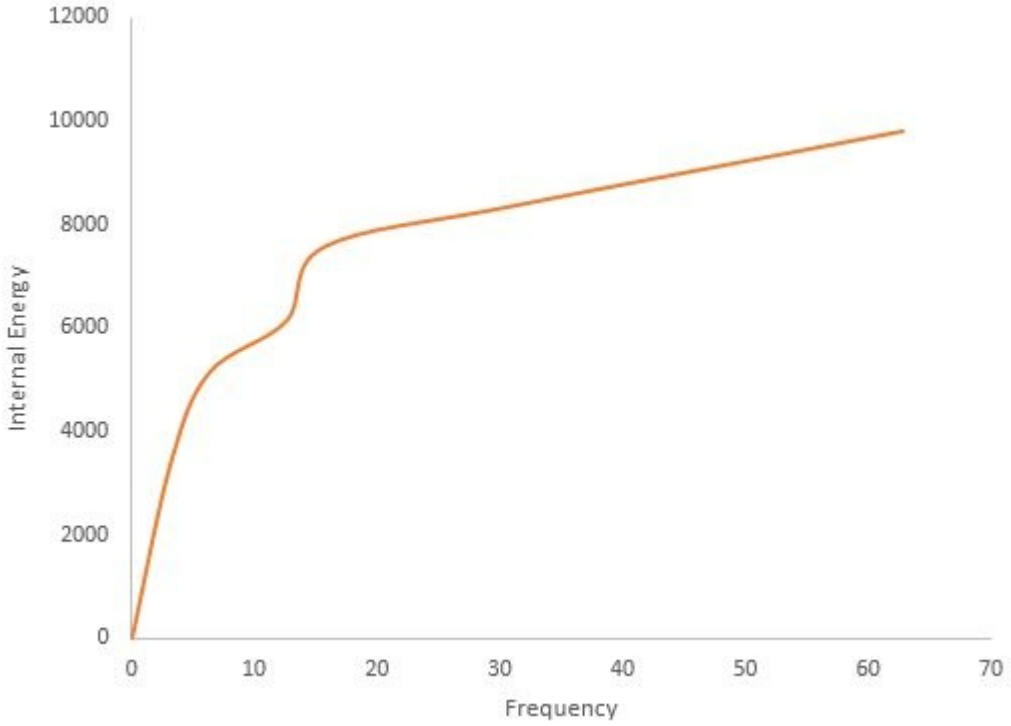

Figure 4.4: Internal energy vs frequency

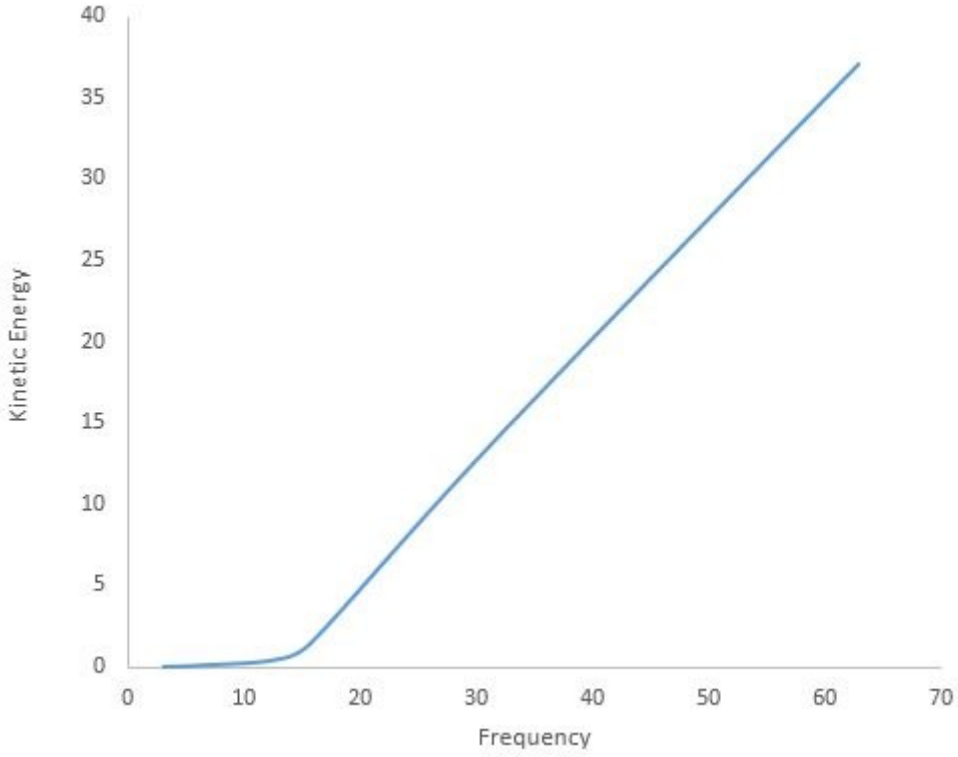

Figure 4.5: Kinetic energy vs frequency

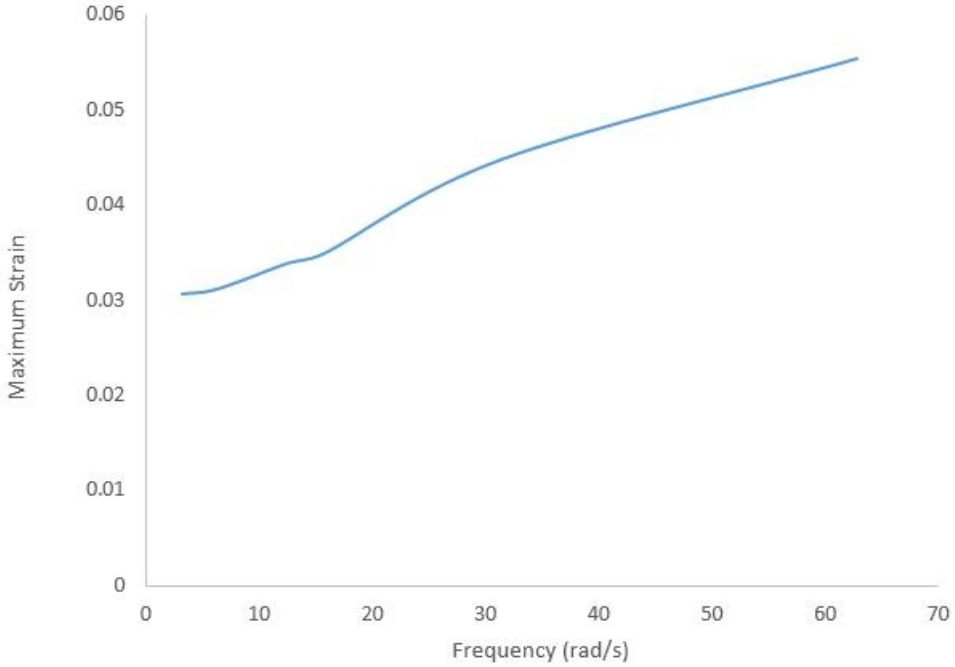

Figure 4.6: Maximum strain vs frequency

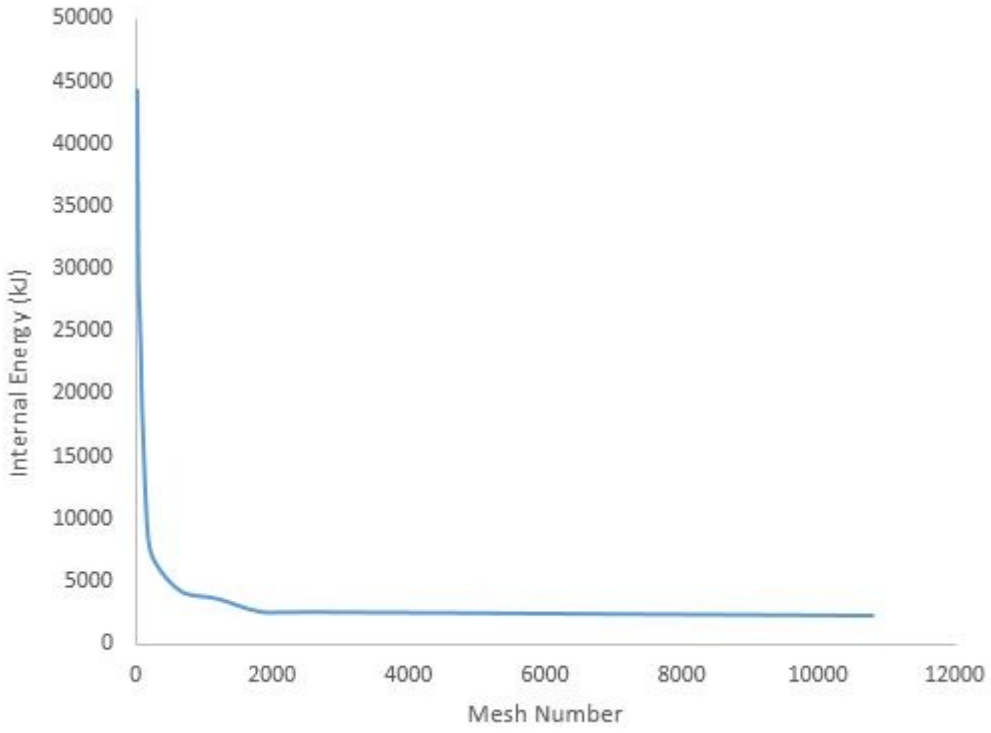

Figure 4.7: Internal energy vs mesh number

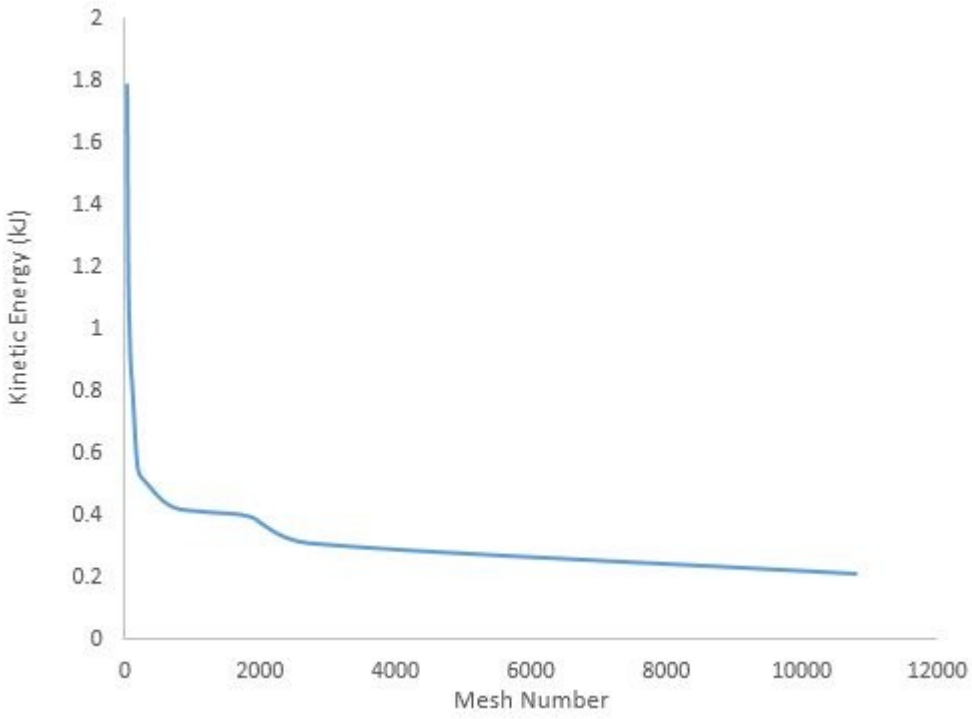

Figure 4.8: Kinetic energy vs mesh number

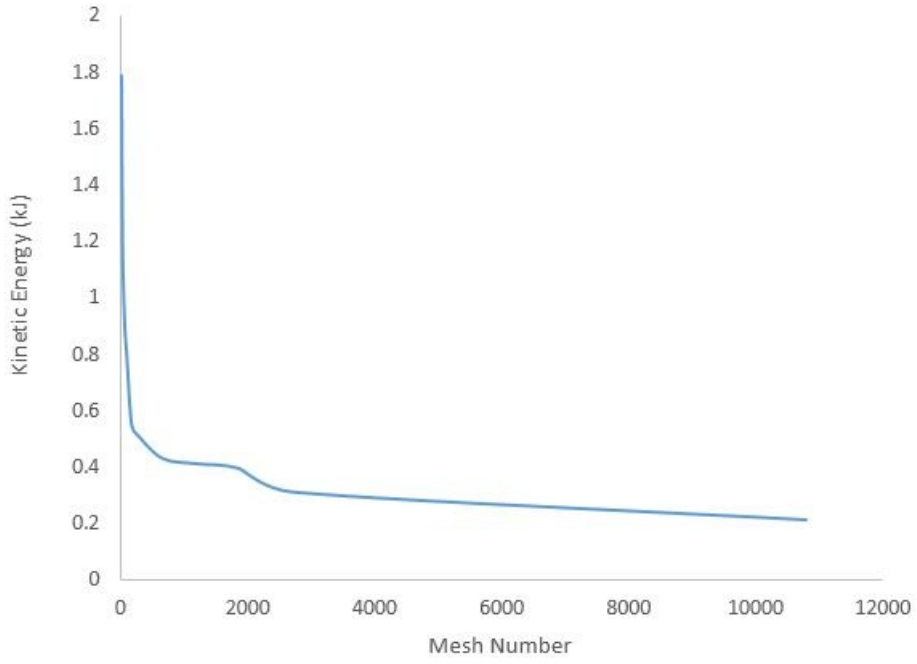

Figure 4.9: Maximum strain vs mesh number

CHAPTER 5

RESULTS

In this chapter, results of the analyses considering different kinematic hardening rules and yield functions are presented. Models have been run for both uniaxial and biaxial loading conditions.

5.1 Uniaxial Ratcheting

In this section, results of uniaxial ratcheting of a solid rod are presented for von-Mises yield criterion and six different kinematic hardening rules are used. Mechanical properties of the material are given in Table 5.1. The contstants K and n characterizes the stress-strain diagram of material according to the model $\sigma = K\epsilon^n$. The dimensions of this work piece are given in Figure 5.1. Stress and strain controlled ratcheting results are included in all subsections. While one end of the rod was hold fixed, loading or displacement was applied from the other end during the analyses. For each model, except Prager, analyses for four different mean stresses and four different alternating stresses were performed for stress controlled cycling.

$\sigma_y(MPa)$	$\sigma_u(MPa)$	$E(MPa)$	ν	$K(MPa)$	n
241	420	200000	0.3	564	0.17

Table 5.1: Mechanical properties of the material

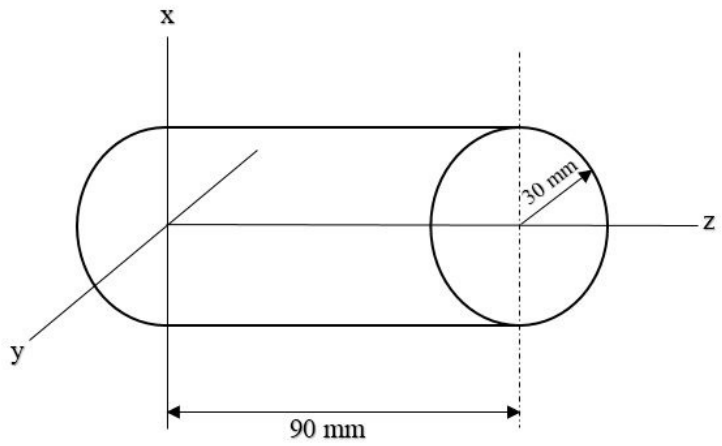

Figure 5.1: Specimen of uniaxial analyses

5.1.1 Prager Model

Since Prager model did not simulate any ratcheting for any loading conditions, only result of stress controlled analyses with 80 MPa mean stress and 220 MPa alternating stress is given in Figure 5.2.

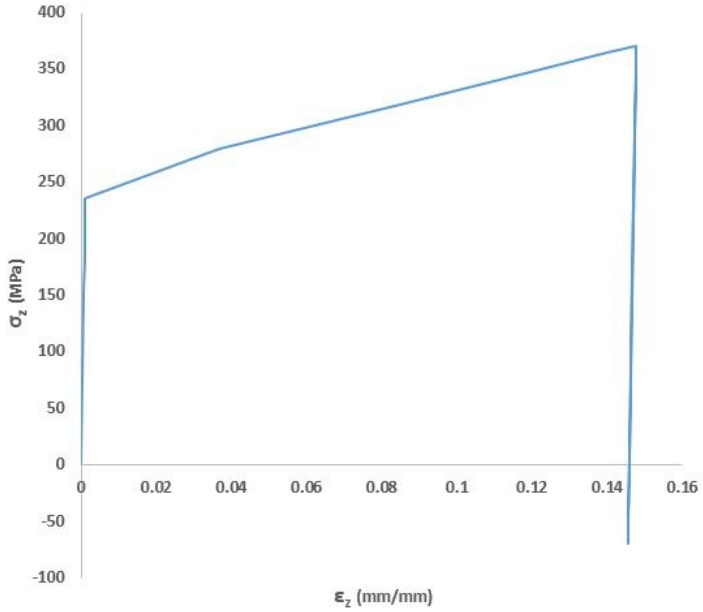

Figure 5.2: Stress-strain behavior of Prager model in uniaxial loading for $\sigma_m = 80MPa$, $\sigma_a = 220MPa$

5.1.2 Armstrong-Frederick Model

Four different mean stress values; 40 MPa, 60 MPa, 80 MPa and 100 MPa were applied for A-F model while the alternating stress was taken as 210 MPa for all mean stresses. Figure 5.3 - Figure 5.6 show the variation of the axial strain of the bar, ϵ_z, for mean stress values 40 MPa, 60 MPa, 80 MPa and 100 MPa, respectively. In Figure 5.7, the variation of maximum ratcheting strain with respect to number of cycles are shown for different mean stresses at constant alternating stress. It is observed that accumulated strain increases with increasing mean stress.

Four different alternating stress values; 150 MPa, 180 MPa, 210 MPa and 240 MPa were applied for A-F model while mean stress was kept at 80 MPa for all alternating stresses. Figure 5.8 - Figure 5.11 show the variation of the axial strain of the bar, ϵ_z, for alternating stress values 150 MPa, 180 MPa, 210 MPa and 240 MPa, respectively. In Figure 5.12, the variation of ratcheting strain with respect to number of cycles are shown for different alternating stresses at constant mean stress. It is seen that increasing alternating stress increases the amount of ratcheting strain.

Figure 5.13 shows the stress strain response for symmetric strain cycling with an amplitude of $\epsilon_z = 0.002mm/mm$. After several cycles of hardening, the material has shaken down and strain hardening has stopped.

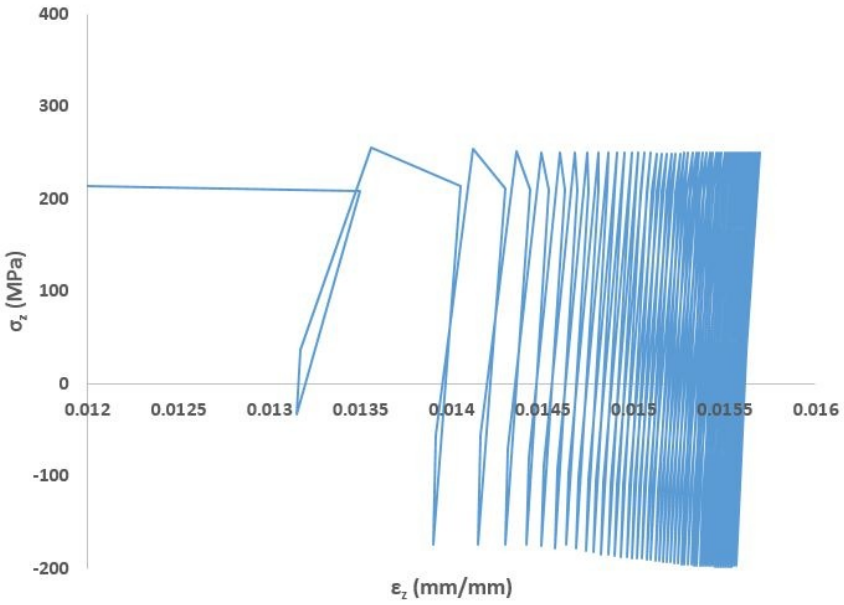

Figure 5.3: A-F model with $\sigma_m = 40MPa$ and $\sigma_a = 210MPa$

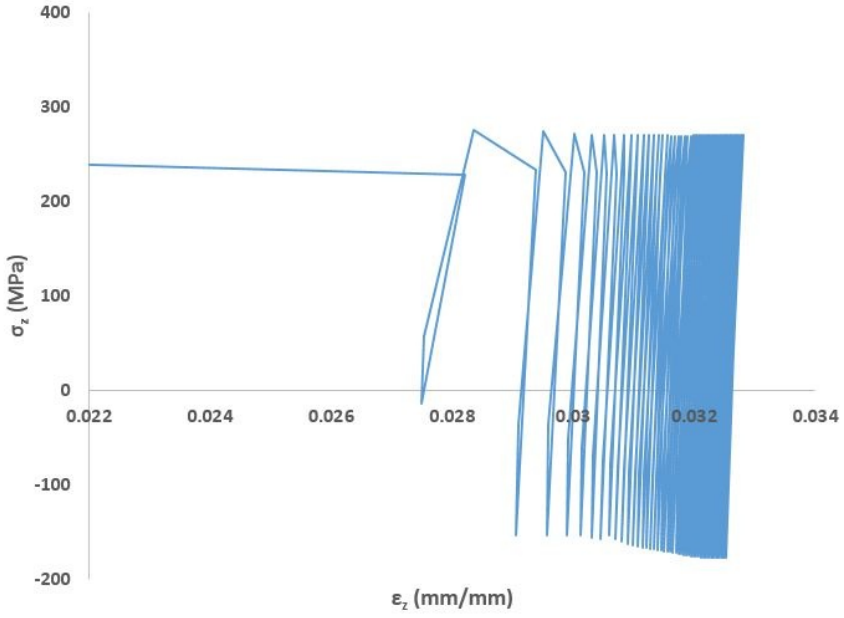

Figure 5.4: A-F model with $\sigma_m = 60MPa$ and $\sigma_a = 210MPa$

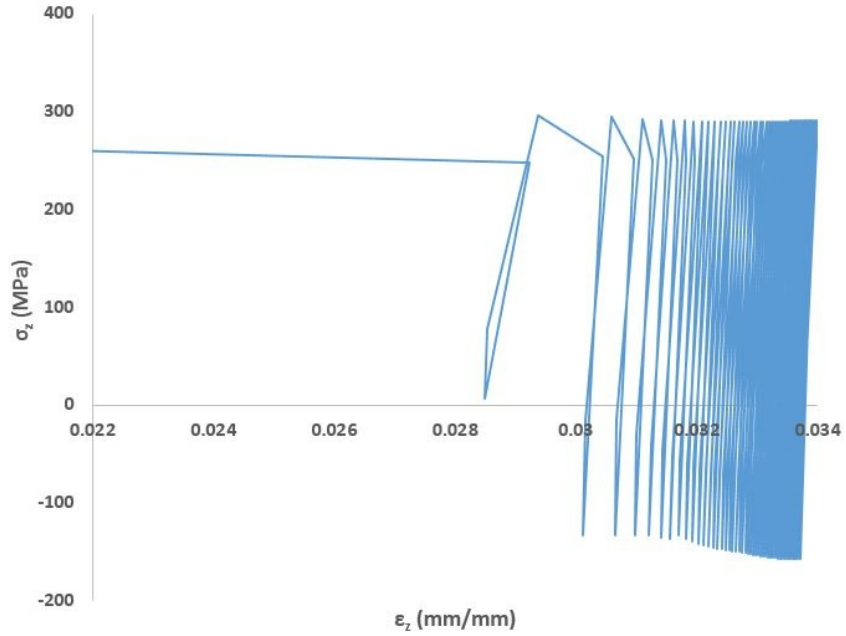

Figure 5.5: A-F model with $\sigma_m = 80MPa$ and $\sigma_a = 210MPa$

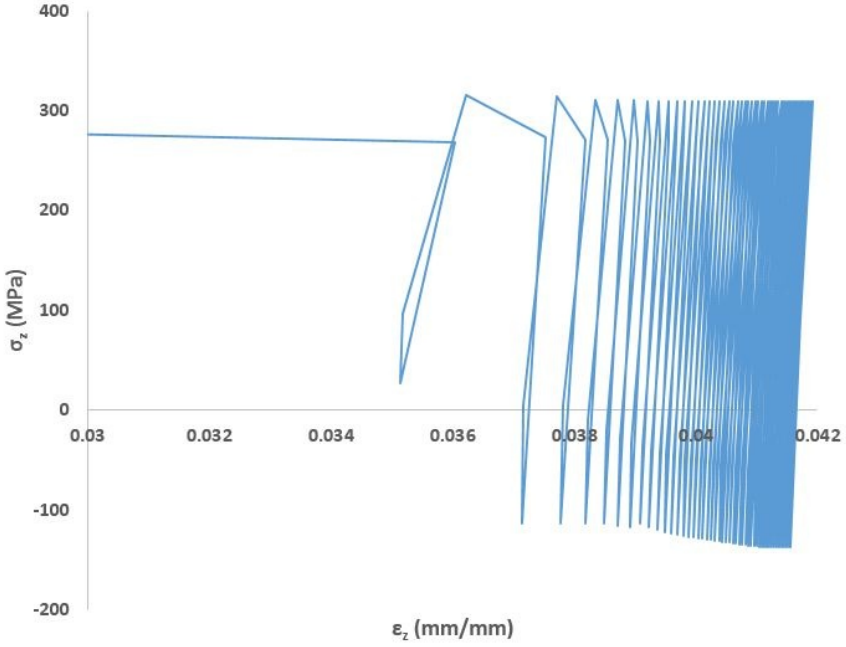

Figure 5.6: A-F model with $\sigma_m = 100MPa$ and $\sigma_a = 210MPa$

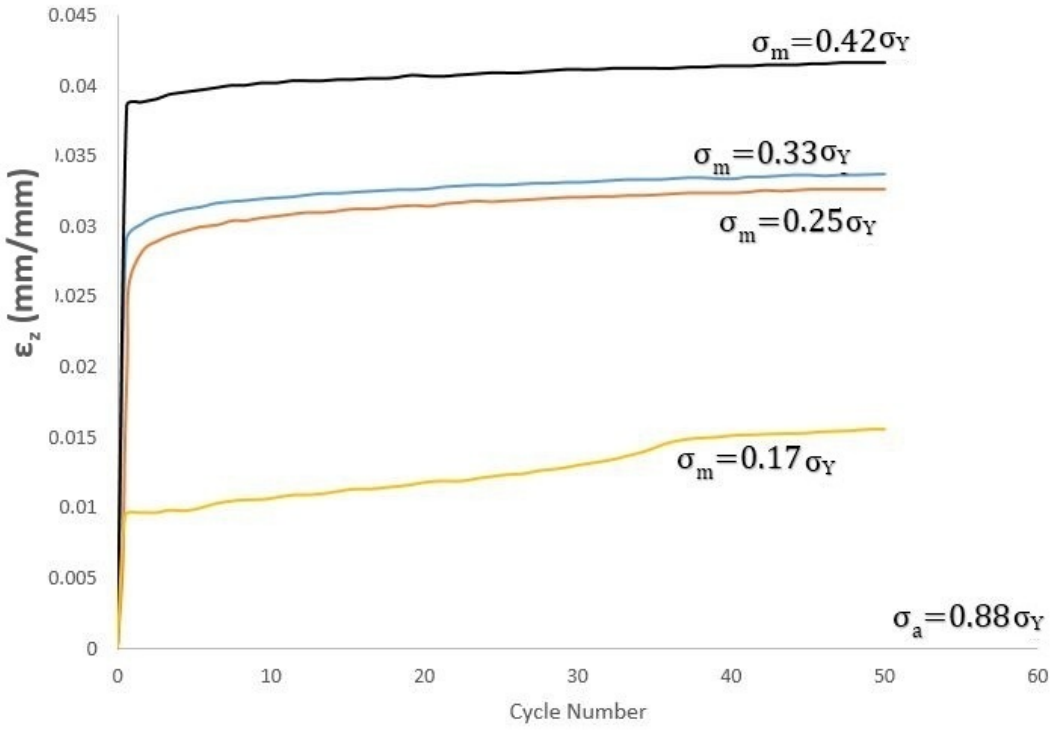

Figure 5.7: Variation of ratcheting strain for different mean stress values for A-F model where σ_Y is the initial yield stress of the material

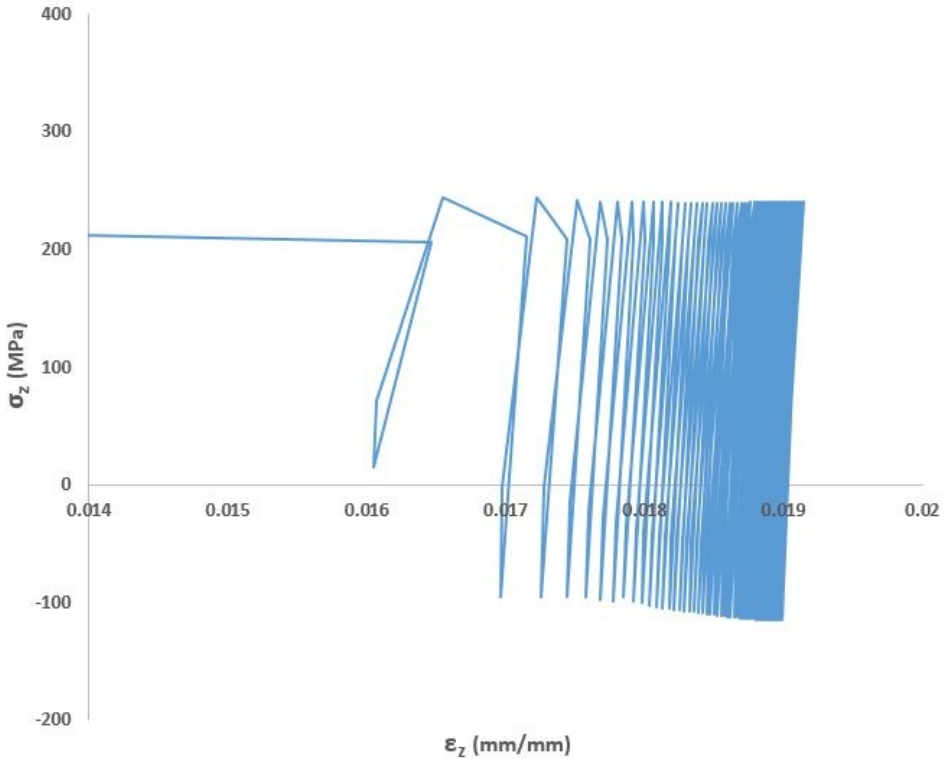

Figure 5.8: A-F model with $\sigma_m = 80MPa$ and $\sigma_a = 150MPa$

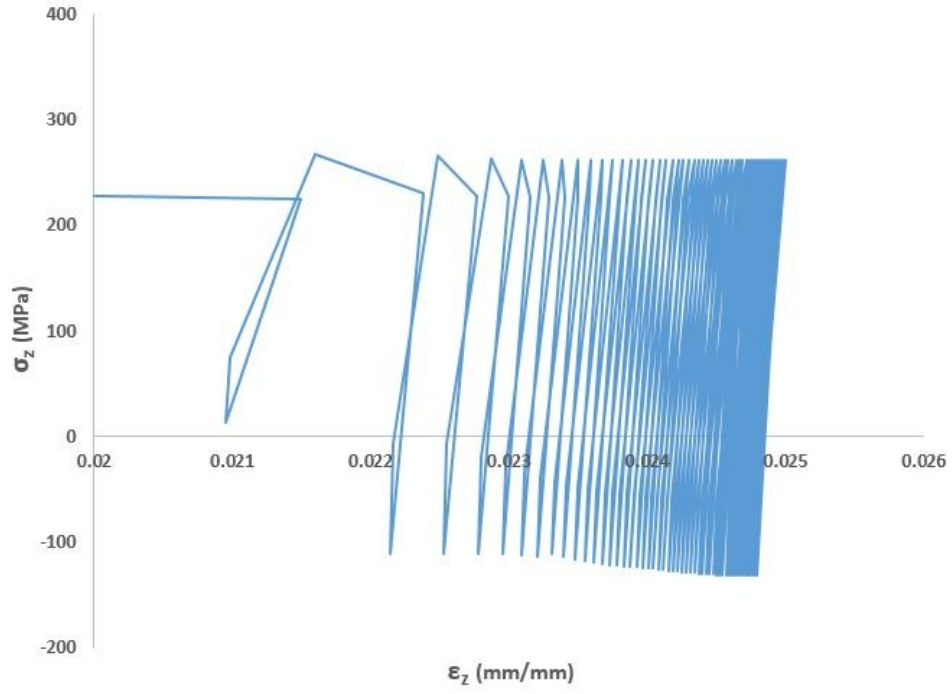

Figure 5.9: A-F model with $\sigma_m = 80MPa$ and $\sigma_a = 180MPa$

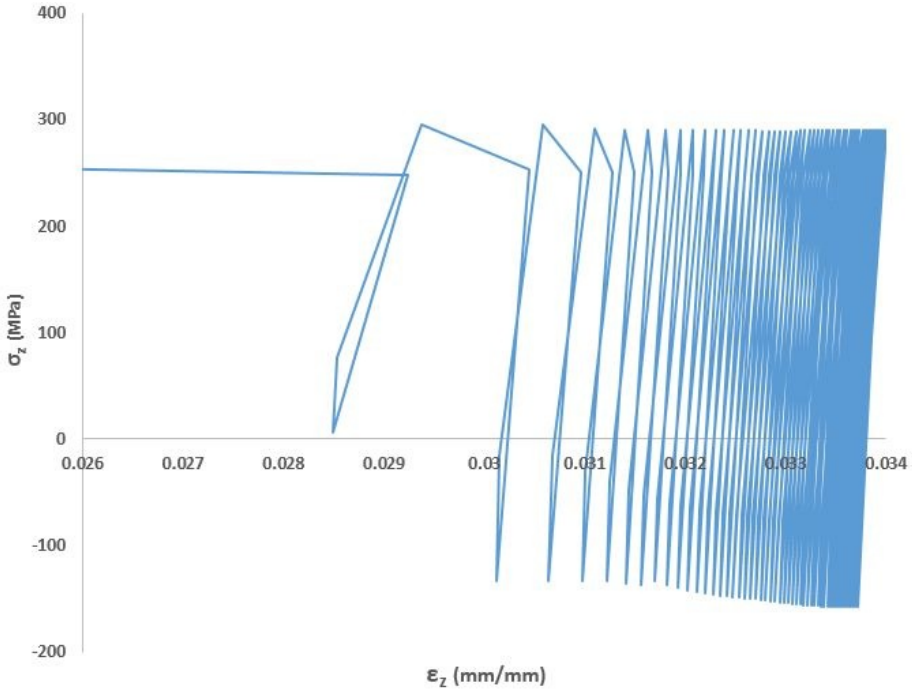

Figure 5.10: A-F model with $\sigma_m = 80MPa$ and $\sigma_a = 210MPa$

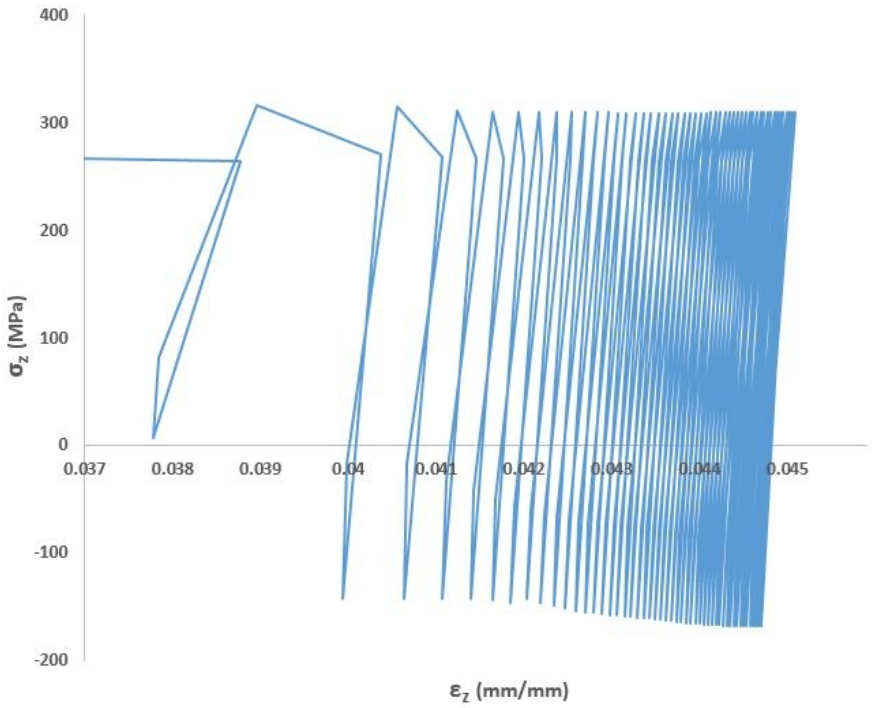

Figure 5.11: A-F model with $\sigma_m = 80MPa$ and $\sigma_a = 240MPa$

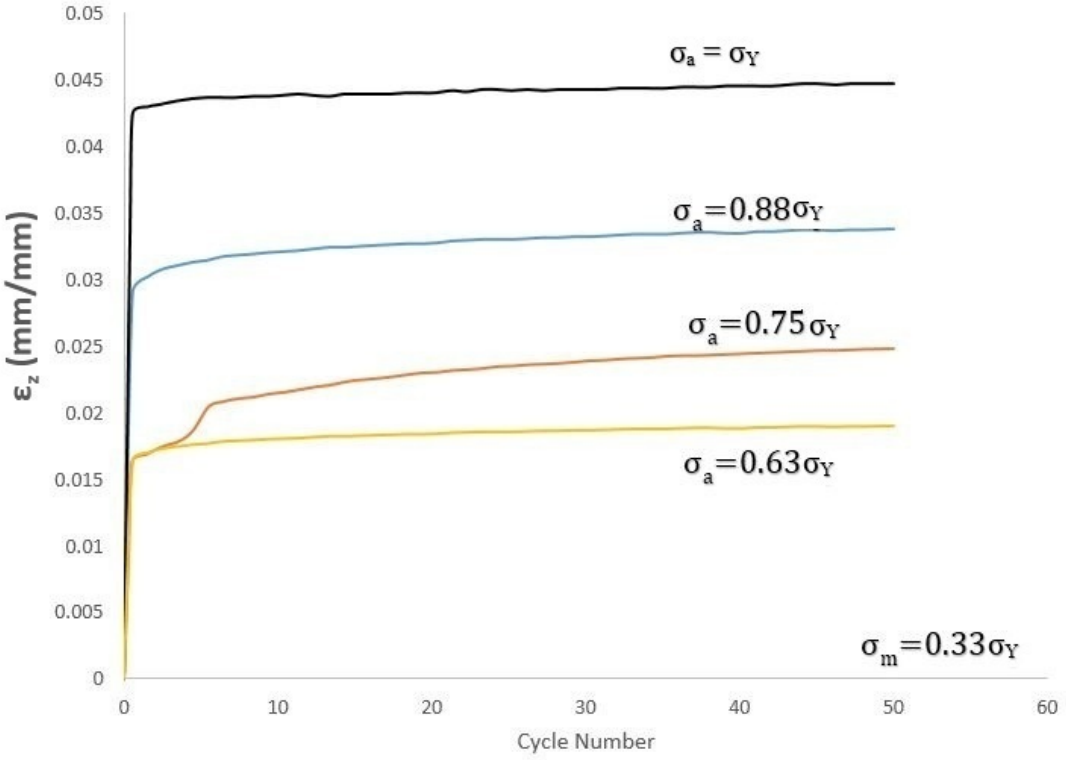

Figure 5.12: Variation of ratcheting strain for different alternating stress values for A-F model where σ_Y is the initial yield stress of the material

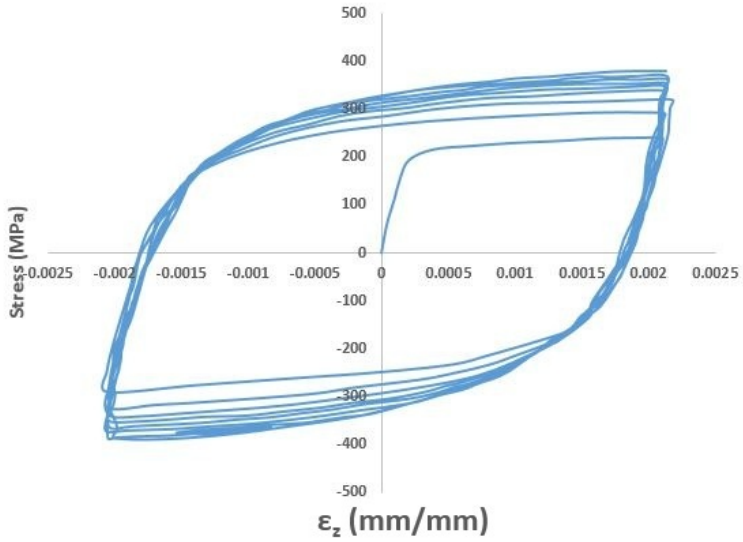

Figure 5.13: Cyclic hardening of A-F model with $\epsilon_a = 0.002$

5.1.3 Burlet-Cailletaud Model

Since this model's results are the same as with A-F model, they are not included separately to avoid repetition.

5.1.4 Chaboche Model

Four different mean stress values; 40 MPa, 60 MPa, 80 MPa and 100 MPa were applied for Chaboche model while the alternating stress was taken as 210 MPa for all mean stresses. Figure 5.14 - Figure 5.17 show the variation of the axial strain of the bar, ϵ_z, for mean stress values 40 MPa, 60 MPa, 80 MPa and 100 MPa, respectively. In Figure 5.18, the variation of maximum ratcheting strain with respect to number of cycles are shown for different mean stresses at constant alternating stress. It is concluded that increase in the mean stress increases the ratcheting strain.

Four different alternating stress values; 150 MPa, 180 MPa, 210 MPa and 240 MPa were applied for Chaboche model while mean stress was kept at 80 MPa for all alternating stresses. Figure 5.19 - Figure 5.22 show the variation of the axial strain of the bar, ϵ_z, for alternating stress values 150 MPa, 180 MPa, 210 MPa and 240 MPa, respectively. In Figure 5.23, the variation of ratcheting strain with respect to number of cycles are shown for different alternating stresses at constant alternating stress. It is concluded that increase in the alternating stress increases the ratcheting strain.

Figure 5.24 shows the stress strain response for symmetric strain cycling with an amplitude of $\epsilon_z = 0.002mm/mm$. In every strain cycle, hardening was observed. Shakedown was seen in this model after several cycles.

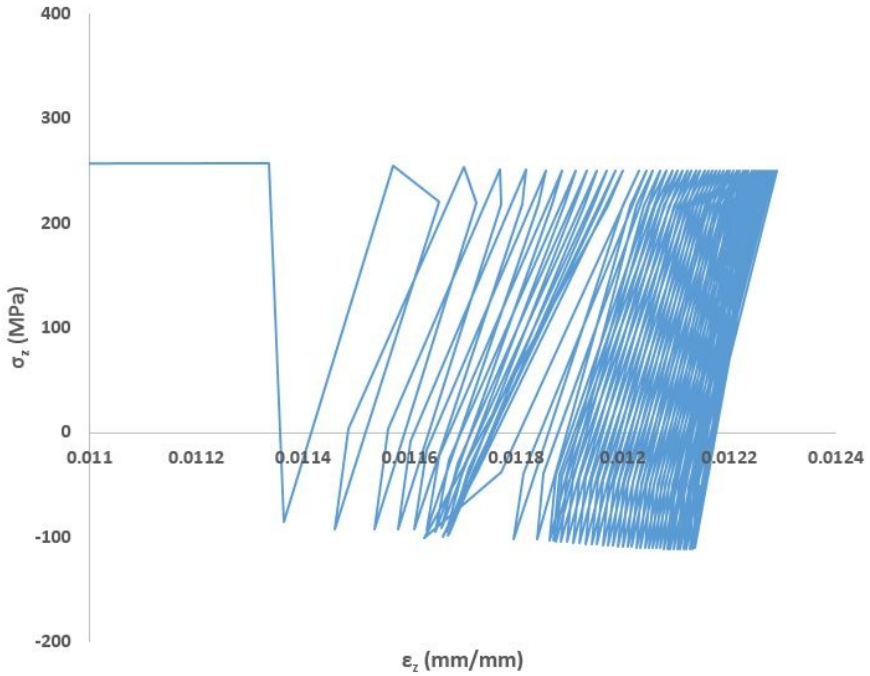

Figure 5.14: Chaboche model with $\sigma_m = 40MPa$ and $\sigma_a = 210MPa$

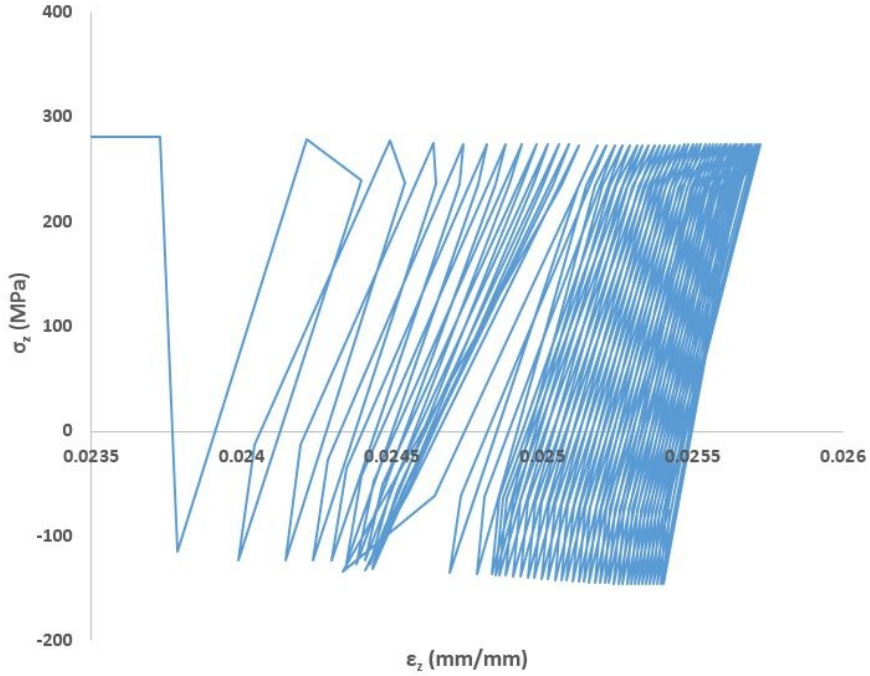

Figure 5.15: Chaboche model with $\sigma_m = 60MPa$ and $\sigma_a = 210MPa$

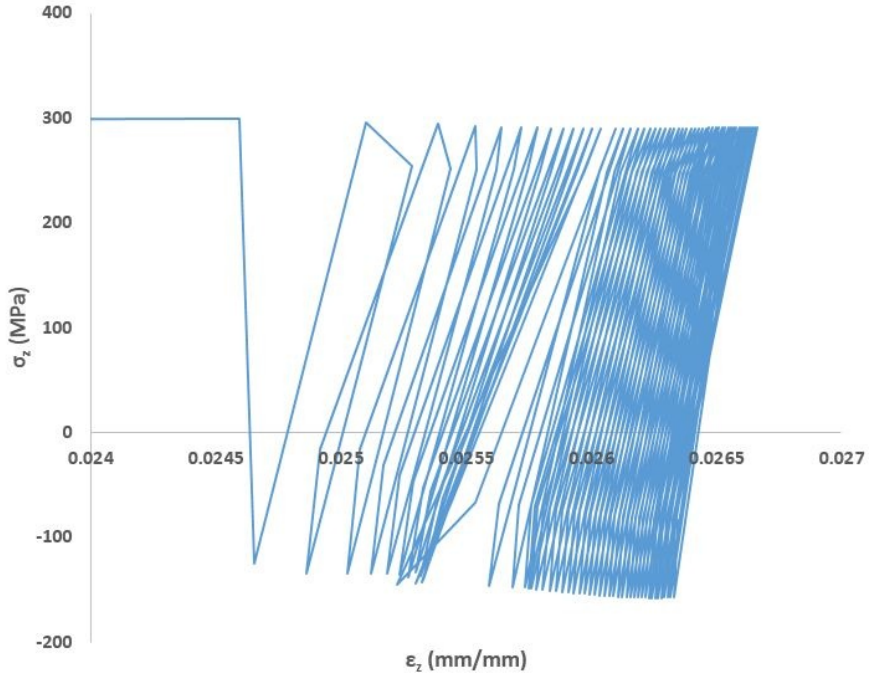

Figure 5.16: Chaboche model with $\sigma_m = 80MPa$ and $\sigma_a = 210MPa$

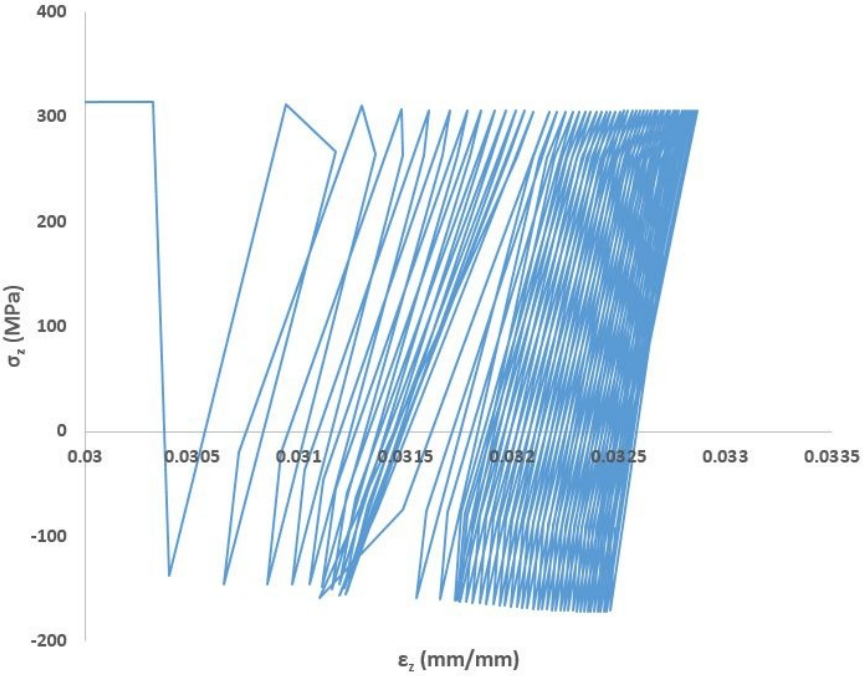

Figure 5.17: Chaboche model with $\sigma_m = 100MPa$ and $\sigma_a = 210MPa$

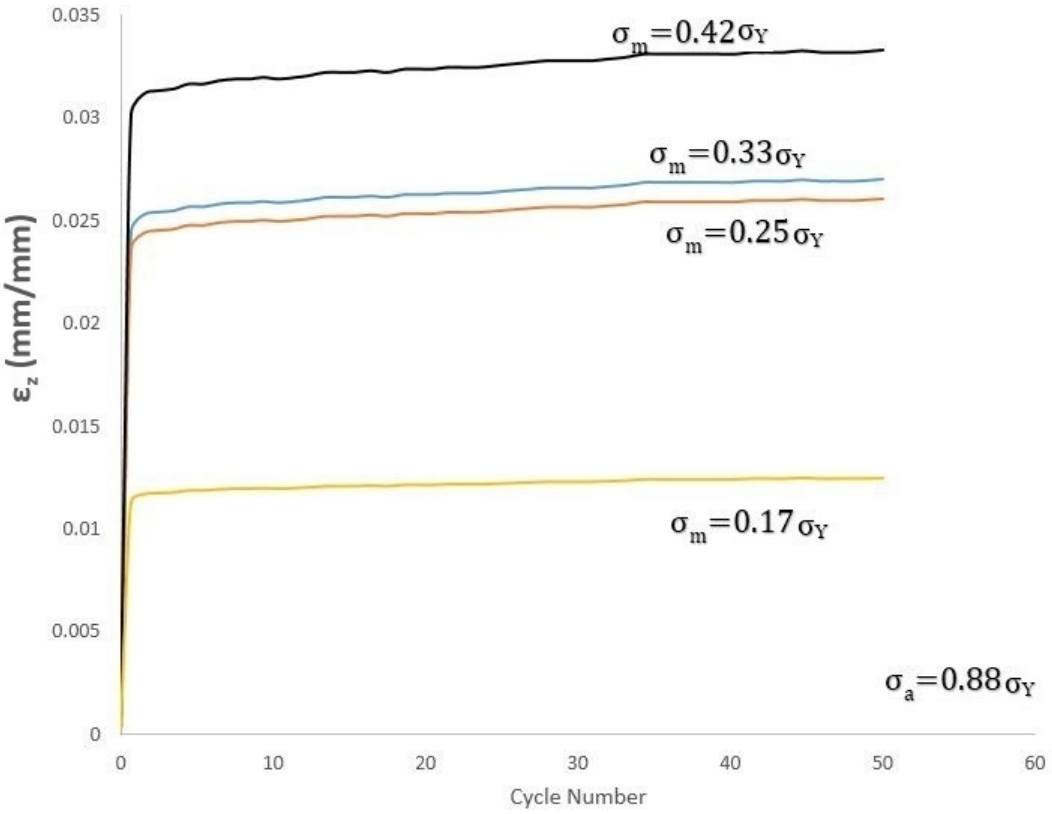

Figure 5.18: Variation of ratcheting strain for different mean stress values for Chaboche model where σ_Y is the initial yield stress of the material

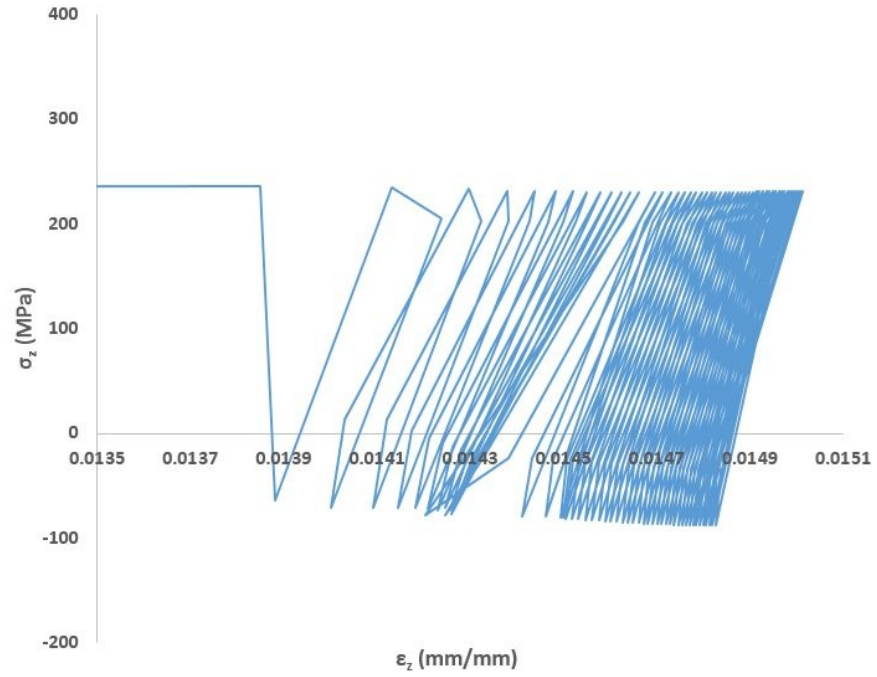

Figure 5.19: Chaboche model with $\sigma_m = 80MPa$ and $\sigma_a = 150MPa$

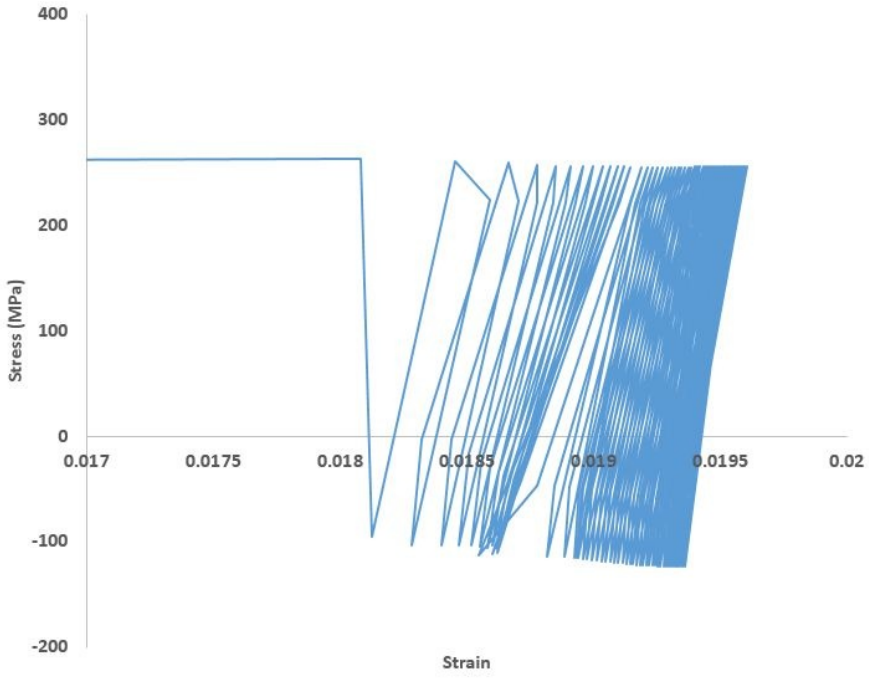

Figure 5.20: Chaboche model with $\sigma_m = 80MPa$ and $\sigma_a = 150MPa$

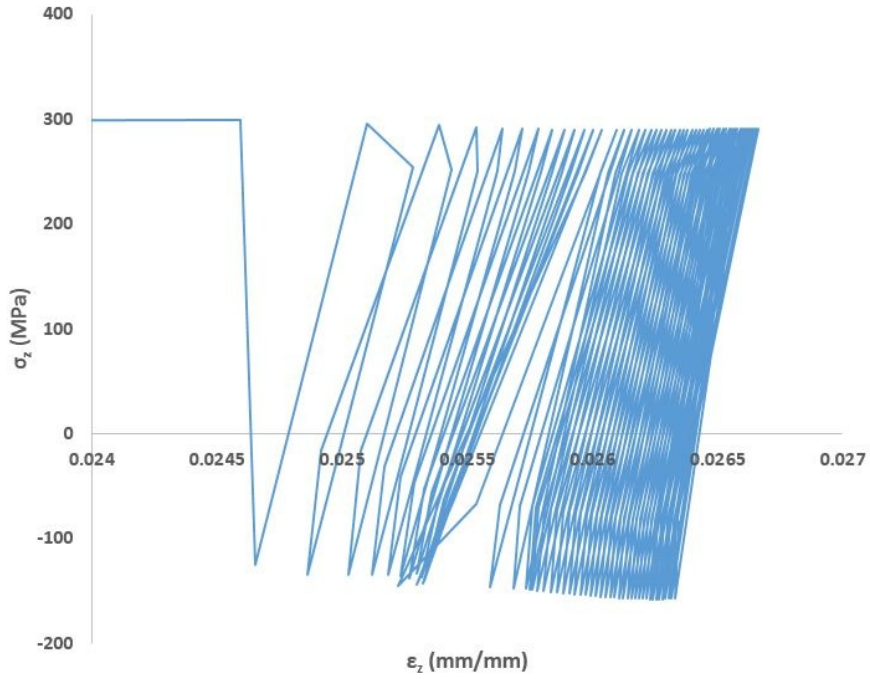

Figure 5.21: Chaboche model with $\sigma_m = 80MPa$ and $\sigma_a = 210MPa$

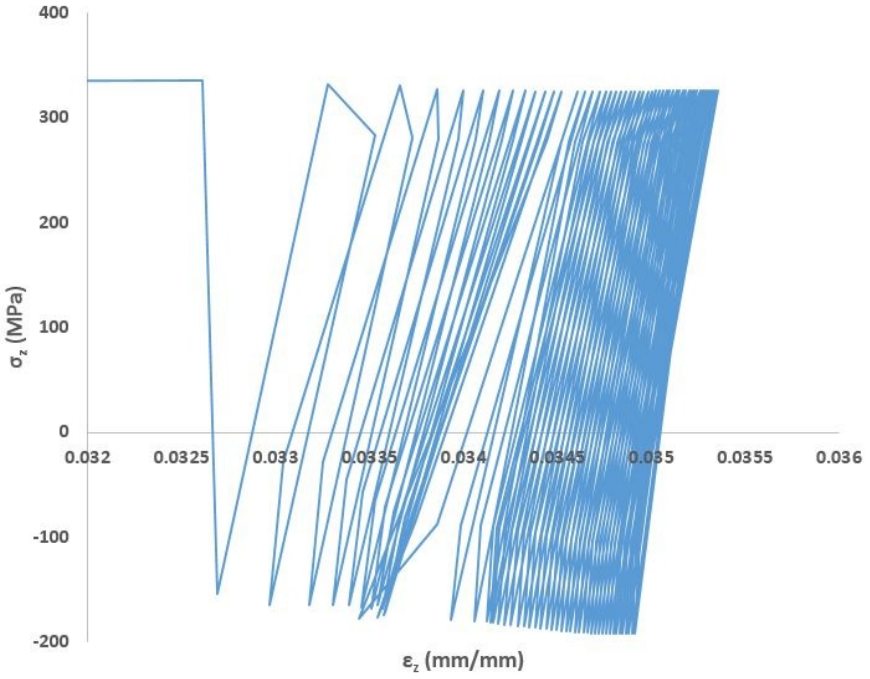

Figure 5.22: Chaboche model with $\sigma_m = 80MPa$ and $\sigma_a = 240MPa$

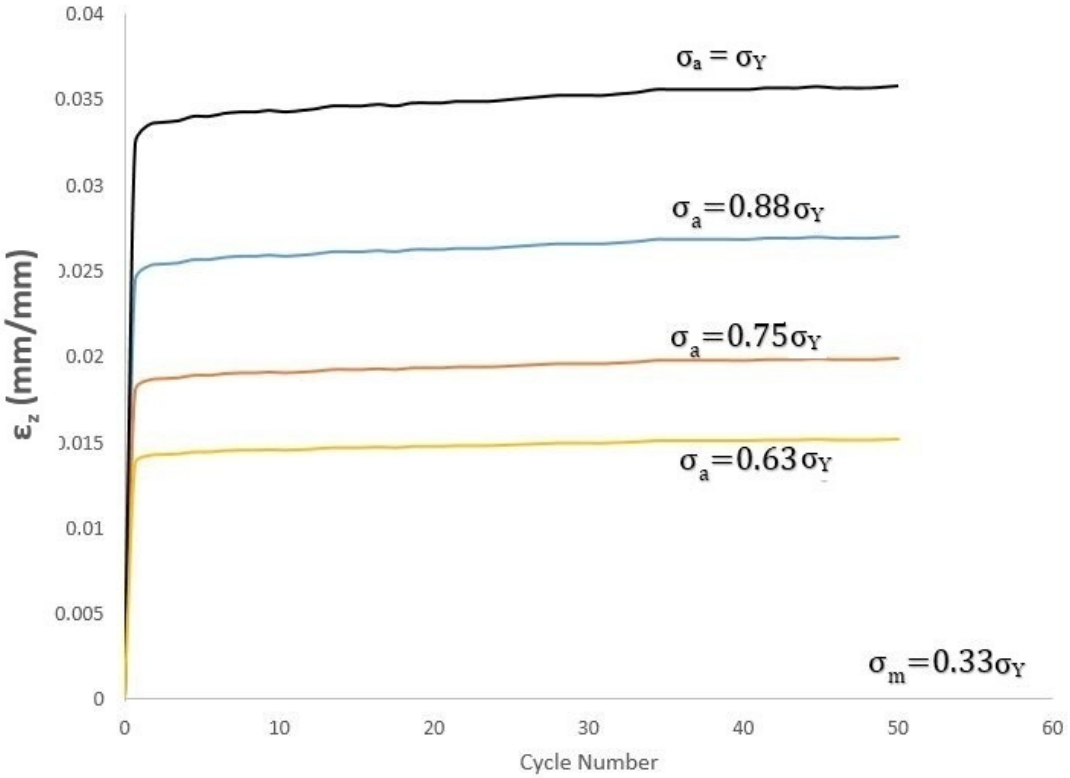

Figure 5.23: Variation of ratcheting strain for different alternating stress values for Chaboche model where σ_Y is the initial yield stress of the material

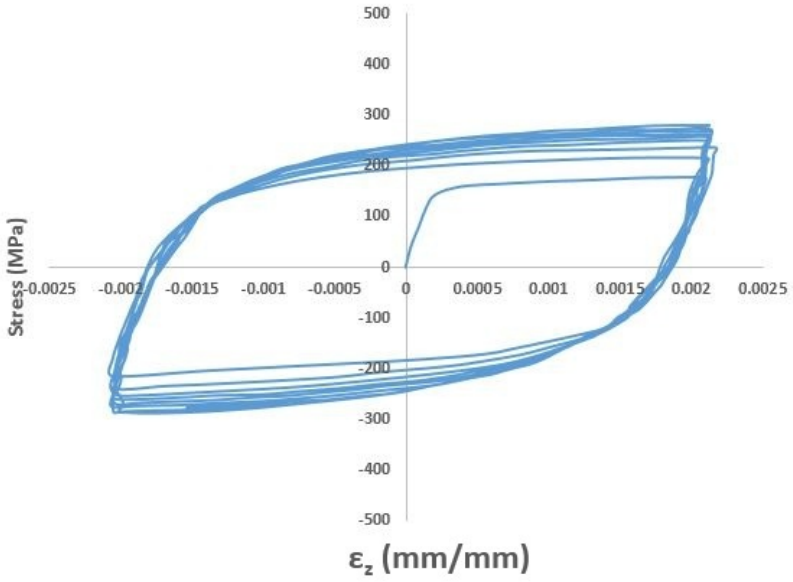

Figure 5.24: Cyclic hardening of Chaboche model with $\epsilon_a = 0.002$

5.1.5 Bari-Hassan Model

Four different mean stress values; 40 MPa, 60 MPa, 80 MPa and 100 MPa were applied for B-H model while the alternating stress was taken as 210 MPa for all mean stresses. Figure 5.25 - Figure 5.28 show the variation of the axial strain of the bar, ϵ_z, for mean stress values 40 MPa, 60 MPa, 80 MPa and 100 MPa, respectively. In Figure 5.29, the variation of maximum ratcheting strain with respect to number of cycles are shown for different mean stresses at constant alternating stress. It is observed that accumulated strain increases with increasing mean stress.

Four different alternating stress values; 150 MPa, 180 MPa, 210 MPa and 240 MPa were applied for B-H model while mean stress was kept at 80 MPa for all alternating stresses. Figure 5.30 - Figure 5.33 show the variation of the axial strain of the bar, ϵ_z, for alternating stress values 150 MPa, 180 MPa, 210 MPa and 240 MPa, respectively. In Figure 5.34, the variation of ratcheting strain with respect to number of cycles are shown for different alternating stresses at constant mean stress. The conclusion is increasing alternating stress increases the amount of ratcheting strain.

Figure 5.35 shows the stress strain response for symmetric strain cycling with an amplitude of $\epsilon_z = 0.002mm/mm$. After several cycles of hardening, the material has shaken down and strain hardening has stopped.

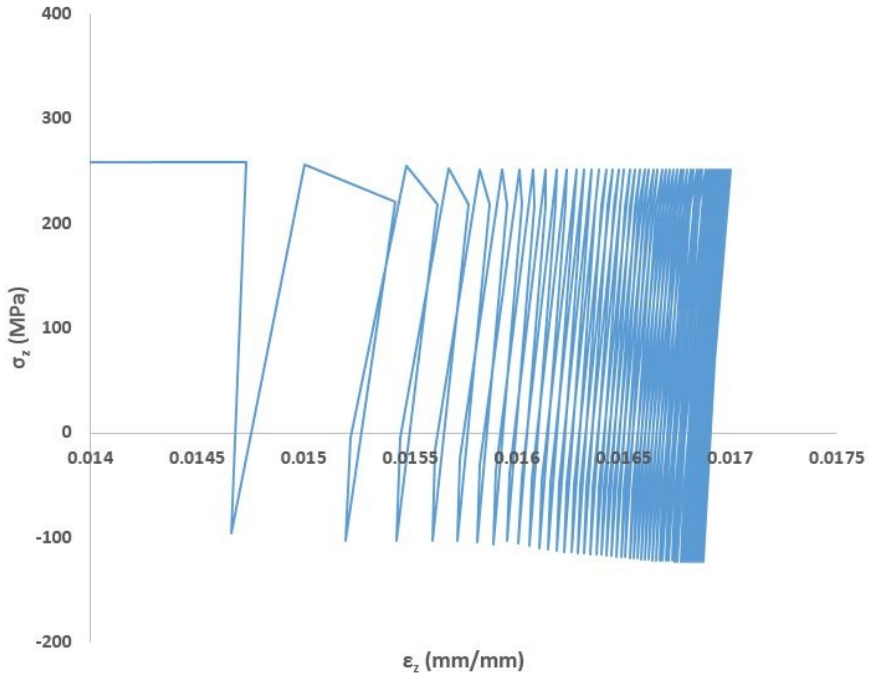

Figure 5.25: B-H model with $\sigma_m = 40MPa$ and $\sigma_a = 210MPa$

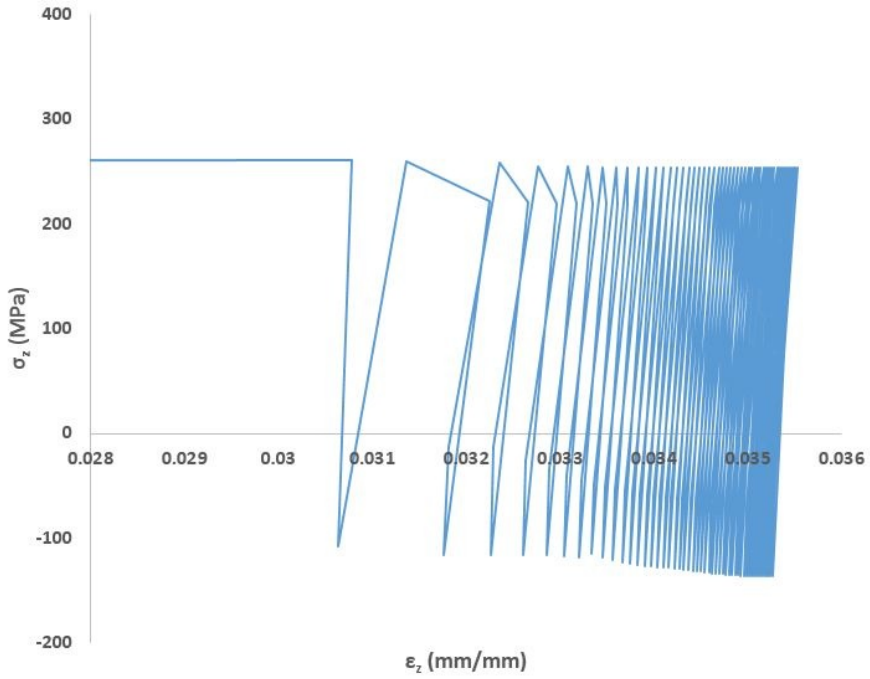

Figure 5.26: B-H model with $\sigma_m = 60MPa$ and $\sigma_a = 210MPa$

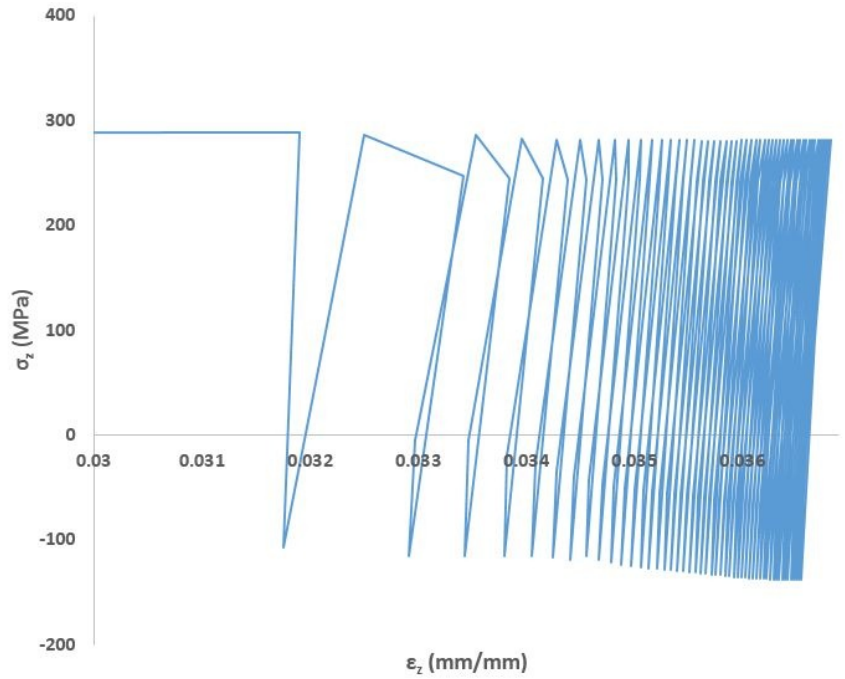

Figure 5.27: B-H model with $\sigma_m = 80MPa$ and $\sigma_a = 210MPa$

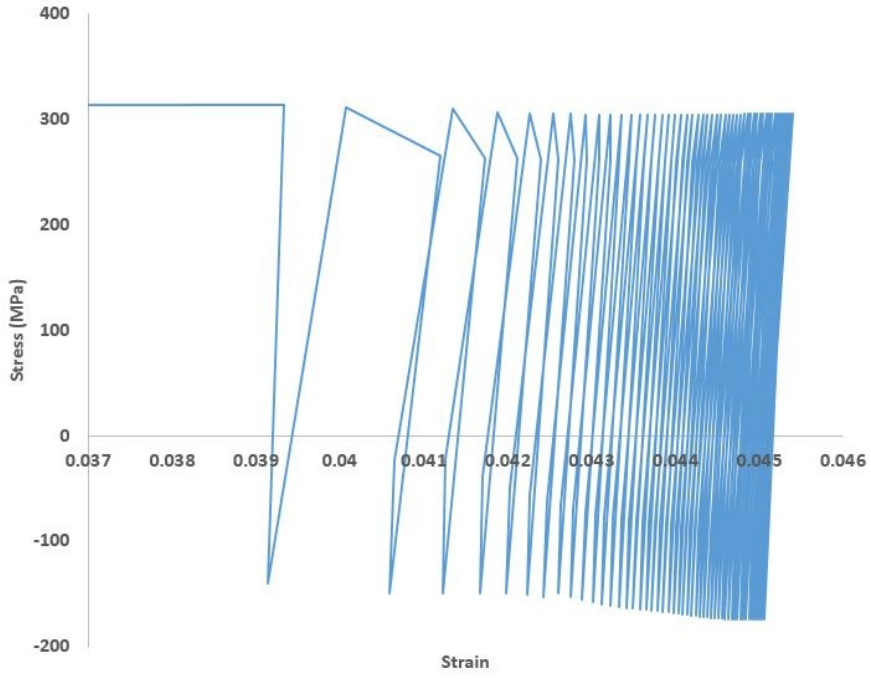

Figure 5.28: B-H model with $\sigma_m = 10MPa$ and $\sigma_a = 210MPa$

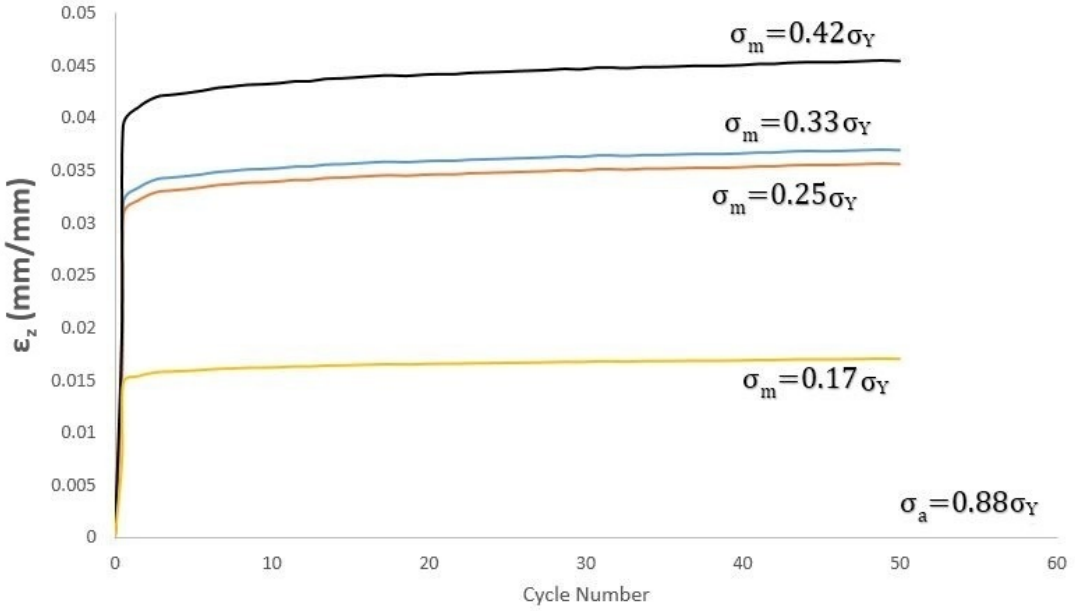

Figure 5.29: Variation of ratcheting strain for different mean stress values for B-H model where σ_Y is the initial yield stress of the material

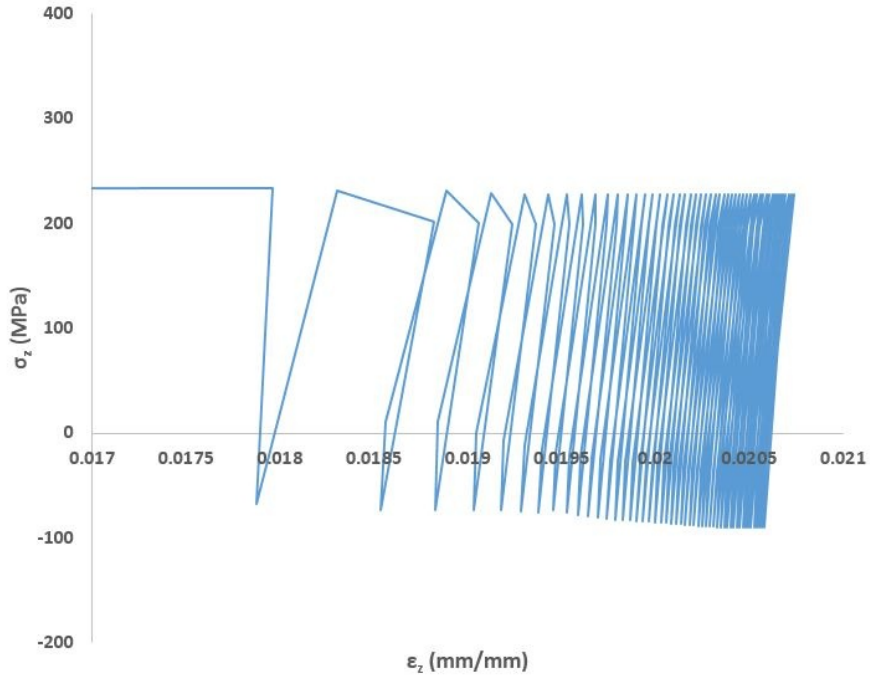

Figure 5.30: B-H model with $\sigma_m = 80MPa$ and $\sigma_a = 150MPa$

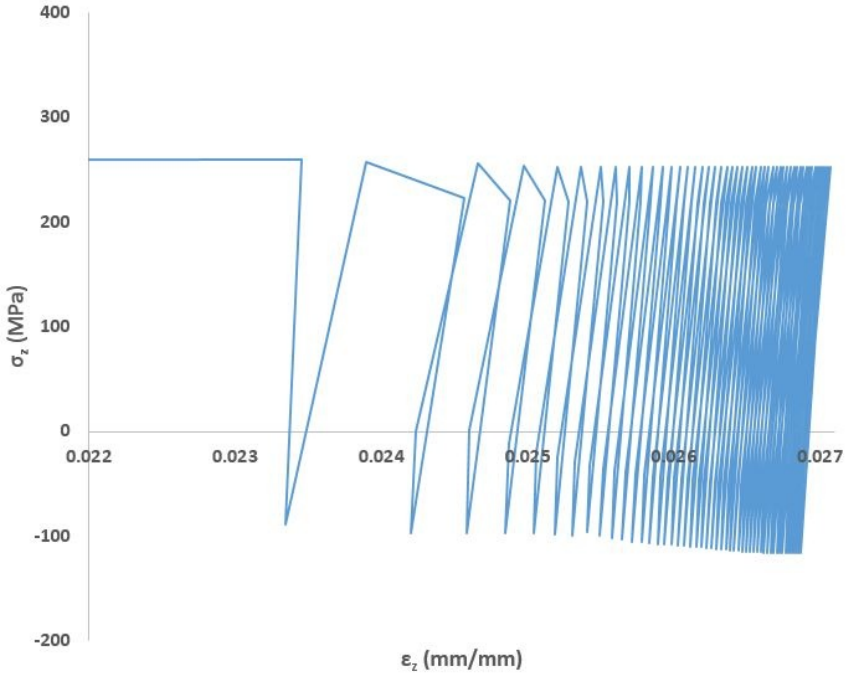

Figure 5.31: B-H model with $\sigma_m = 80MPa$ and $\sigma_a = 180MPa$

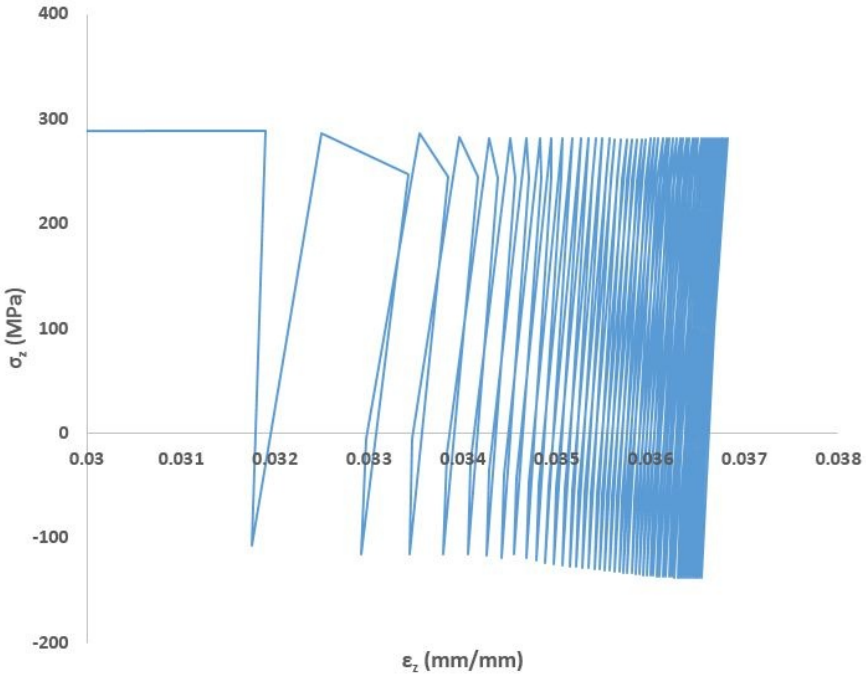

Figure 5.32: B-H model with $\sigma_m = 80MPa$ and $\sigma_a = 210MPa$

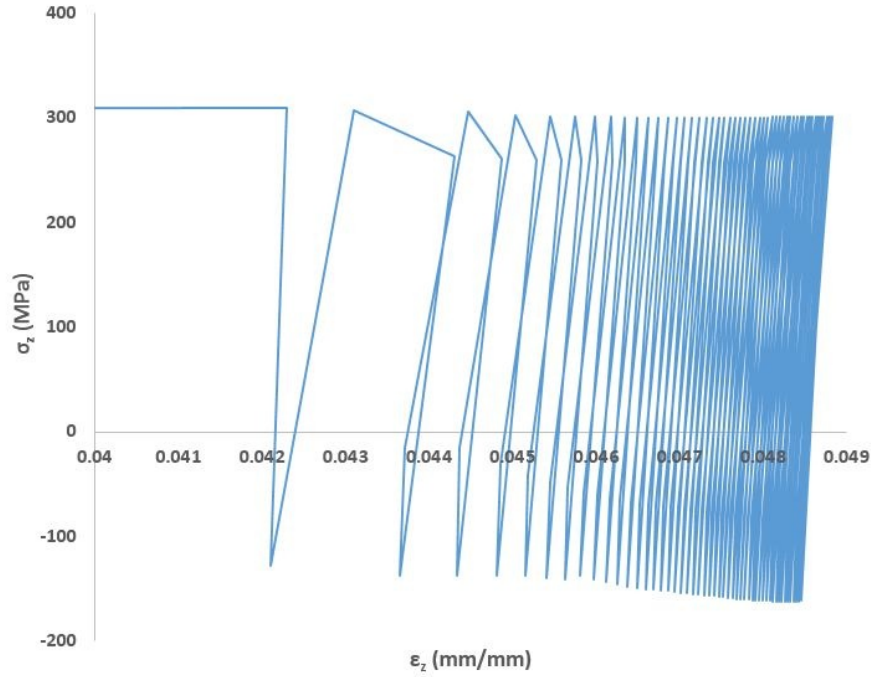

Figure 5.33: B-H model with $\sigma_m = 80MPa$ and $\sigma_a = 240MPa$

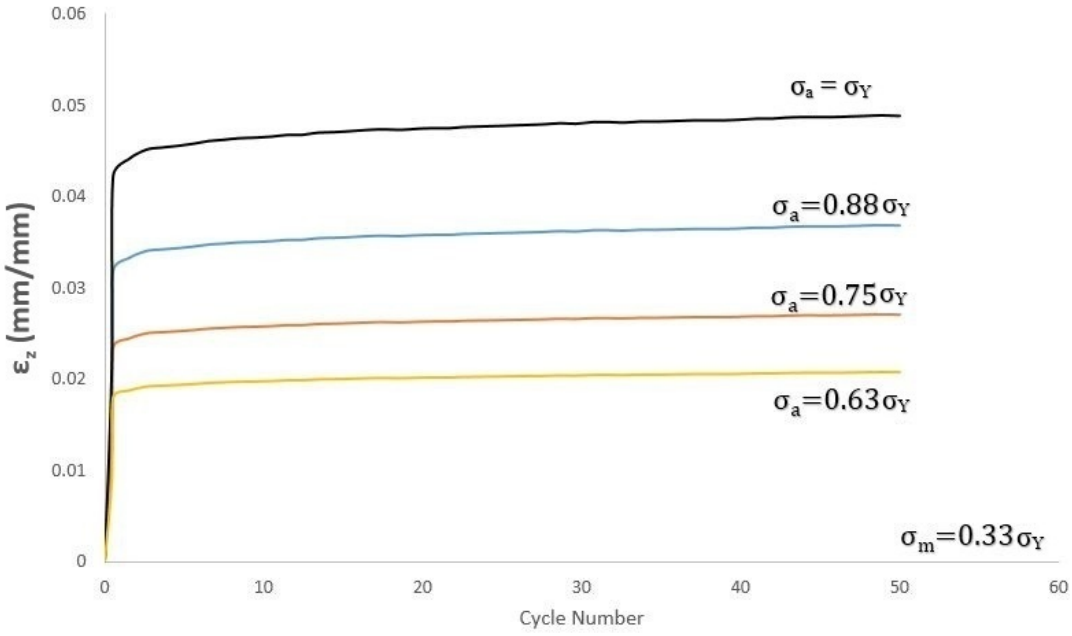

Figure 5.34: Variation of ratcheting strain for different alternating stress values for B-H model where σ_Y is the initial yield stress of the material

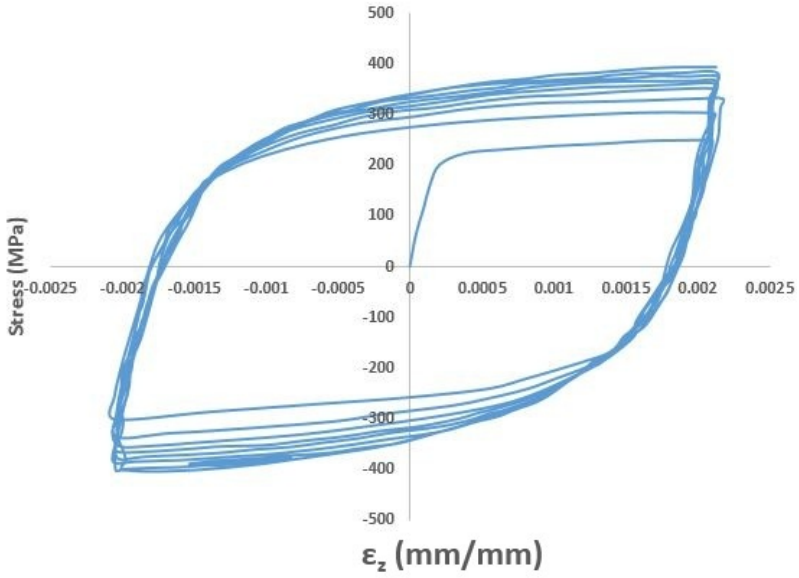

Figure 5.35: Cyclic hardening of B-H model with $\epsilon_a = 0.002$

5.1.6 Ohno-Wang Model

Four different mean stress values; 40 MPa, 60 MPa, 80 MPa and 100 MPa were applied for O-W model while the alternating stress was taken as 210 MPa for all mean stresses. Figure 5.36 - Figure 5.39 show the variation of the axial strain of the bar, ϵ_z, for mean stress values 40 MPa, 60 MPa, 80 MPa and 100 MPa, respectively. In Figure 5.40, the variation of maximum ratcheting strain with respect to number of cycles are shown for different mean stresses at constant alternating stress. It is observed that accumulated strain increases with increasing mean stress.

Four different alternating stress values; 150 MPa, 180 MPa, 210 MPa and 240 MPa were applied for O-W model while mean stress was kept at 80 MPa for all alternating stresses. Figure 5.41 - Figure 5.44 show the variation of the axial strain of the bar, ϵ_z, for alternating stress values 150 MPa, 180 MPa, 210 MPa and 240 MPa, respectively. In Figure 5.45, he variation of ratcheting strain with respect to number of cycles are shown for different alternating stresses at constant mean stress. The conclusion is increasing alternating stress increases the amount of ratcheting strain.

Figure 5.46 shows the stress strain response for symmetric strain cycling with an

amplitude of $\epsilon_z = 0.002mm/mm$. After several cycles of hardening, the material has shaken down and strain hardening has stopped.

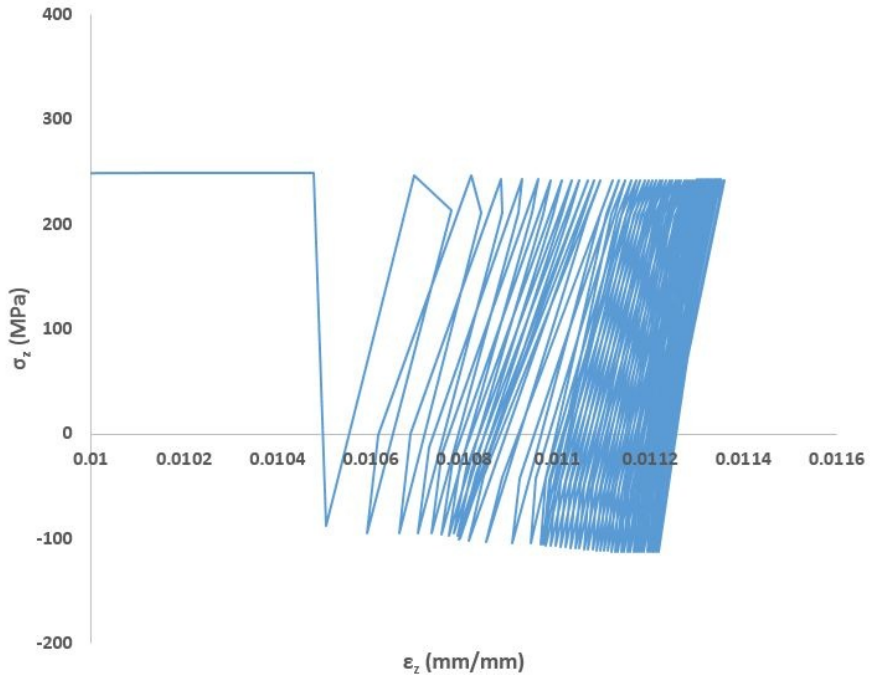

Figure 5.36: O-W model with $\sigma_m = 40MPa$ and $\sigma_a = 210MPa$

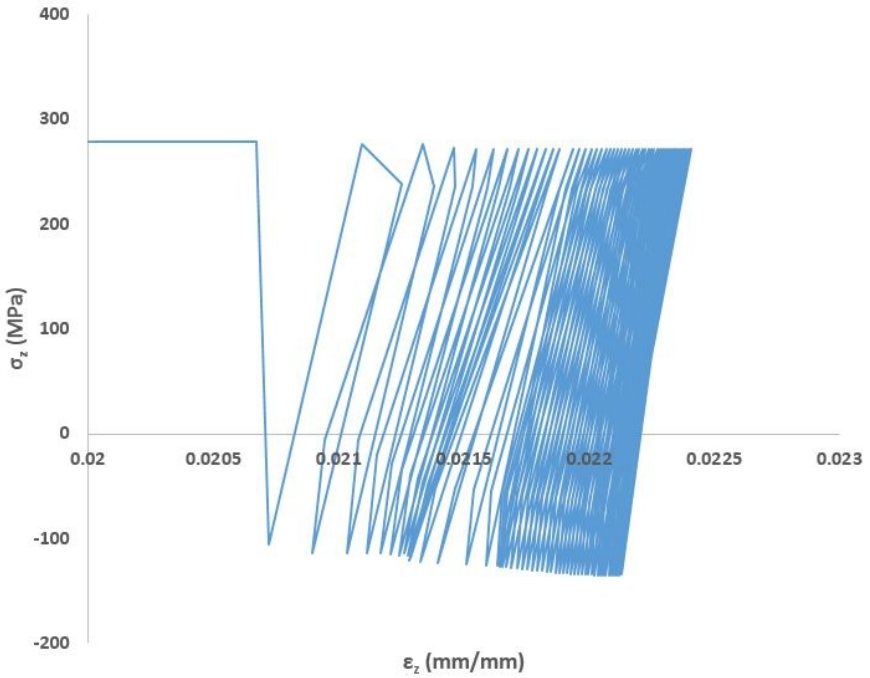

Figure 5.37: O-W model with $\sigma_m = 60MPa$ and $\sigma_a = 210MPa$

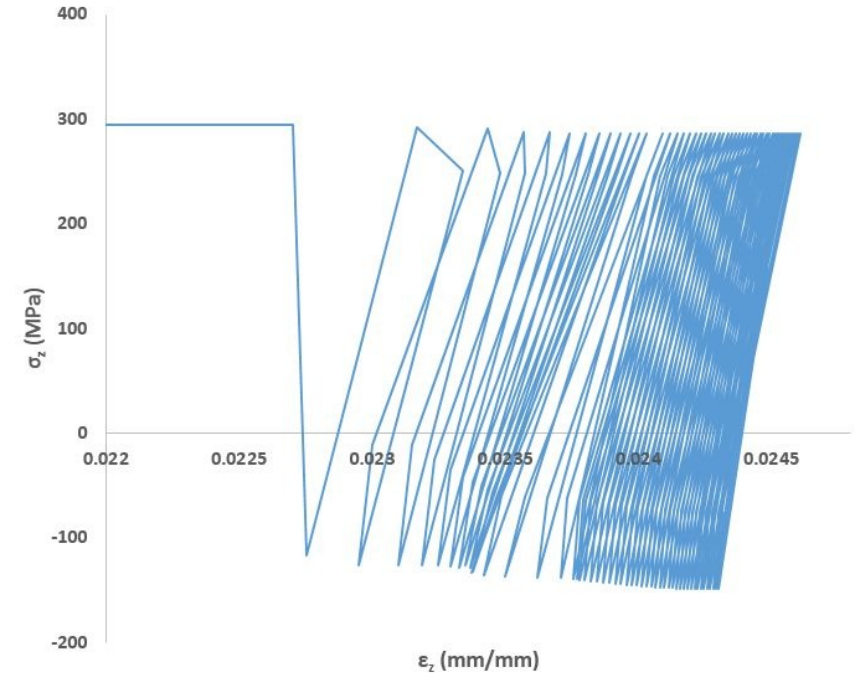

Figure 5.38: O-W model with $\sigma_m = 80MPa$ and $\sigma_a = 210MPa$

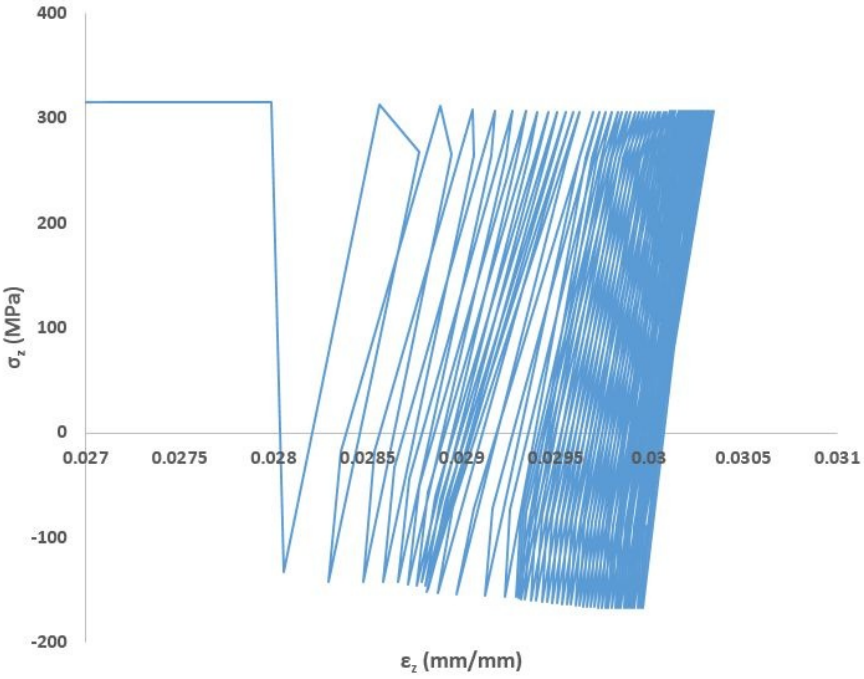

Figure 5.39: O-W model with $\sigma_m = 100MPa$ and $\sigma_a = 210MPa$

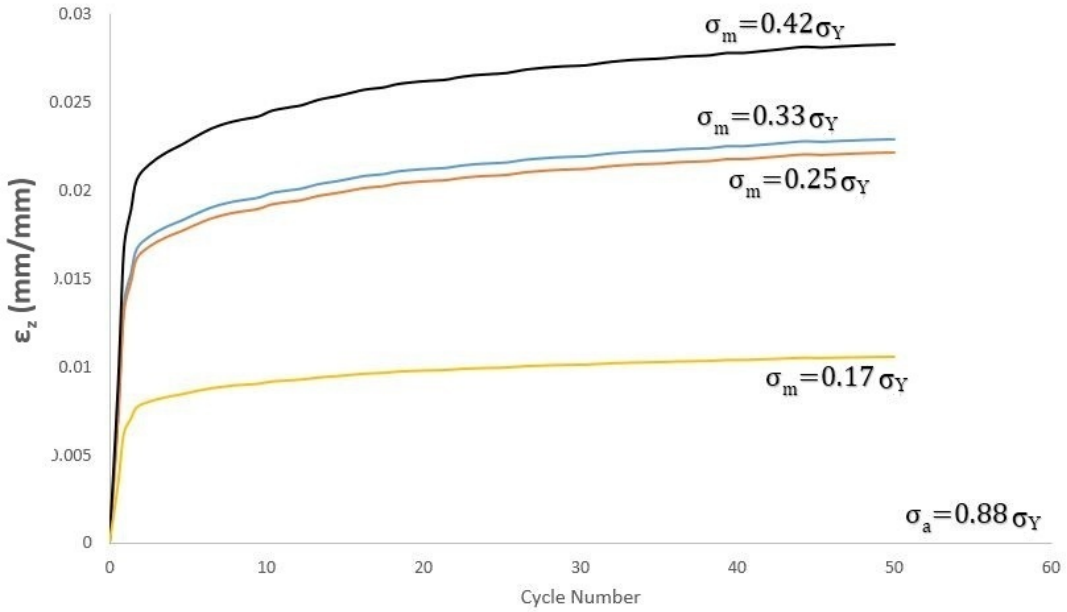

Figure 5.40: Variation of ratcheting strain for different mean stress values for O-W model where σ_Y is the initial yield stress of the material

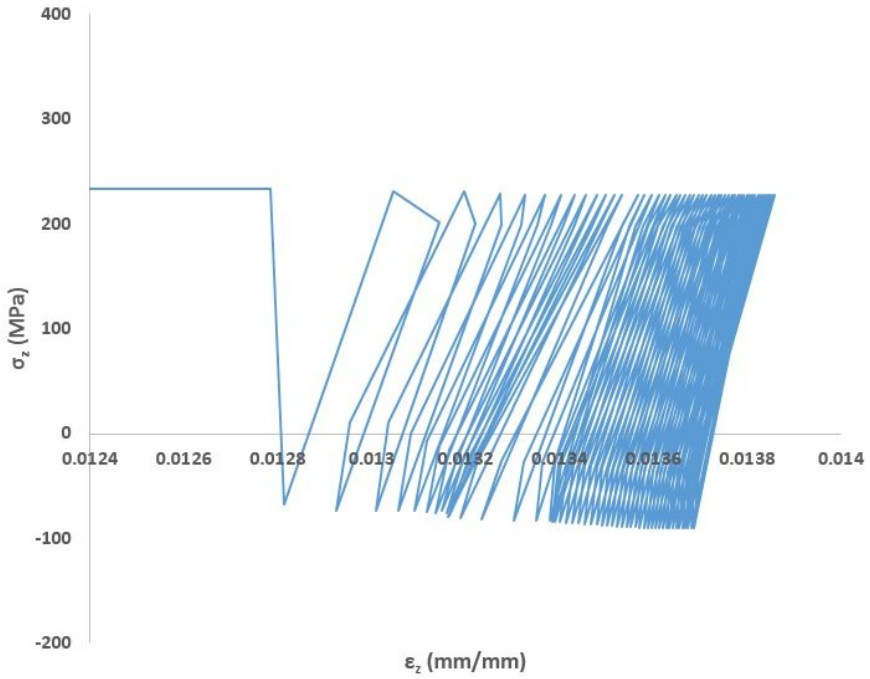

Figure 5.41: O-W model with $\sigma_m = 80MPa$ and $\sigma_a = 150MPa$

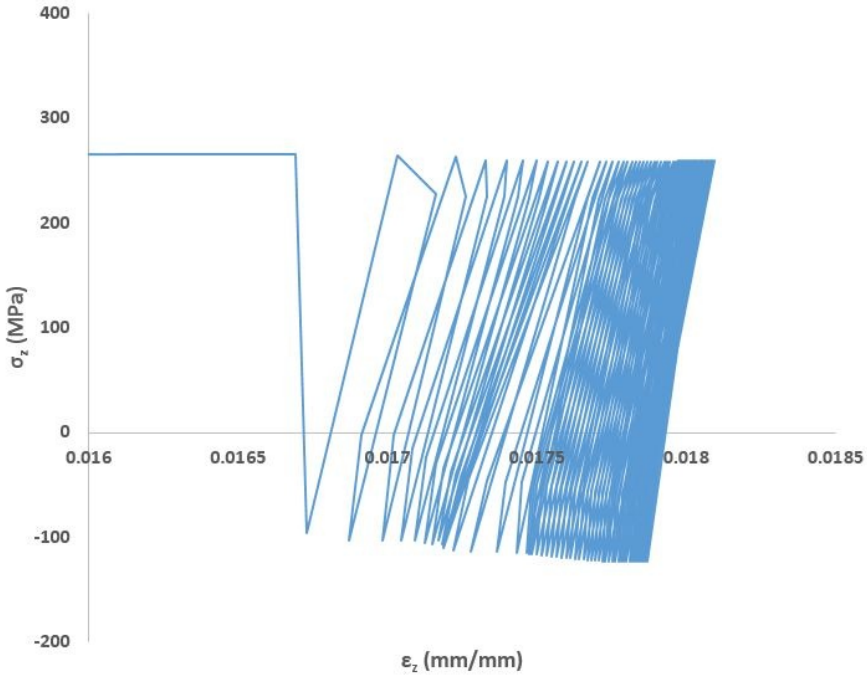

Figure 5.42: O-W model with $\sigma_m = 80MPa$ and $\sigma_a = 180MPa$

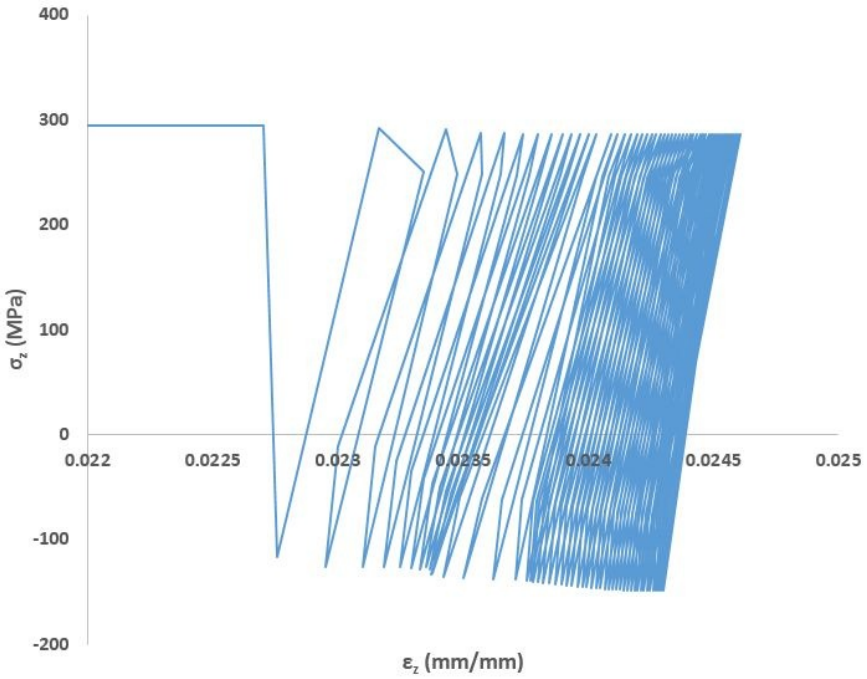

Figure 5.43: O-W model with $\sigma_m = 80MPa$ and $\sigma_a = 210MPa$

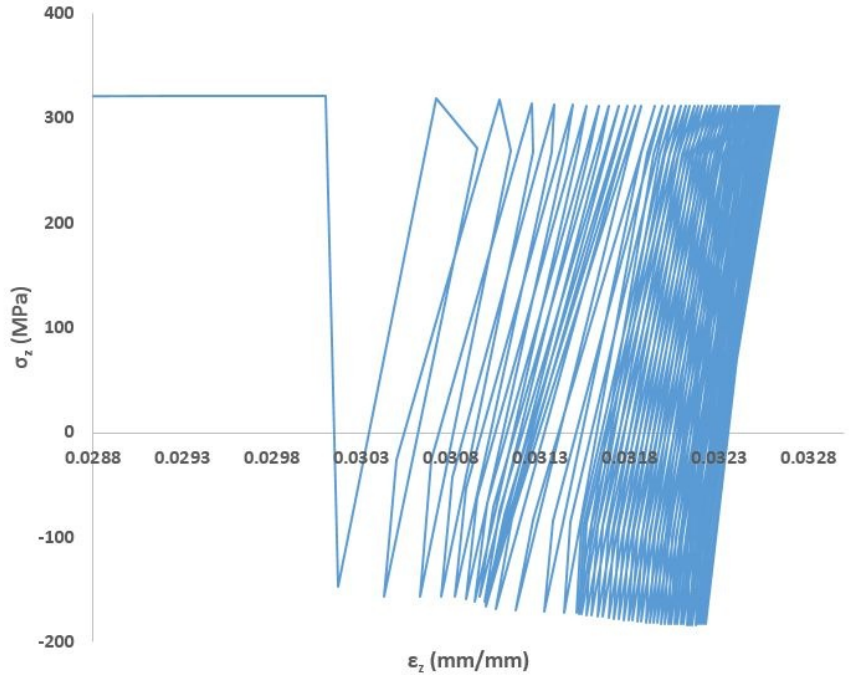

Figure 5.44: O-W model with $\sigma_m = 80MPa$ and $\sigma_a = 240MPa$

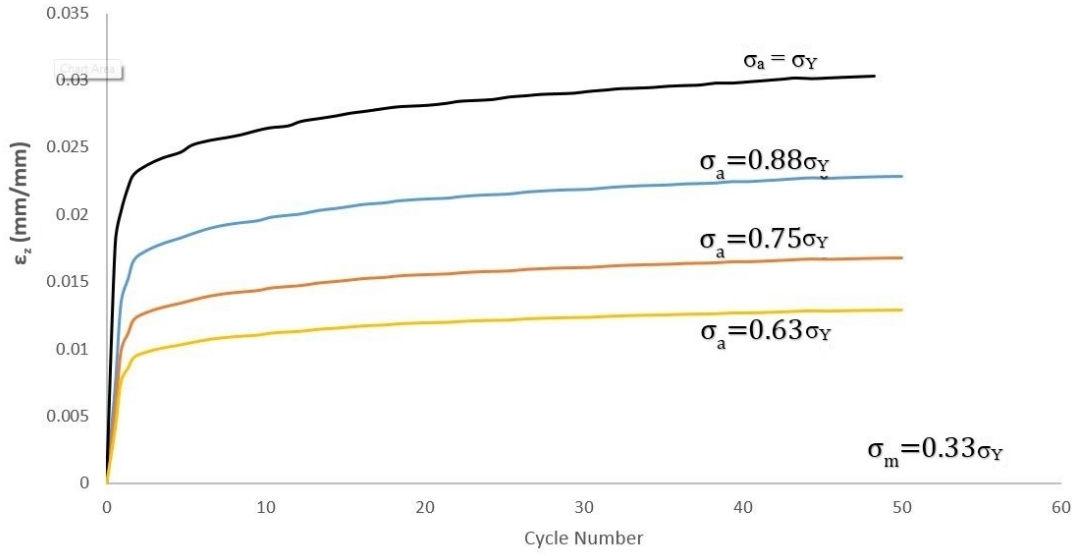

Figure 5.45: Variation of ratcheting strain for different alternating stress values for O-W model where σ_Y is the initial yield stress of the material

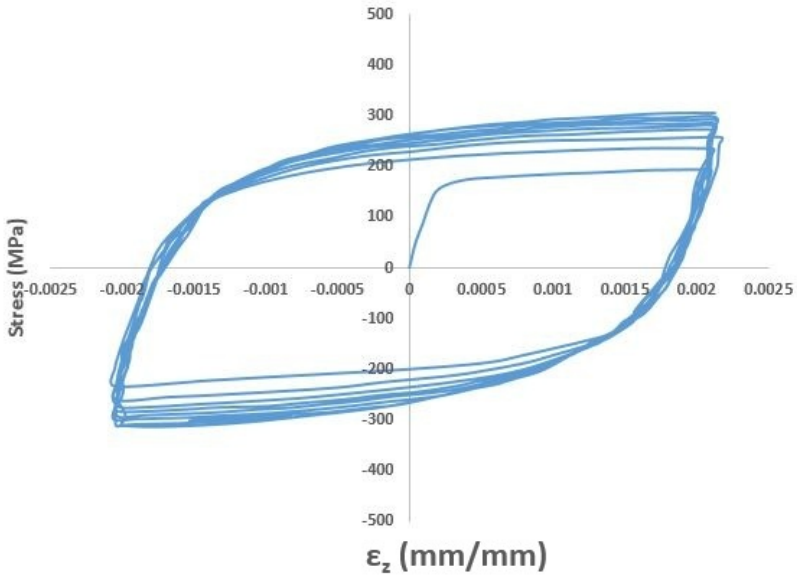

Figure 5.46: Cyclic hardening of O-W model with $\epsilon_a = 0.002mm/mm$

5.1.7 Comparison of the Results of Uniaxial Ratcheting for Different Kinematic Hardening Models

Comparison of the maximum strain accumulations is given in Figure 5.47 - Figure 5.50 for different mean stress values of $\sigma_m = 40MPa$, $\sigma_m = 60MPa$, $\sigma_m = 80MPa$, $\sigma_m = 100MPa$ respectively at constant alternating stress $\sigma_a = 210MPa$ and for different alternating stress values $\sigma_a = 150MPa$, $\sigma_a = 180MPa$, $\sigma_a = 210MPa$, $\sigma_a = 240MPa$ in Figure 5.51 - Figure 5.54 respectively at constant mean stress $\sigma_m = 80MPa$.

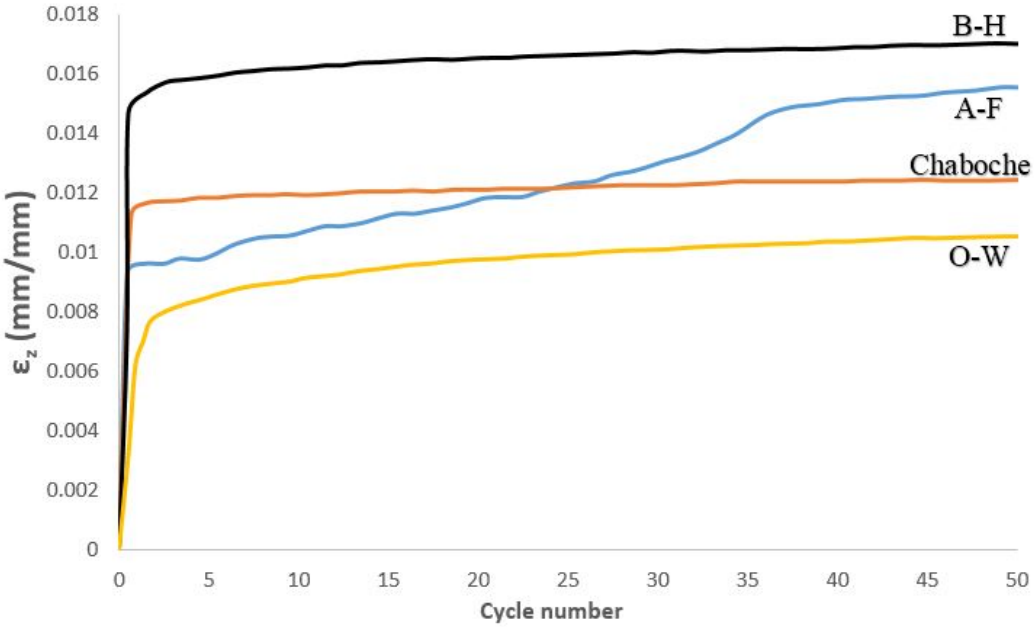

Figure 5.47: Comparison of models with $\sigma_m = 40MPa$ and $\sigma_a = 210MPa$

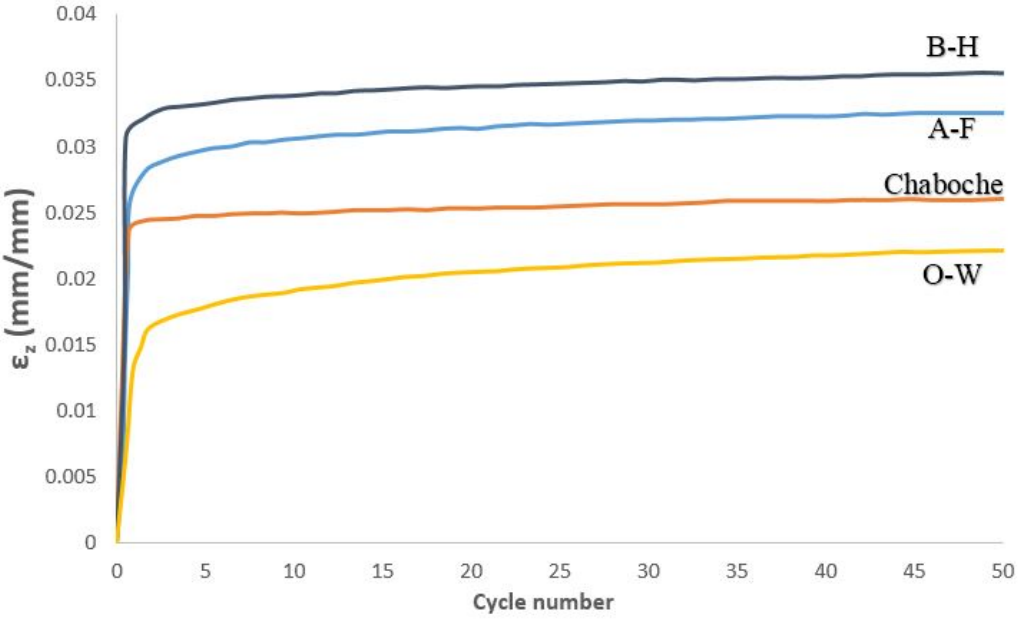

Figure 5.48: Comparison of models with $\sigma_m = 60MPa$ and $\sigma_a = 210MPa$

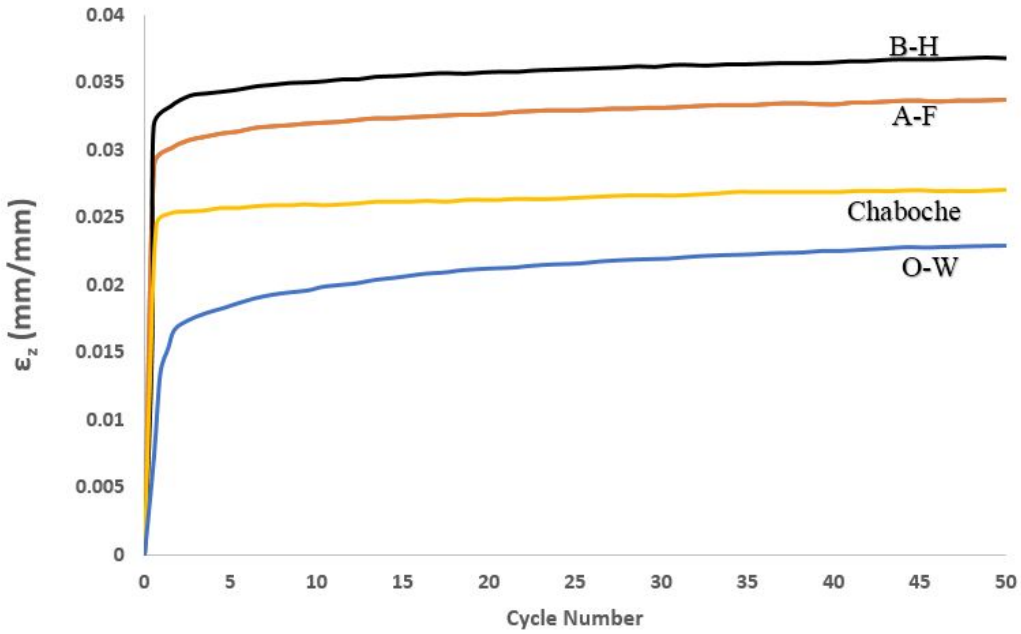

Figure 5.49: Comparison of models with $\sigma_m = 80MPa$ and $\sigma_a = 210MPa$

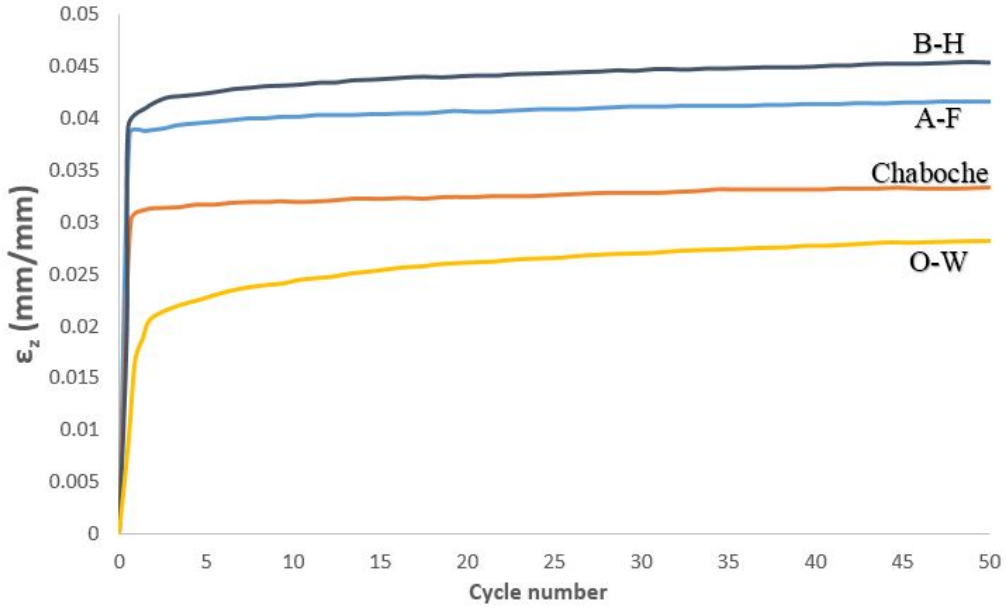

Figure 5.50: Comparison of models with $\sigma_m = 100MPa$ and $\sigma_a = 210MPa$

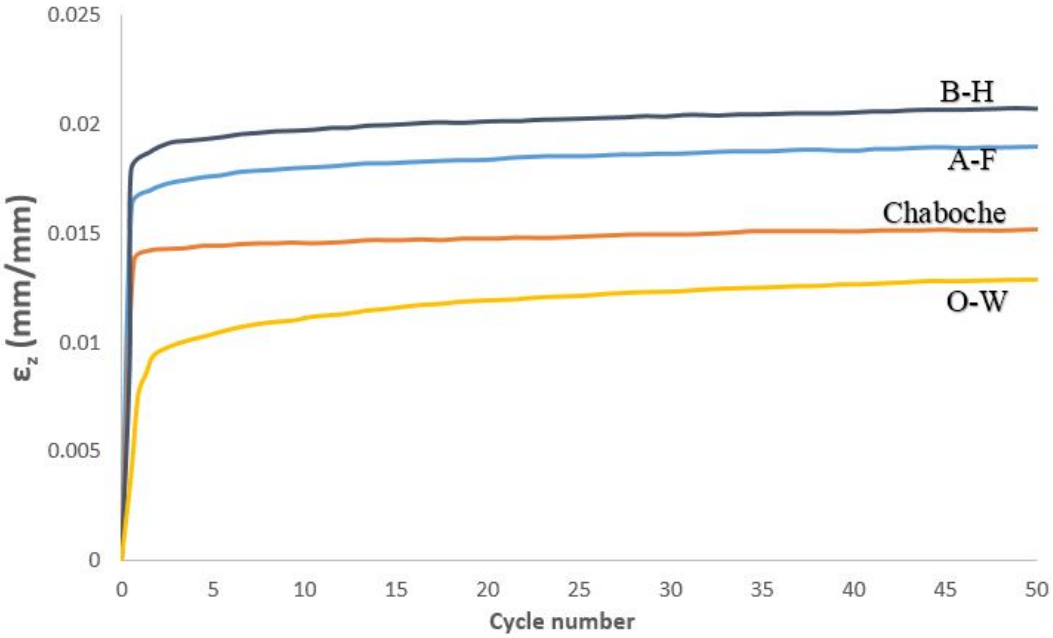

Figure 5.51: Comparison of models with $\sigma_a = 150MPa$ and $\sigma_m = 80MPa$

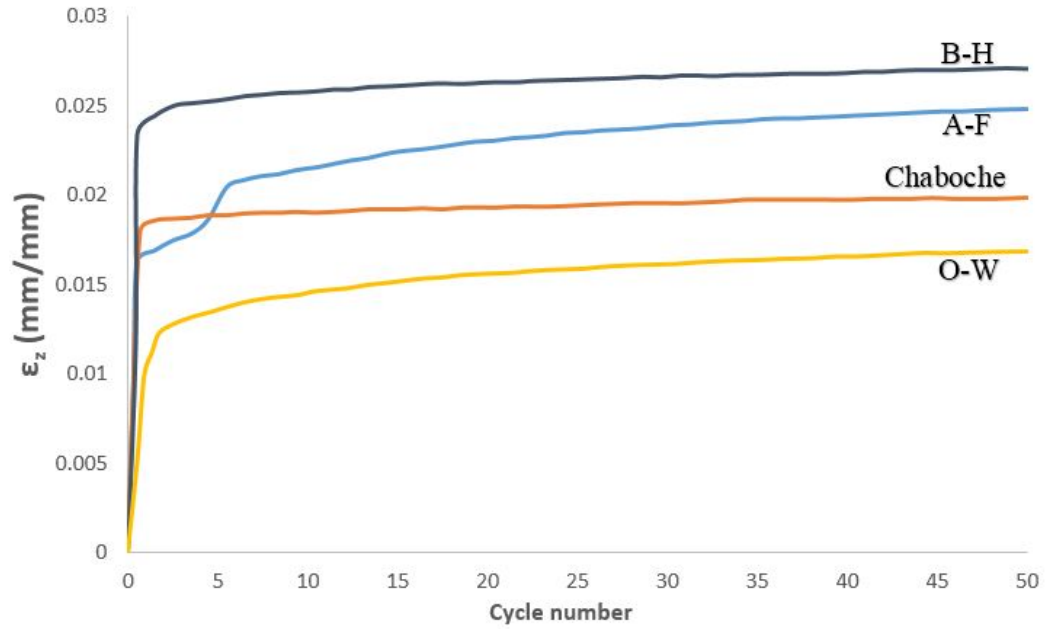

Figure 5.52: Comparison of models with $\sigma_a = 180MPa$ and $\sigma_m = 80MPa$

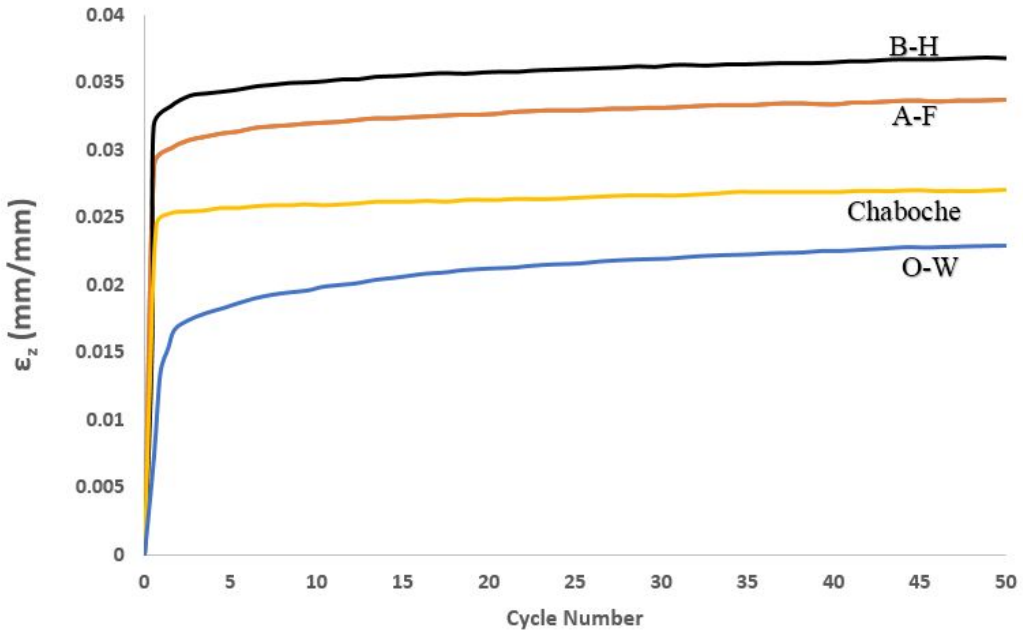

Figure 5.53: Comparison of models with $\sigma_a = 210MPa$ and $\sigma_m = 80MPa$

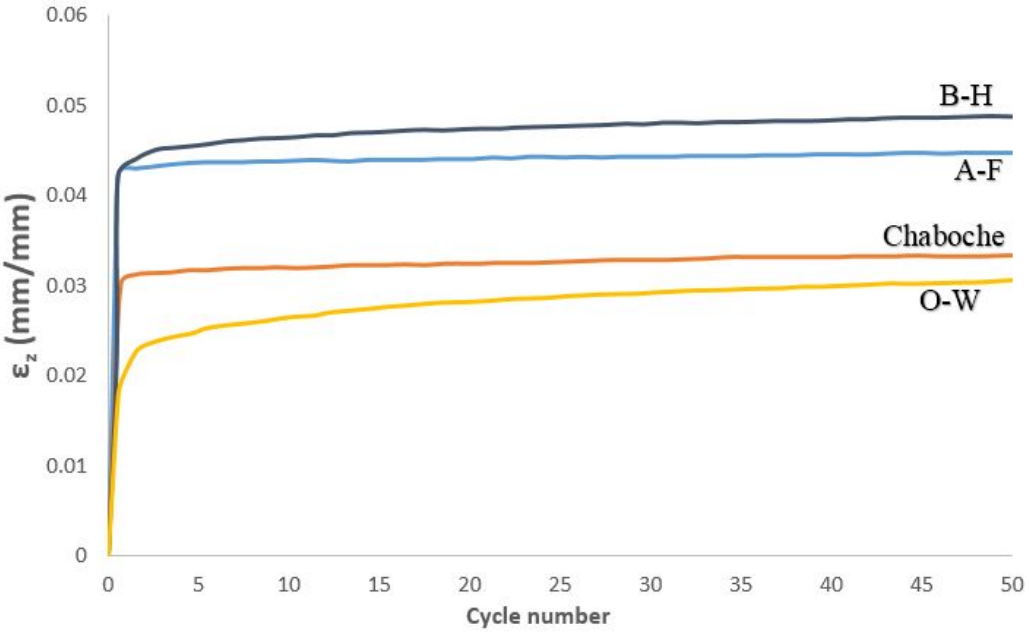

Figure 5.54: Comparison of models with $\sigma_a = 240MPa$ and $\sigma_m = 80MPa$

Prager model was expected to give closed hysteresis loops for each load cycle. The model model did not give any amount of ratcheting with cyclic loading as seen in

Figure 5.2. Although this model gives acceptable results for simple tension or compression tests, it can not be used to simulate cyclic loading. Neither the increasing deformation nor the shakedown phenomena can be observed since there is no open hysteresis loops.

A-F model gave high amount of ratcheting compared to the other proposed ones. It was concluded that shakedown (cessation of accumulation of strain) started to occur after a cycle number of about 40 for A-F model. Another observation was the fact that for low mean stresses, the accumulation rate increases for this model. On the other hand, ratcheting values are observed to be higher and accumulation rates are observed to be lower as mean stress or alternating stresses increase. However, A-F model is easily applicable because of its simplicity in coding. Also, since the number of iterations are not too much compared to the recent models, elapsed time for this model to complete the analysis is shorter. The over prediction of this model also holds for strain controlled loading.

The line of yield surface shift is the same for all load cycles in uniaxial loading. Therefore, the inner product of the surface normal **n** with itself in the second term become unity and results are the same with A-F model for uniaxial ratcheting of B-C model. The only effect of this modification on second term can only be observed in biaxial loading.

Originally, Chaboche model has been created to compensate the high strain values given by A-F model. However, the procedure for parameter determination, made the first version of the model fail. When a fourth partition having a threshold value was introduced, there existed some amount of ratcheting. This amount is observed to give fairly smaller predictions than A-F model. It is one of the most suitable models to simulate uniaxial ratcheting. Shakedown was reached earlier than A-F model in four partitioned Chaboche model. The accumulation rate was not affected much by changing mean and alternating stress values unlike A-F model. However, total accumulated strains have been increased with increasing mean and alternating stress values. The hardening rate is smaller than A-F model in same range of strain cycling.

Regardless of this Dolebelle parameter, first version of B-H model has no difference with A-F or B-C models for uniaxial ratcheting since the radial evanescence term does

not differ. As a result of this inefficiency on uniaxial ratcheting simulation of B-H model, second version has been performed. It was seen that Bari-Hassan model predicts ratcheting more than A-F model. However, shakedown was observed in smaller number of cycles than A-F model.

When the results are analyzed, O-W estimated the least amount of ratcheting among all models in this study. The most important modification was the step function included in the second term. By this way, no strain was accumulated until a certain value of stress and hence, this model is appropriate to give close estimations to actual cases.

As a conclusion of this part, different kinematic hardening models have been analyzed in their response to cyclic loading and accumulation of plastic strain. The simplest analyses were uniaxial loading. B-H model has given the highest amount of ratcheting. A-F model had the second highest amount. The lowest predictions have been done by Chaboche and O-W models. O-W model had the least amount of ratcheting in uniaxial loading.

5.2 Biaxial Ratcheting

In biaxial loading, both stress and strain controlled loading were applied to specimen. A circular hollow tube was used as test specimen with 25.4 mm outside diameter and 1.27 mm thickness as seen in Figure 5.55. Material properties are given in Table 5.1. The hollow tube was subjected to an alternating longitudinal stress or strain while there was a constant internal pressure. Different ranges of stress and strain were applied. In the analyses von Mises yield criterion, Hill yield criterion and Aretz yield criterion were used for different kinematic hardening models.

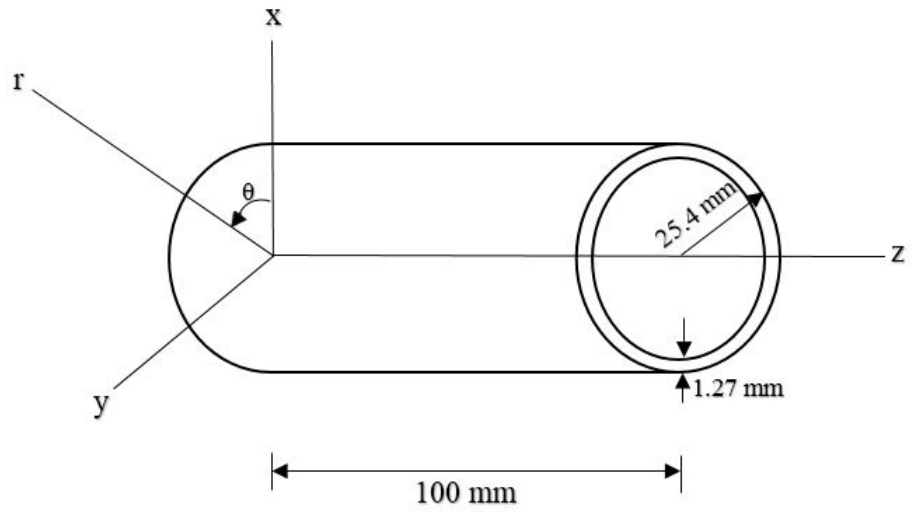

Figure 5.55: Specimen of biaxial analyses

5.2.1 Von Mises Yield Criterion

The von-Mises yield criterion is applied for six different kinematic hardening models.

5.2.1.1 Armstrong-Frederick Model

For A-F model, Figure 5.56 - Figure 5.58 show longitudinal strain versus transverse strain under 3 MPa, 4.7 MPa and 6 MPa internal pressures for strain controlled symmetric cyclic loading with strain amplitude $(\epsilon_z)_a = 0.005 mm/mm$. Figure 5.59 presents cycle number versus transverse strain under different internal pressures with 0.005 mm/mm alternating strain.

Figure 5.60 - Figure 5.62 show longitudinal strain ϵ_z versus tangential strain in strain controlled cyclic loading with strain amplitudes 0.002 mm/mm, 0.005 mm/mm and 0.008 mm/mm and p = 4.7 MPa internal pressure. Figure 5.59 presents cycle number versus tangential strain under different alternating strains with 4.7 MPa internal pressure.

Figure 5.64 - Figure 5.66 show longitudinal strain versus transverse strain in stress controlled analysis under 2.5 MPa, 4 MPa and 5.796 MPa internal pressures and

$\sigma_a = 240MPa$, $\sigma_m = 40MPa$. In Figure 5.67 and Figure 5.68, the accumulation of strain in both directions with changing longitudinal stress are shown.

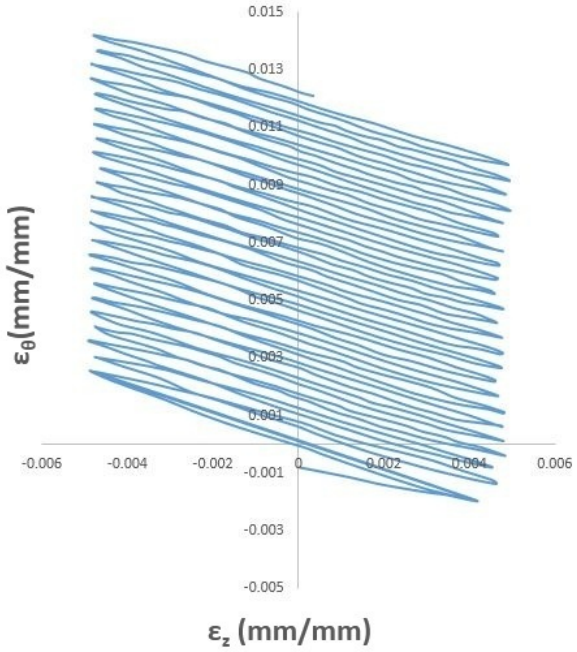

Figure 5.56: A-F model with $p = 3MPa$ and $(\epsilon_z)_a = 0.005mm/mm$

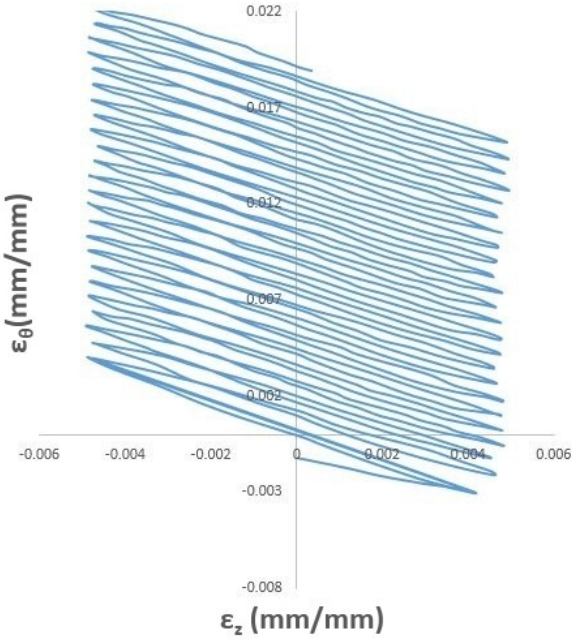

Figure 5.57: A-F model with $p = 4.7MPa$ and $(\epsilon_z)_a = 0.005mm/mm$

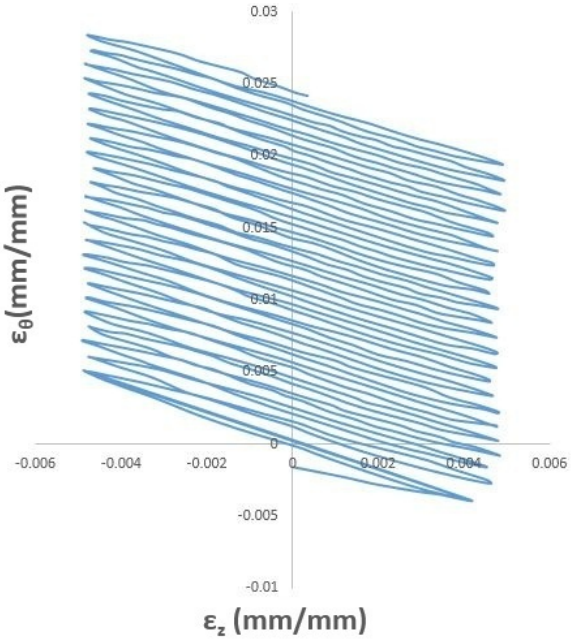

Figure 5.58: A-F model with $p = 6MPa$ and $(\epsilon_z)_a = 0.005mm/mm$

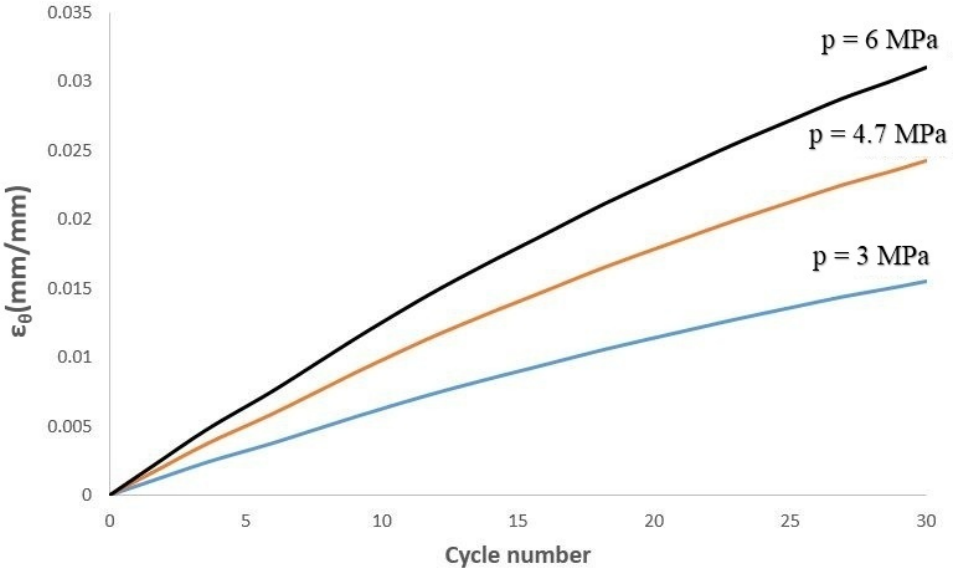

Figure 5.59: A-F model with different internal pressures and constant alternating strain $(\epsilon_z)_a = 0.005mm/mm$

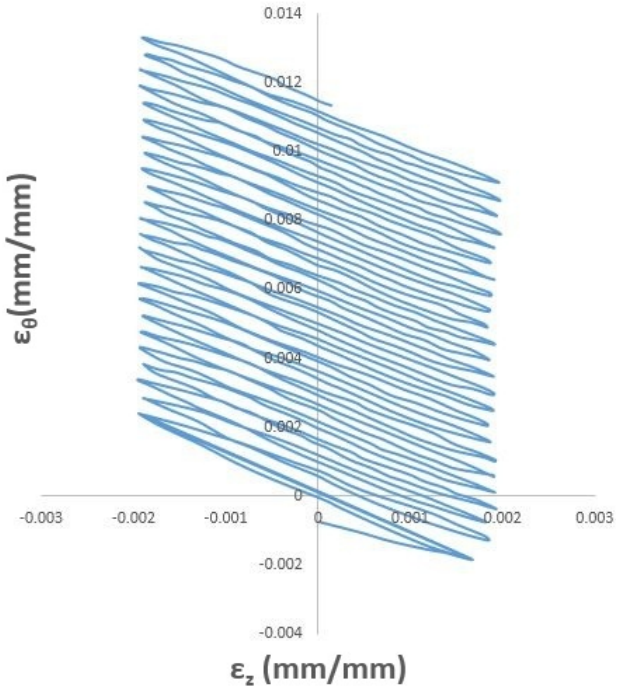

Figure 5.60: A-F model with $p = 4.7MPa$ and $(\epsilon_z)_a = 0.002mm/mm$

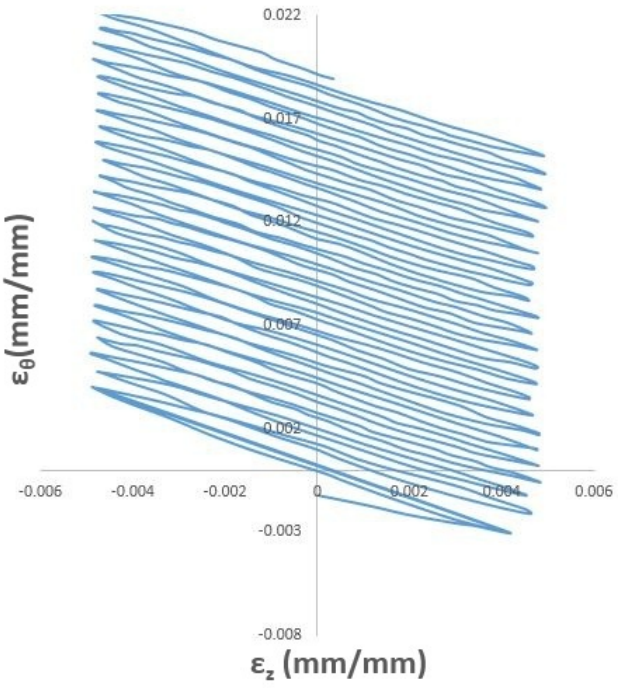

Figure 5.61: A-F model with $p = 4.7MPa$ and $(\epsilon_z)_a = 0.005mm/mm$

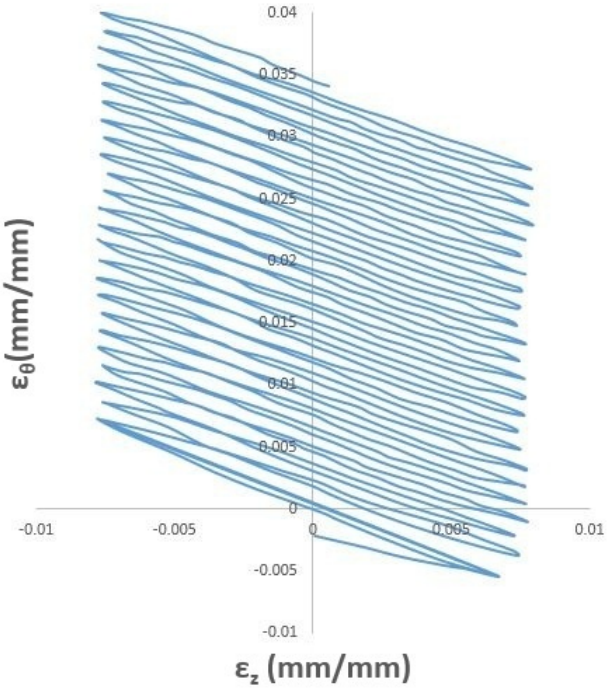

Figure 5.62: A-F model with $p = 4.7MPa$ and $(\epsilon_z)_a = 0.008mm/mm$

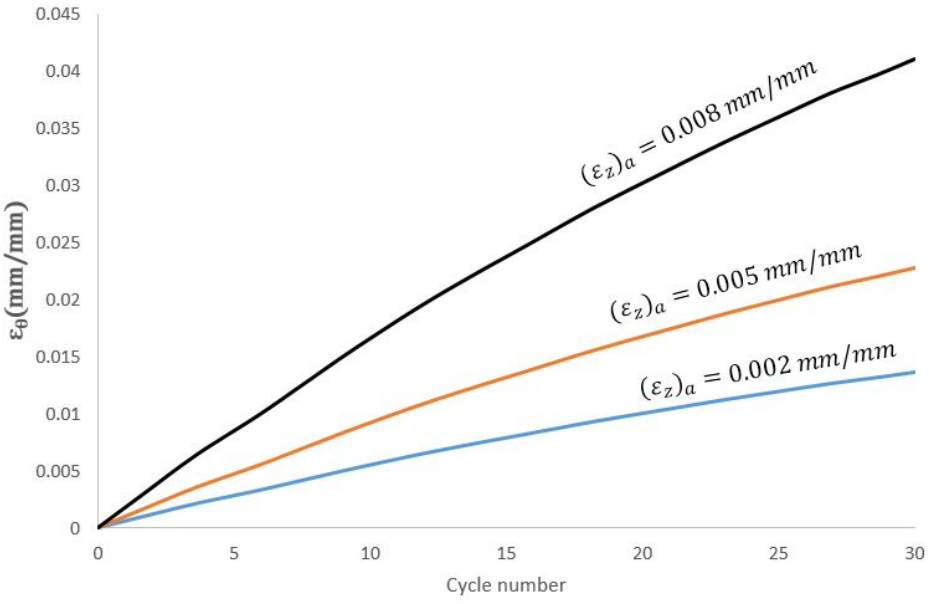

Figure 5.63: A-F model with different alternating strains and $p = 4.7MPa$

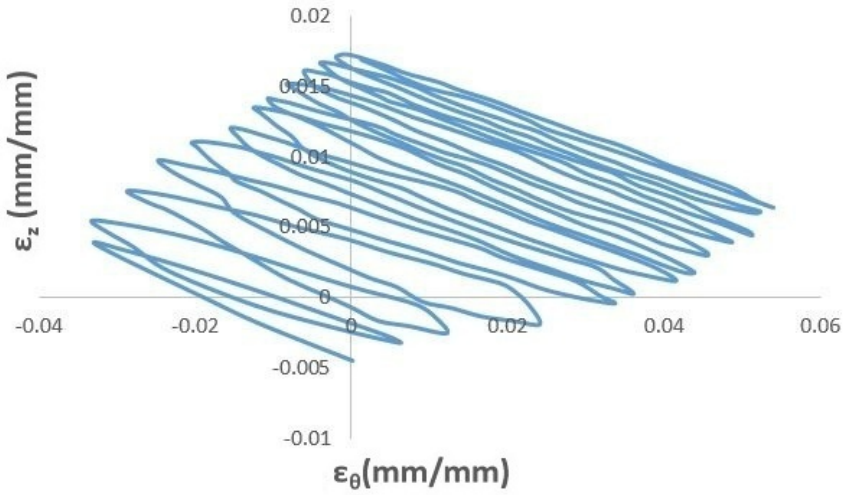

Figure 5.64: A-F model with $p = 2.5MPa$ and $\sigma_a = 240MPa, \sigma_m = 40MPa$

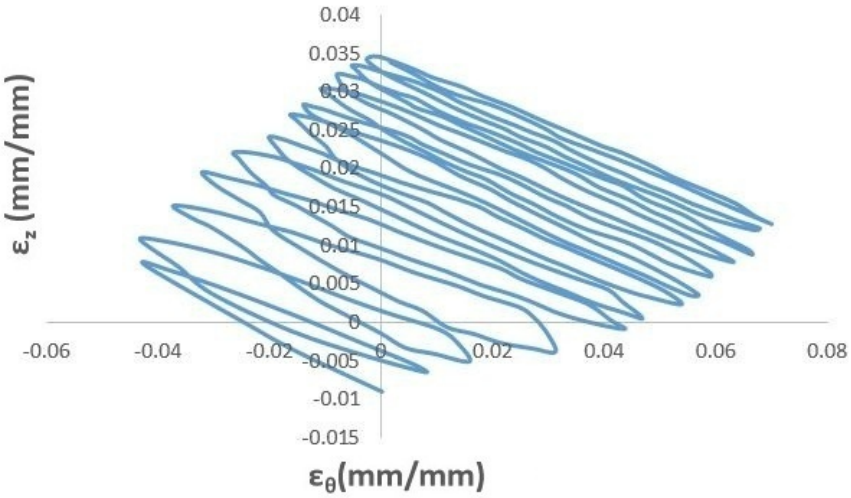

Figure 5.65: A-F model with $p = 4MPa$ and $\sigma_a = 240MPa, \sigma_m = 40MPa$

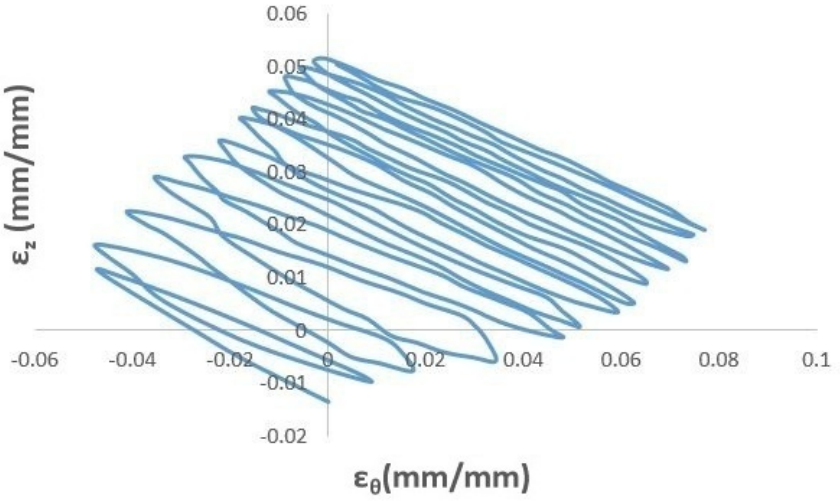

Figure 5.66: A-F model with $p = 5.796MPa$ and $\sigma_a = 240MPa, \sigma_m = 40MPa$

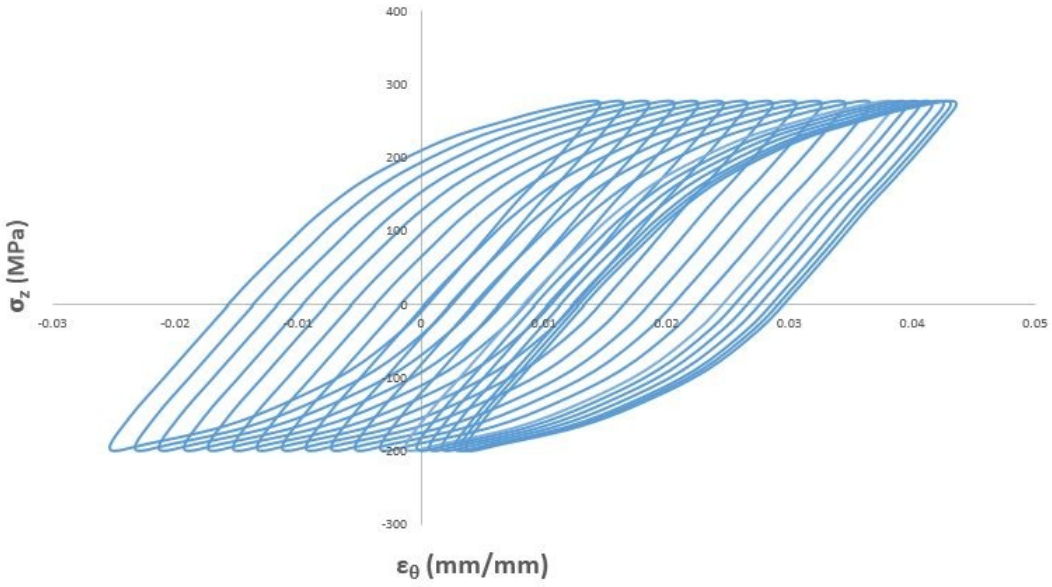

Figure 5.67: Ratcheting in transverse direction in stress controlled loading for A-F model

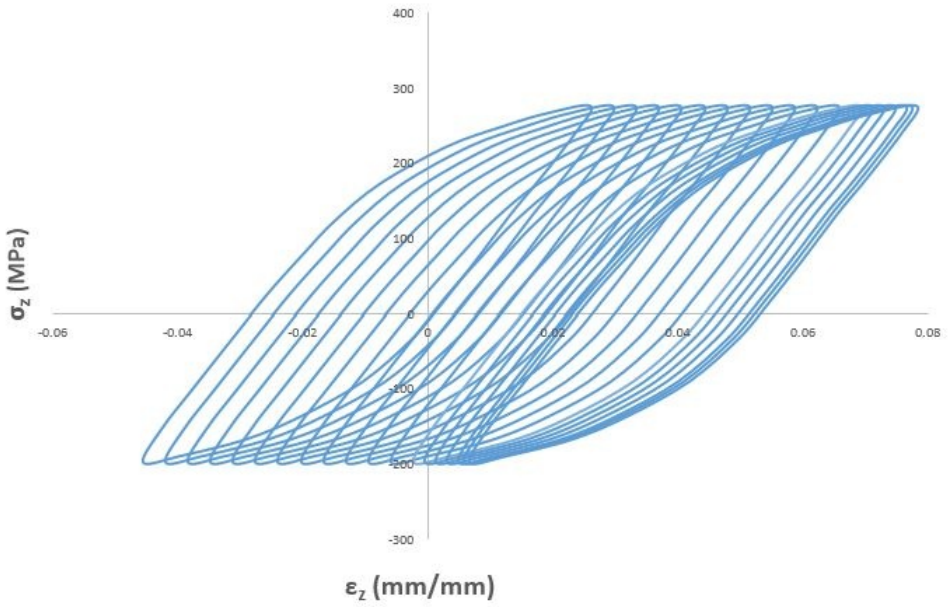

Figure 5.68: Ratcheting in longitudinal direction in stress controlled loading for A-F model

5.2.1.2 Burlet-Cailletaud Model

For B-C model, Figure 5.69 - Figure 5.71 show longitudinal strain versus transverse strain under 3 MPa, 4.7 MPa and 6 MPa internal pressures for strain controlled symmetric cyclic loading with strain amplitude $(\epsilon_z)_a = 0.005mm/mm$. Figure 5.72 presents cycle number versus transverse strain under different internal pressures with 0.005 mm/mm alternating strain.

Figure 5.73 - Figure 5.75 show longitudinal strain ϵ_z versus tangential strain in strain controlled cyclic loading with strain amplitudes 0.002 mm/mm, 0.005 mm/mm and 0.008 mm/mm and p = 4.7 MPa internal pressure. Figure 5.72 presents cycle number versus tangential strain under different alternating strains with 4.7 MPa internal pressure.

Figure 5.77, Figure 5.78 and Figure 5.79 show longitudinal strain versus transverse strain in stress controlled analysis under 2.5 MPa, 4 MPa and 5.796 MPa internal pressures and $\sigma_a = 240MPa$, $\sigma_m = 40MPa$.

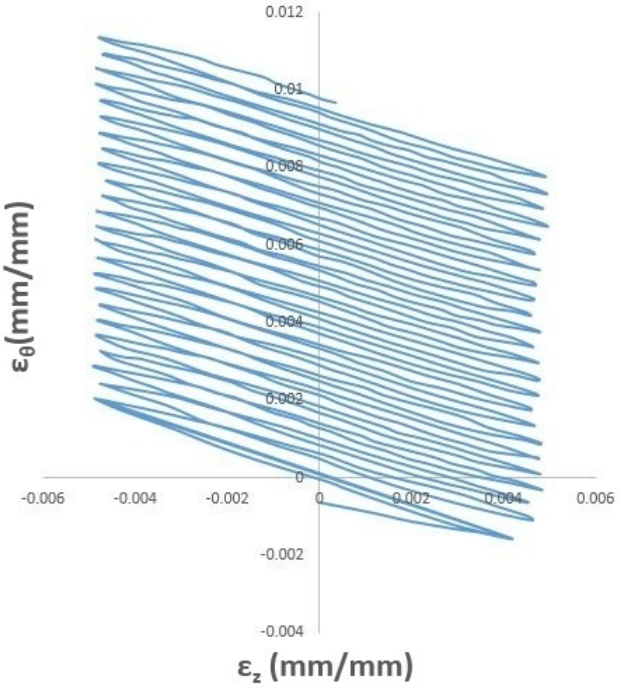

Figure 5.69: B-C model with $p = 3MPa$ and $(\epsilon_z)_a = 0.005mm/mm$

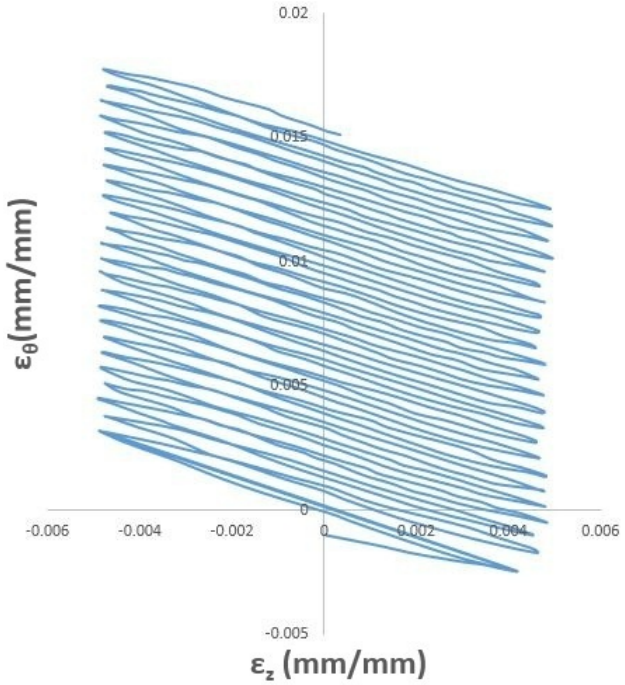

Figure 5.70: B-C model with $p = 4.7MPa$ and $(\epsilon_z)_a = 0.005mm/mm$

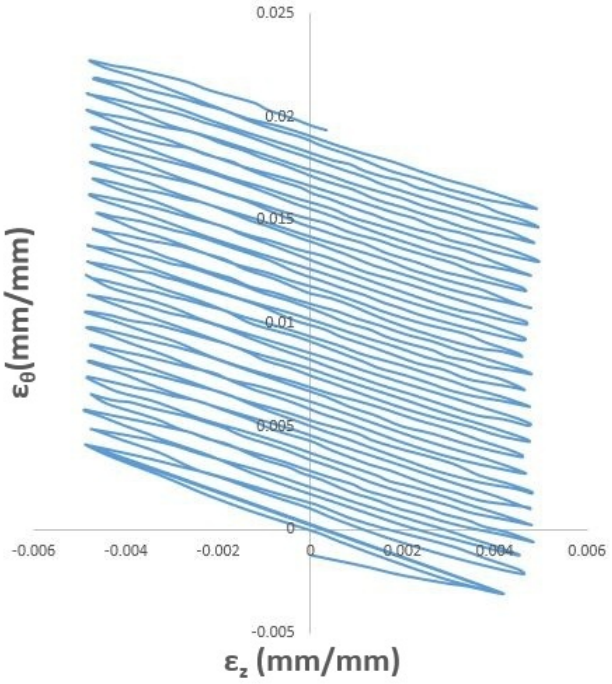

Figure 5.71: B-C model with $p = 6MPa$ and $(\epsilon_z)_a = 0.005mm/mm$

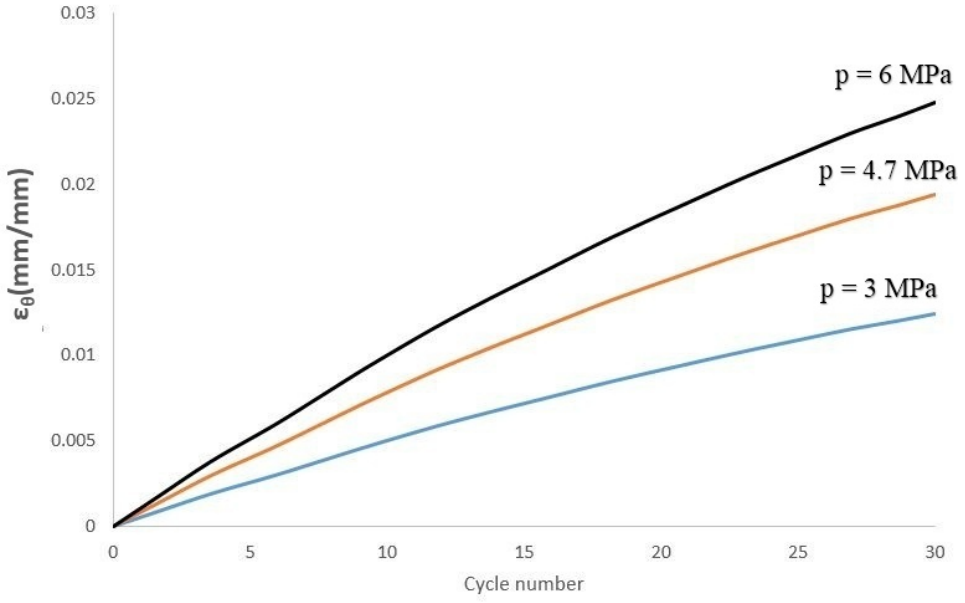

Figure 5.72: B-C model with different internal pressures and and constant alternating strain $(\epsilon_z)_a = 0.005mm/mm$

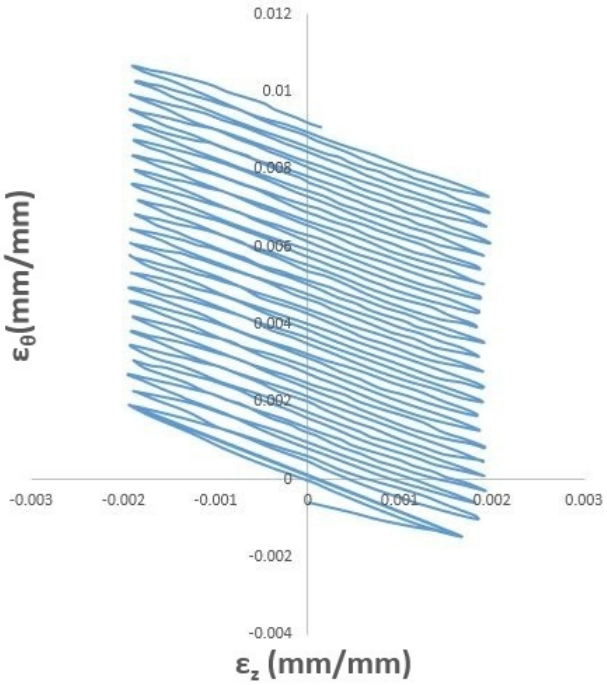

Figure 5.73: B-C model with $p = 4.7MPa$ and $(\epsilon_z)_a = 0.002mm/mm$

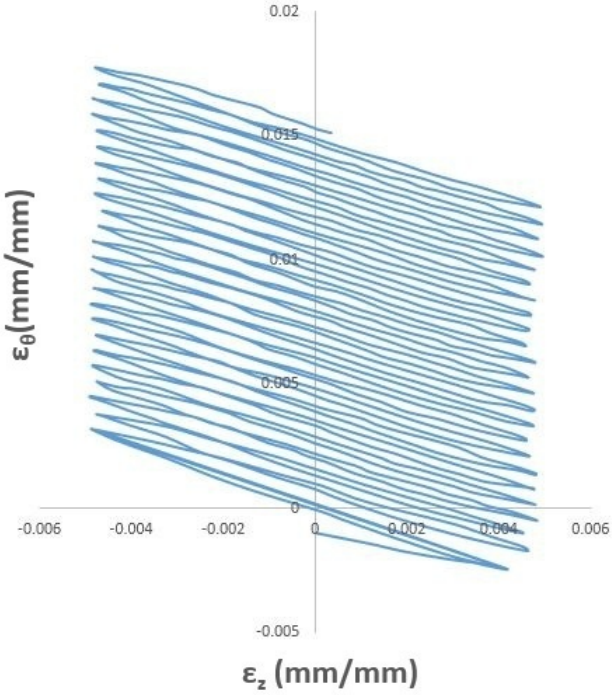

Figure 5.74: B-C model with $p = 4.7MPa$ and $(\epsilon_z)_a = 0.005mm/mm$

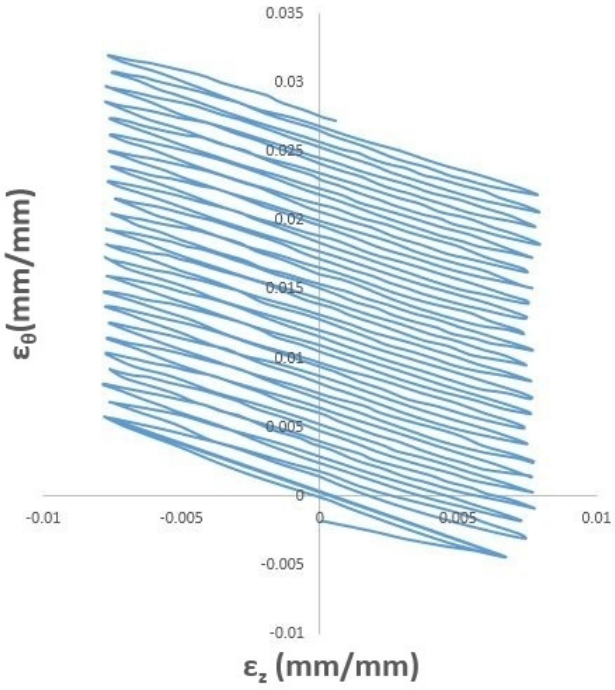

Figure 5.75: B-C model with $p = 4.7MPa$ and $(\epsilon_z)_a = 0.008mm/mm$

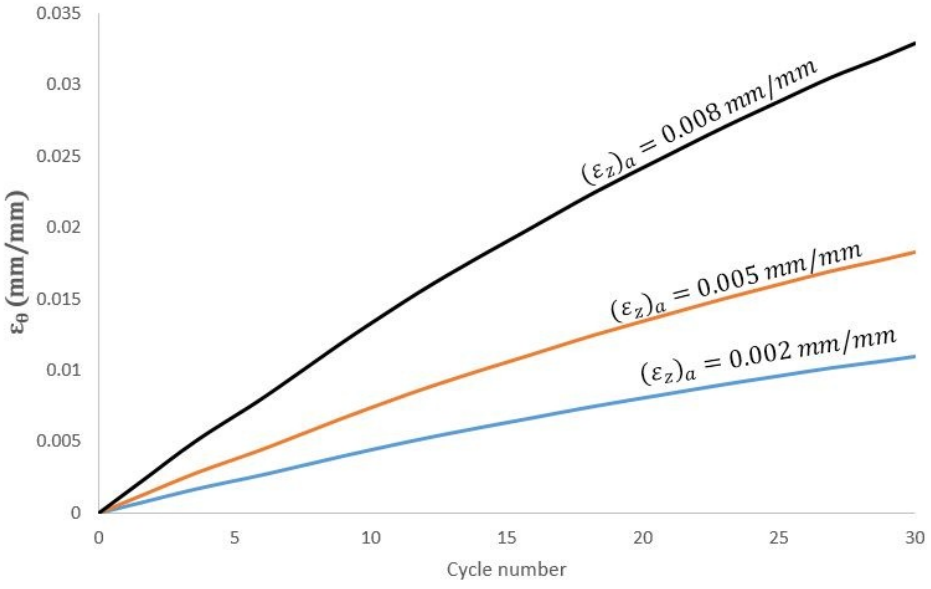

Figure 5.76: B-C model with different alternating strains and $p = 4.7MPa$

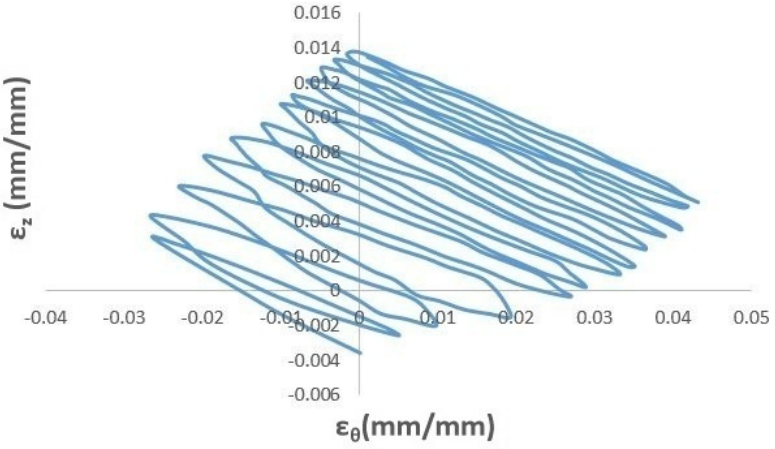

Figure 5.77: B-C model with $p = 2.5MPa$ and $\sigma_a = 240MPa, \sigma_m = 40MPa$

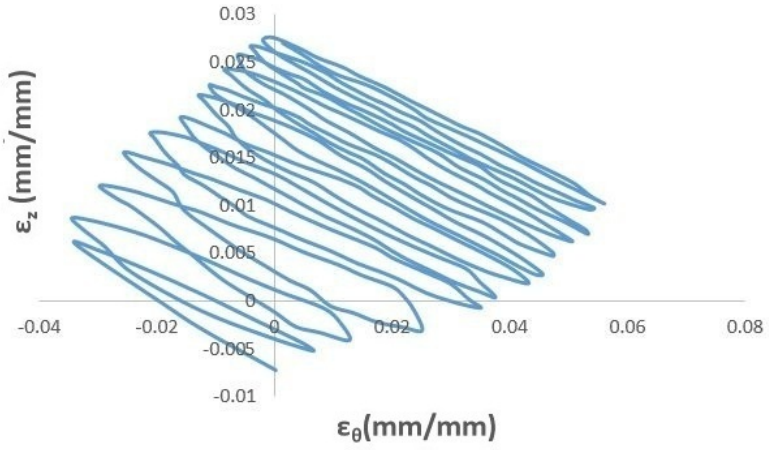

Figure 5.78: B-C model with $p = 4MPa$ and $\sigma_a = 240MPa, \sigma_m = 40MPa$

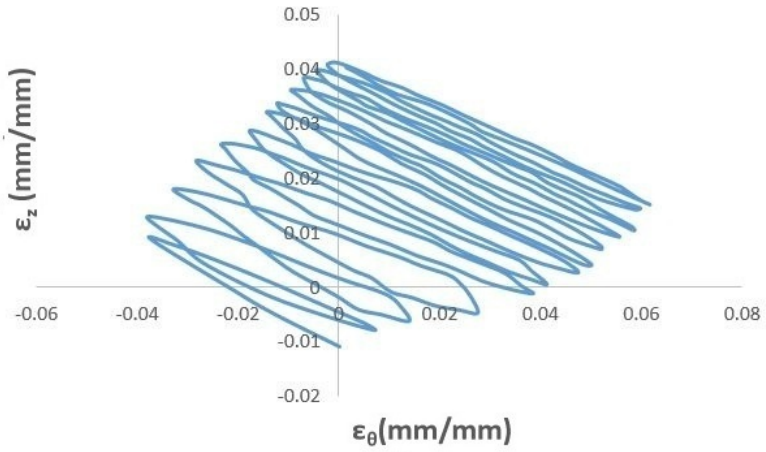

Figure 5.79: B-C model with $p = 5.796MPa$ and $\sigma_a = 240MPa, \sigma_m = 40MPa$

5.2.1.3 Chaboche Model

For Chaboche model, Figure 5.80 - Figure 5.82 show longitudinal strain versus transverse strain under 3 MPa, 4.7 MPa and 6 MPa internal pressures for strain controlled symmetric cyclic loading with strain amplitude $(\epsilon_z)_a = 0.005mm/mm$. Figure 5.83 presents cycle number versus transverse strain under different internal pressures with 0.005 mm/mm alternating strain.

Figure 5.84 - Figure 5.86 show longitudinal strain ϵ_z versus tangential strain in strain controlled cyclic loading with strain amplitudes 0.002 mm/mm, 0.005 mm/mm and 0.008 mm/mm and p = 4.7 MPa internal pressure. Figure 5.83 presents cycle number versus tangential strain under different alternating strains with 4.7 MPa internal pressure.

Figure 5.88, Figure 5.89 and Figure 5.90 show longitudinal strain versus transverse strain in stress controlled analysis under 2.5 MPa, 4 MPa and 5.796 MPa internal pressures and $\sigma_a = 240MPa$, $\sigma_m = 40MPa$.

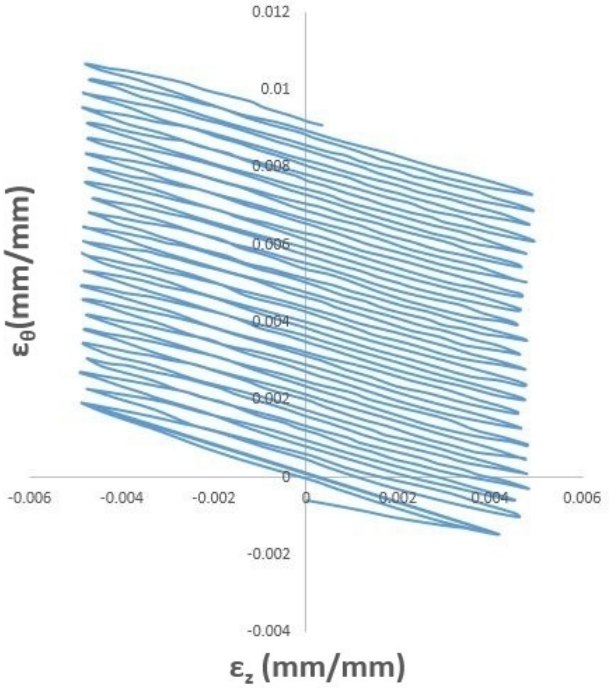

Figure 5.80: Chaboche model with $p = 3MPa$ and $(\epsilon_z)_a = 0.005mm/mm$

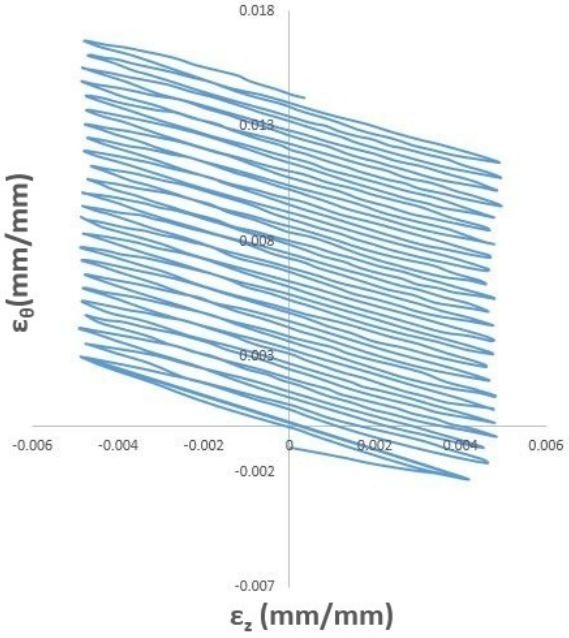

Figure 5.81: Chaboche model with $p = 4.7MPa$ and $(\epsilon_z)_a = 0.005mm/mm$

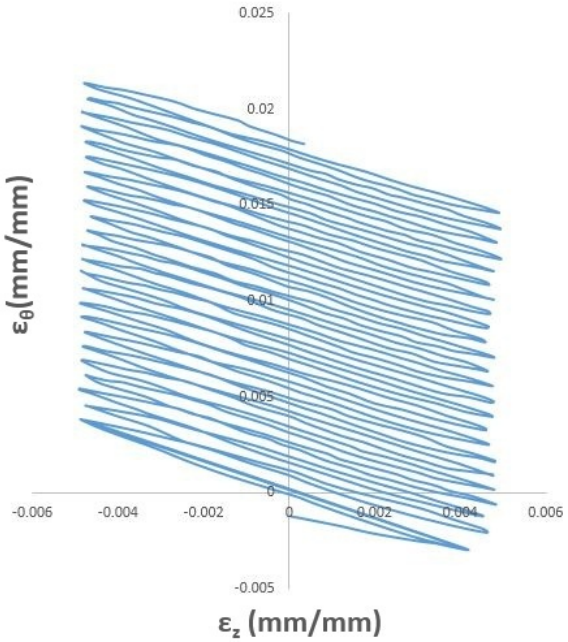

Figure 5.82: Chaboche model with $p = 6MPa$ and $(\epsilon_z)_a = 0.005mm/mm$

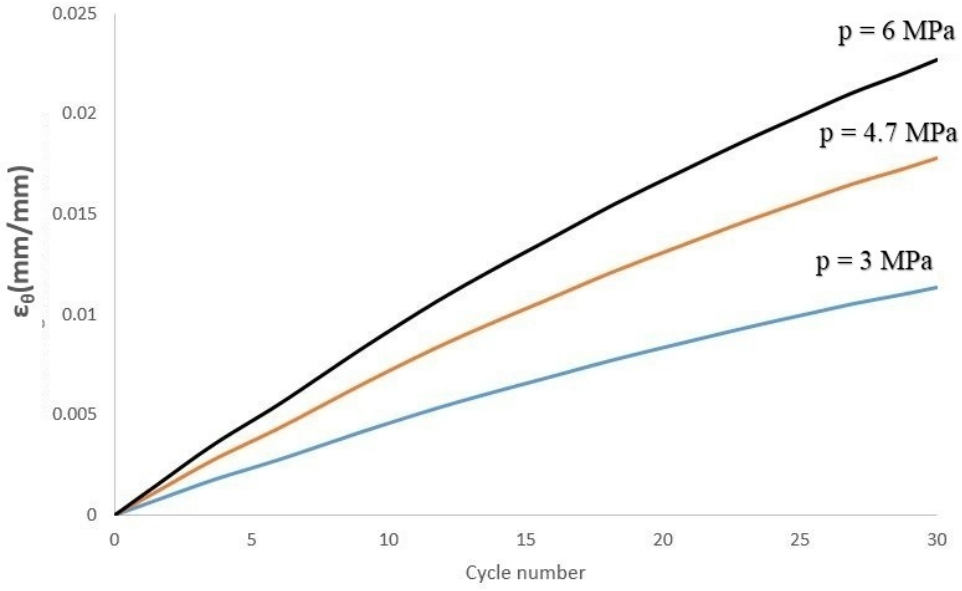

Figure 5.83: Chaboche model with different internal pressures and constant alternating strain $(\epsilon_z)_a = 0.005mm/mm$

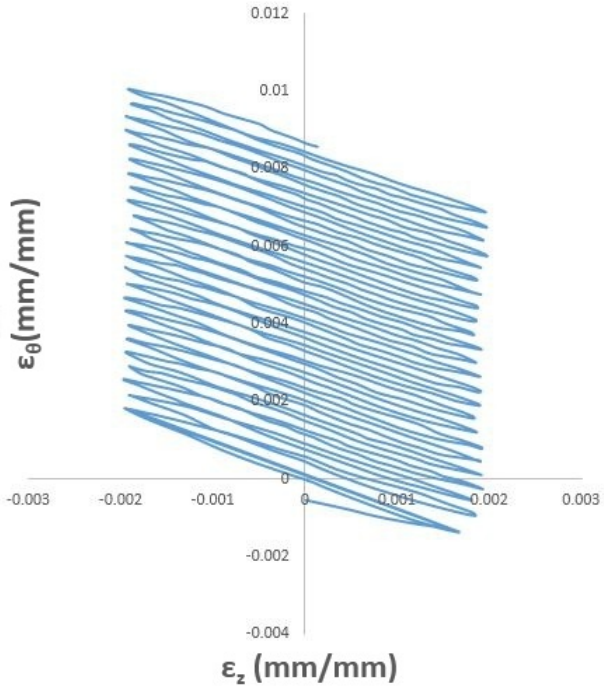

Figure 5.84: Chaboche model with $p = 4.7MPa$ and $(\epsilon_z)_a = 0.002mm/mm$

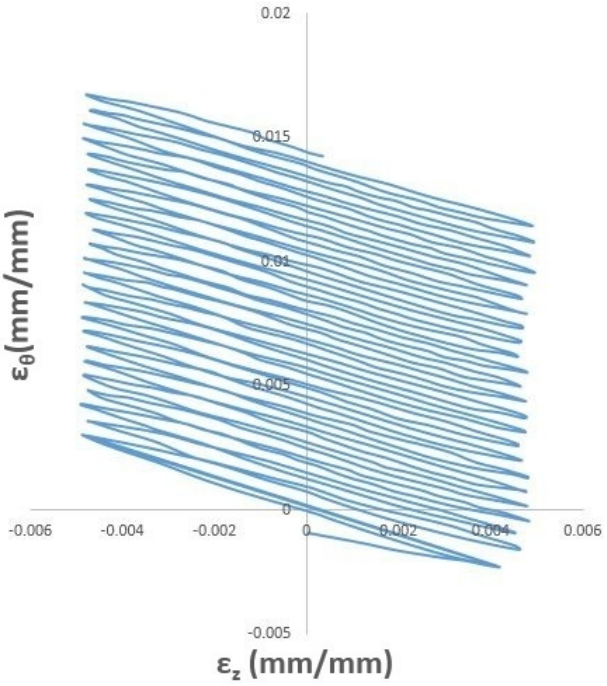

Figure 5.85: Chaboche model with $p = 4.7MPa$ and $(\epsilon_z)_a = 0.005mm/mm$

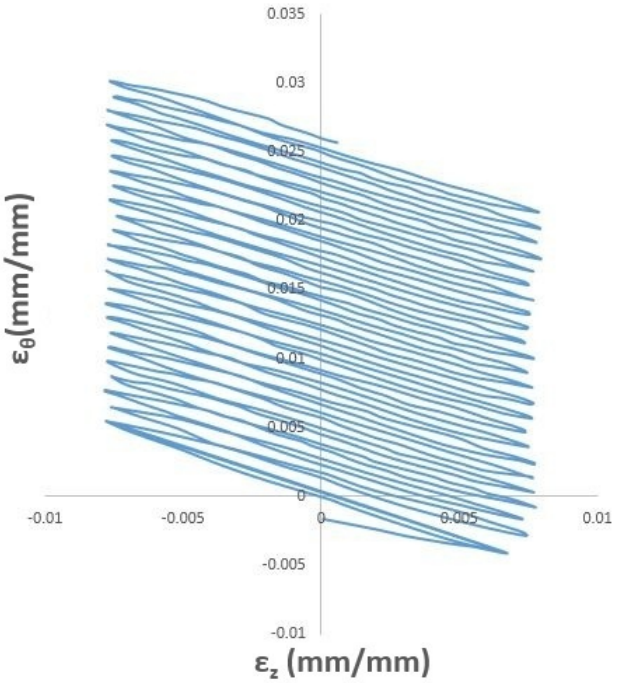

Figure 5.86: Chaboche model with $p = 4.7MPa$ and $(\epsilon_z)_a = 0.008mm/mm$

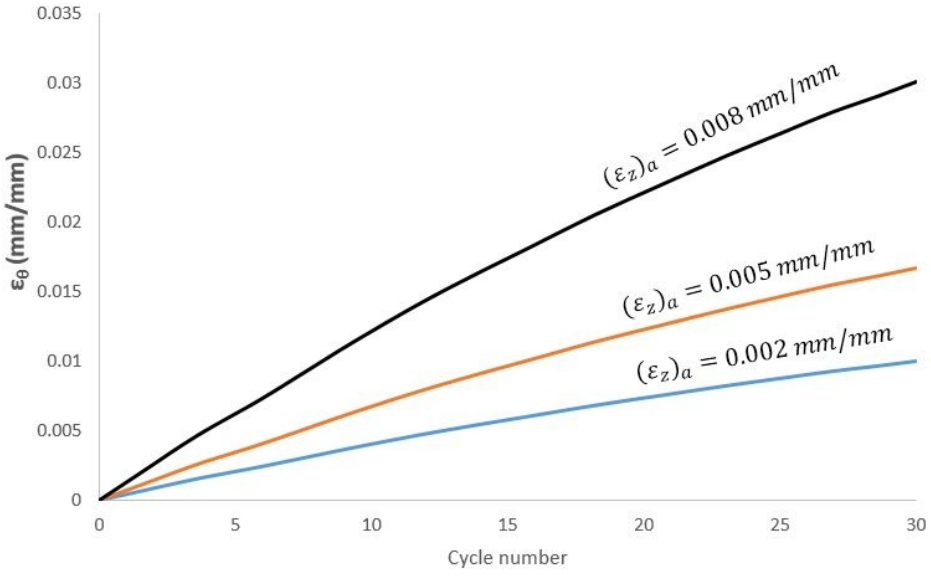

Figure 5.87: Chaboche model with different alternating strains and $p = 4.7MPa$

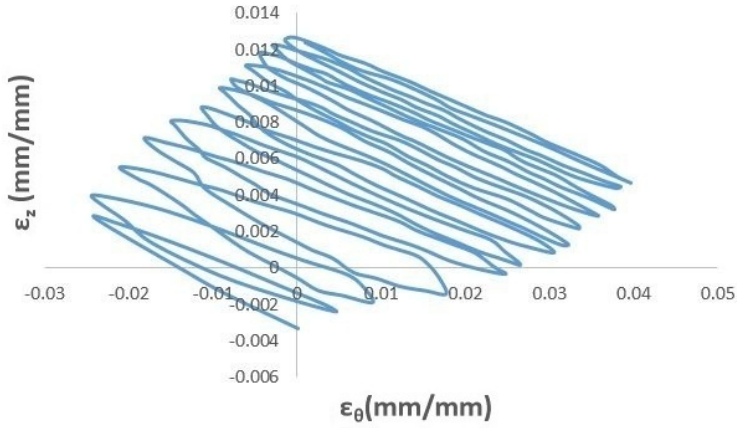

Figure 5.88: Chaboche model with $p = 2.5MPa$ and $\sigma_a = 240MPa, \sigma_m = 40MPa$

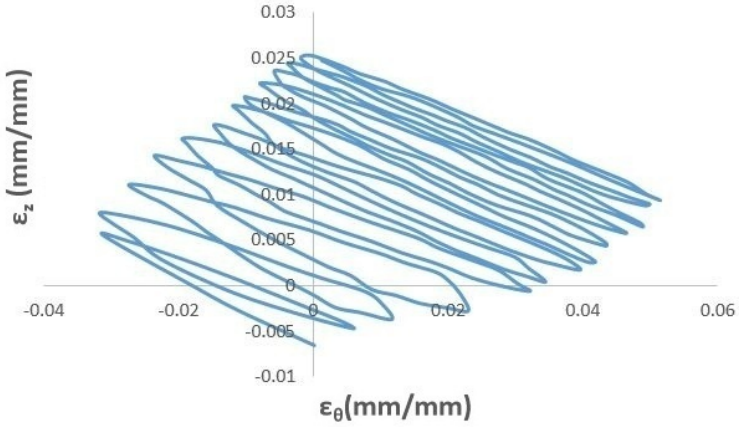

Figure 5.89: Chaboche model with $p = 4MPa$ and $\sigma_a = 240MPa, \sigma_m = 40MPa$

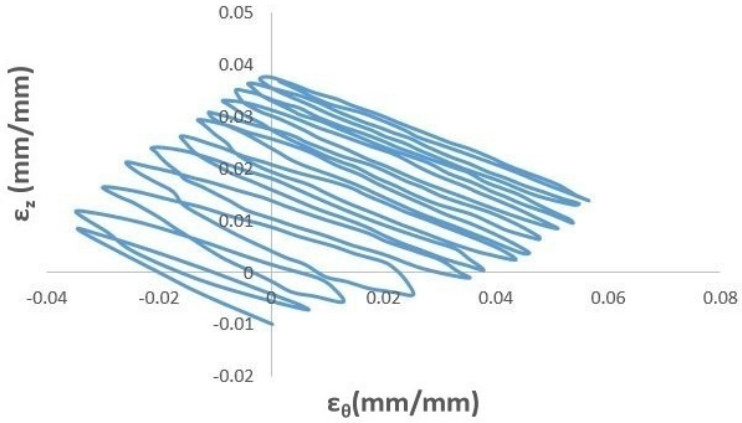

Figure 5.90: Chaboche model with $p = 5.796MPa$ and $\sigma_a = 240MPa, \sigma_m = 40MPa$

5.2.1.4 Bari-Hassan Model

For B-H model, Figure 5.91 - Figure 5.93 show longitudinal strain versus transverse strain under 3 MPa, 4.7 MPa and 6 MPa internal pressures for strain controlled symmetric cyclic loading with strain amplitude $(\epsilon_z)_a = 0.005mm/mm$. Figure 5.94 presents cycle number versus transverse strain under different internal pressures with 0.005 mm/mm alternating strain.

Figure 5.95 - Figure 5.97 show longitudinal strain ϵ_z versus tangential strain in strain controlled cyclic loading with strain amplitudes 0.002 mm/mm, 0.005 mm/mm and 0.008 mm/mm and p = 4.7 MPa internal pressure. Figure 5.59 presents cycle number versus tangential strain under different alternating strains with 4.7 MPa internal pressure.

Figure 5.99, Figure 5.100 and Figure 5.101 show longitudinal strain versus transverse strain in stress controlled analysis under 2.5 MPa, 4 MPa and 5.796 MPa internal pressures and $\sigma_a = 240MPa$, $\sigma_m = 40MPa$.

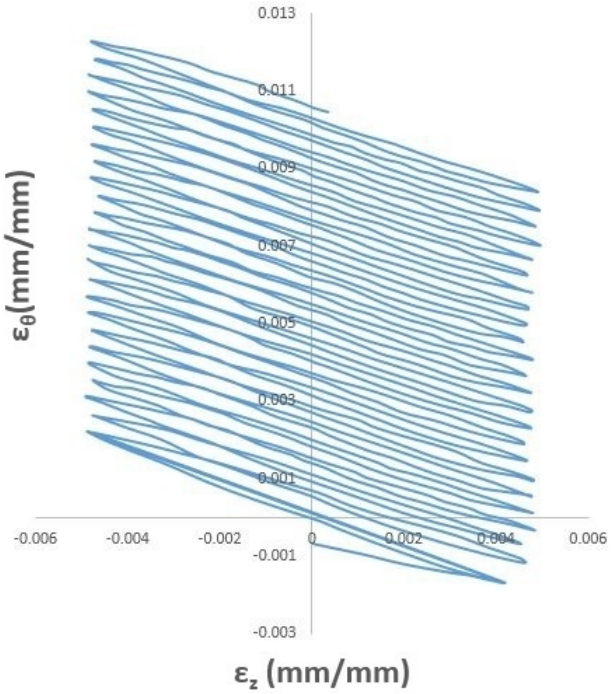

Figure 5.91: B-H model with $p = 3MPa$ and $(\epsilon_z)_a = 0.005mm/mm$

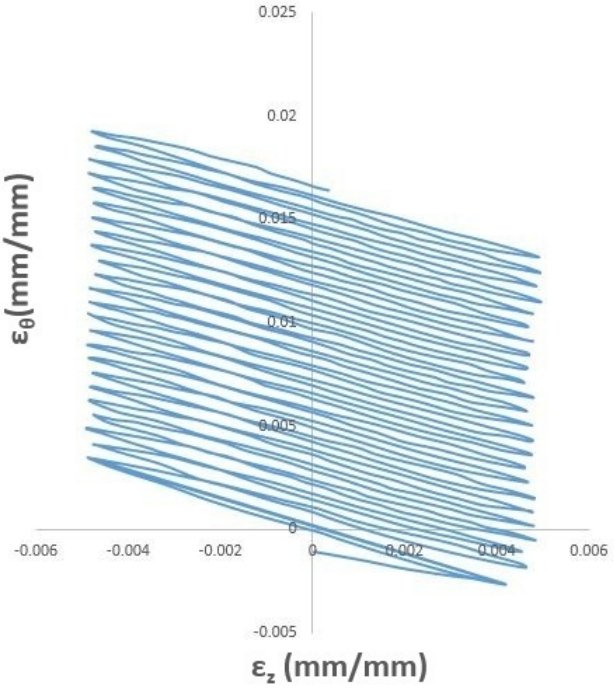

Figure 5.92: B-H model with $p = 4.7MPa$ and $(\epsilon_z)_a = 0.005mm/mm$

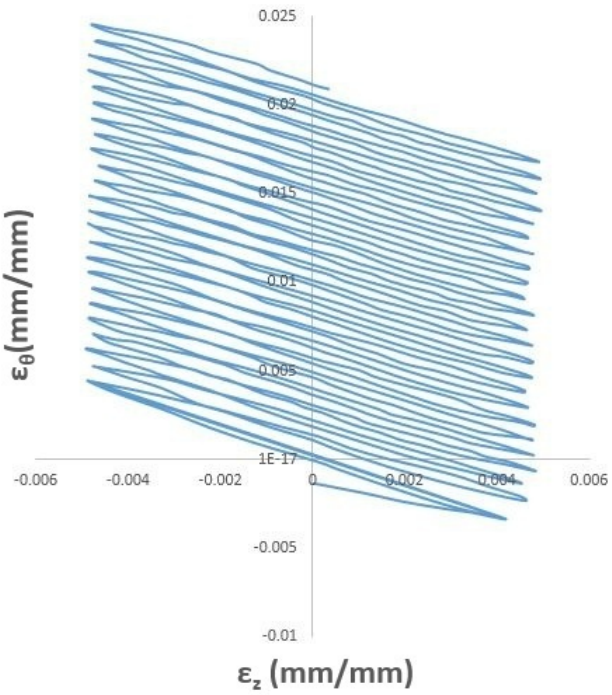

Figure 5.93: B-H model with $p = 6MPa$ and $(\epsilon_z)_a = 0.005mm/mm$

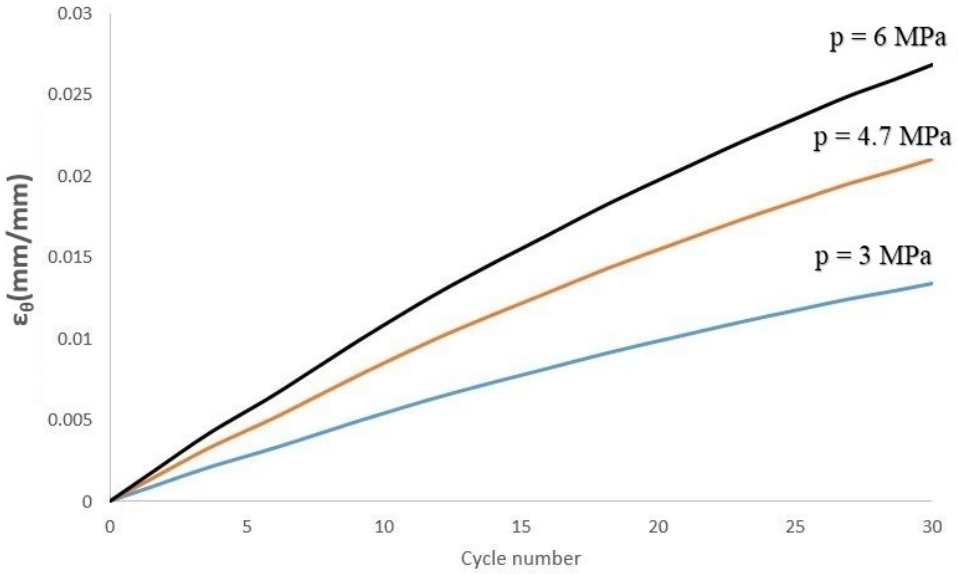

Figure 5.94: B-H model with different internal pressures and constant alternating strain $(\epsilon_z)_a = 0.005mm/mm$

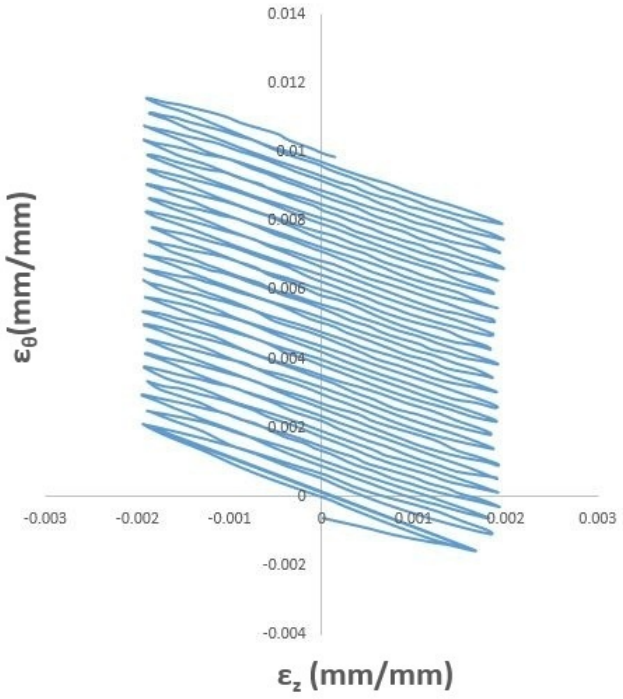

Figure 5.95: B-H model with $p = 4.7MPa$ and $(\epsilon_z)_a = 0.002mm/mm$

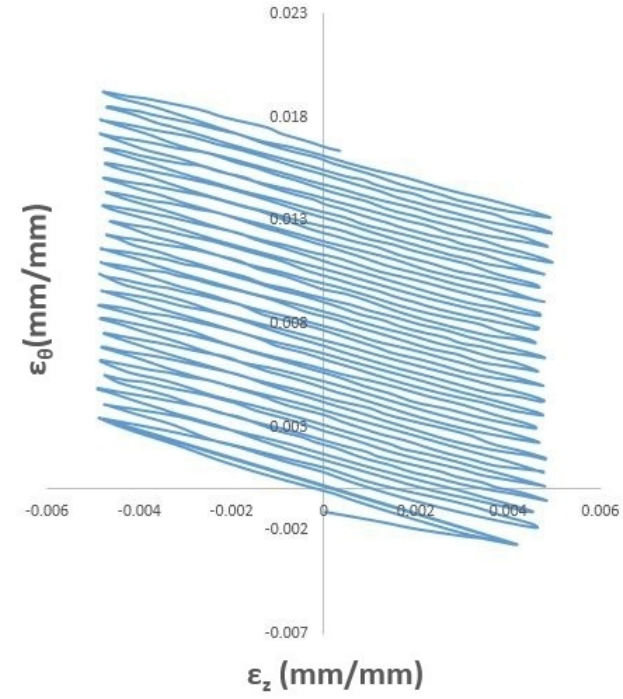

Figure 5.96: B-H model with $p = 4.7MPa$ and $(\epsilon_z)_a = 0.005mm/mm$

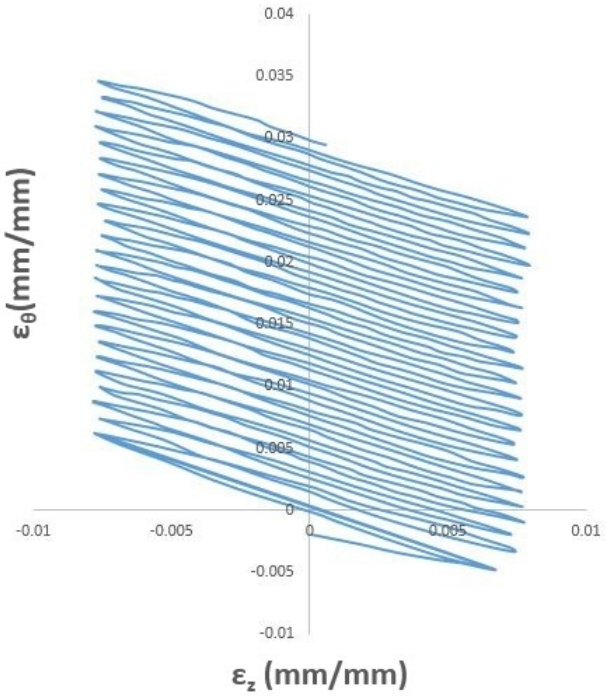

Figure 5.97: B-H model with $p = 4.7MPa$ and $(\epsilon_z)_a = 0.008mm/mm$

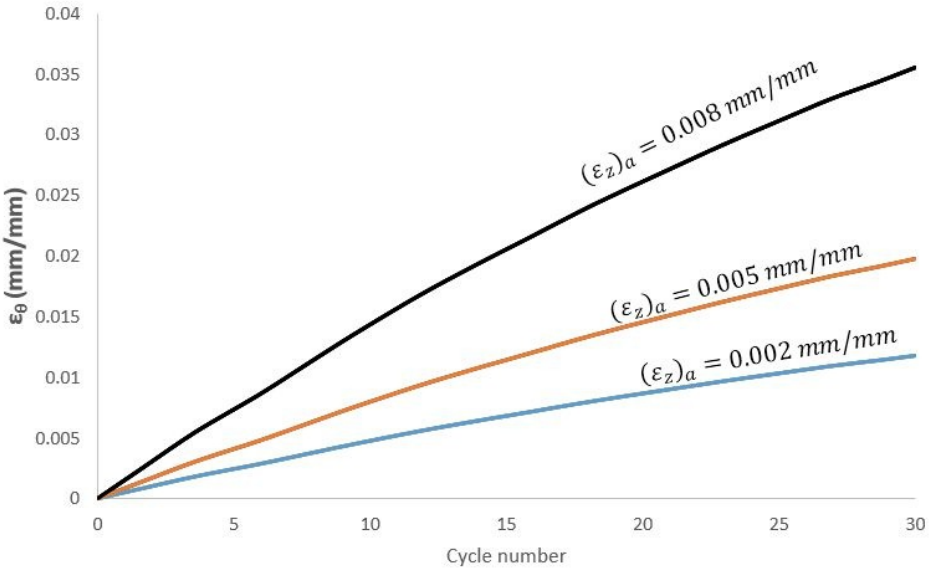

Figure 5.98: B-H model with different alternating strains and $p = 4.7MPa$

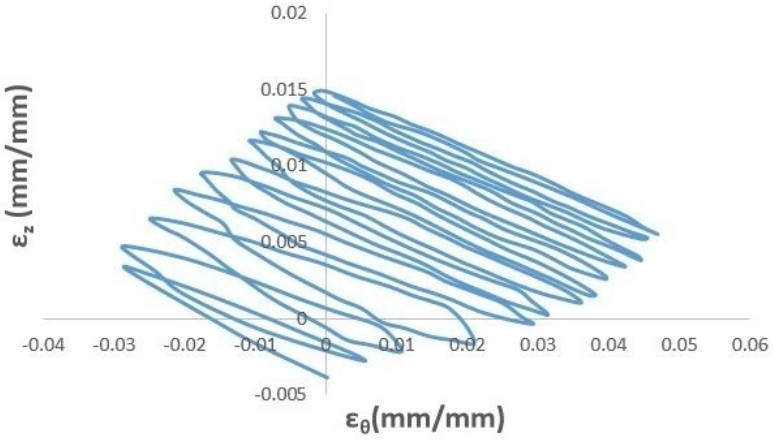

Figure 5.99: B-H model with $p = 2.5MPa$ and $\sigma_a = 240MPa, \sigma_m = 40MPa$

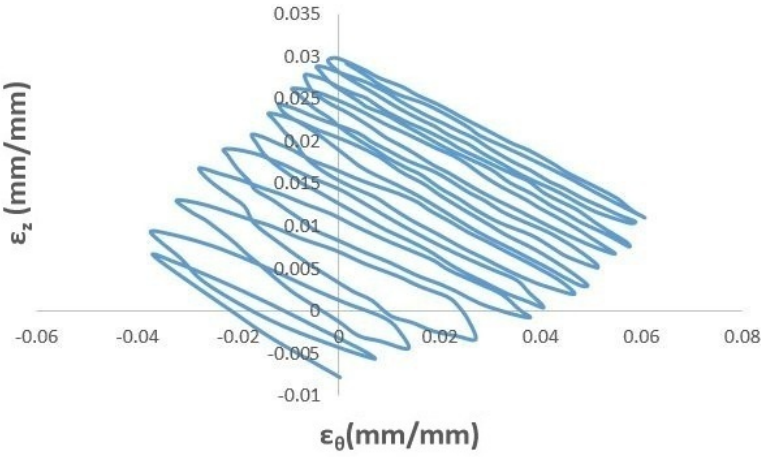

Figure 5.100: B-H model with $p = 4MPa$ and $\sigma_a = 240MPa, \sigma_m = 40MPa$

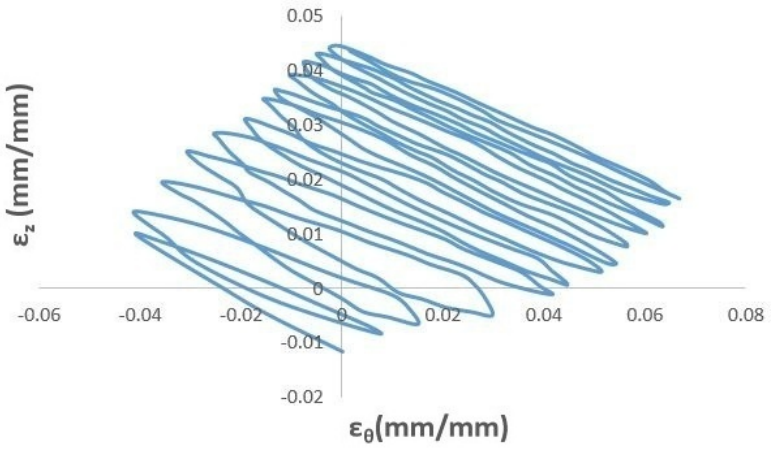

Figure 5.101: B-H model with $p = 5.796MPa$ and $\sigma_a = 240MPa, \sigma_m = 40MPa$

5.2.1.5 Ohno-Wang Model

For O-W model, Figure 5.102 - Figure 5.104 show longitudinal strain versus transverse strain under 3 MPa, 4.7 MPa and 6 MPa internal pressures for strain controlled symmetric cyclic loading with strain amplitude $(\epsilon_z)_a = 0.005mm/mm$. Figure 5.105 presents cycle number versus transverse strain under different internal pressures with 0.005 mm/mm alternating strain.

Figure 5.106 - Figure 5.108 show longitudinal strain ϵ_z versus tangential strain in strain controlled cyclic loading with strain amplitudes 0.002 mm/mm, 0.005 mm/mm and 0.008 mm/mm and p = 4.7 MPa internal pressure. Figure 5.105 presents cycle number versus tangential strain under different alternating strains with 4.7 MPa internal pressure.

Figure 5.110, Figure 5.111 and Figure 5.112 show longitudinal strain versus transverse strain in stress controlled analysis under 2.5 MPa, 4 MPa and 5.796 MPa internal pressures and $\sigma_a = 240MPa$, $\sigma_m = 40MPa$.

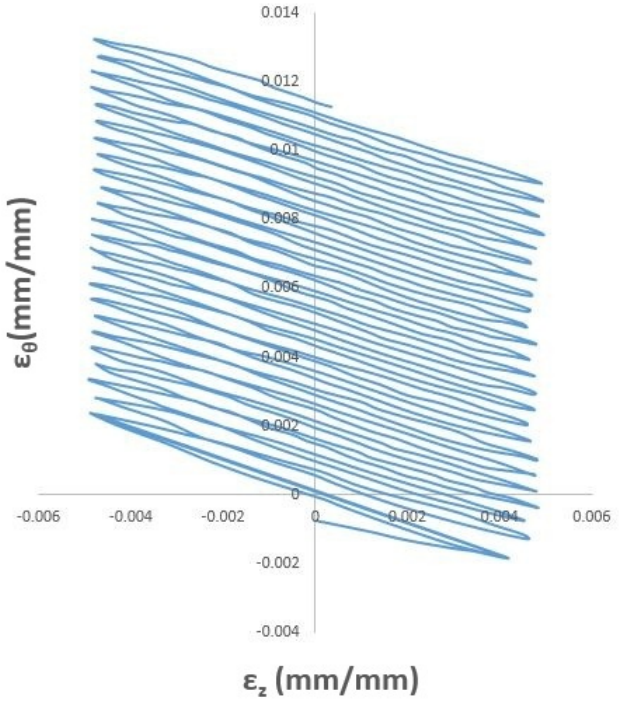

Figure 5.102: O-W model with $p = 3MPa$ and $(\epsilon_z)_a = 0.005mm/mm$

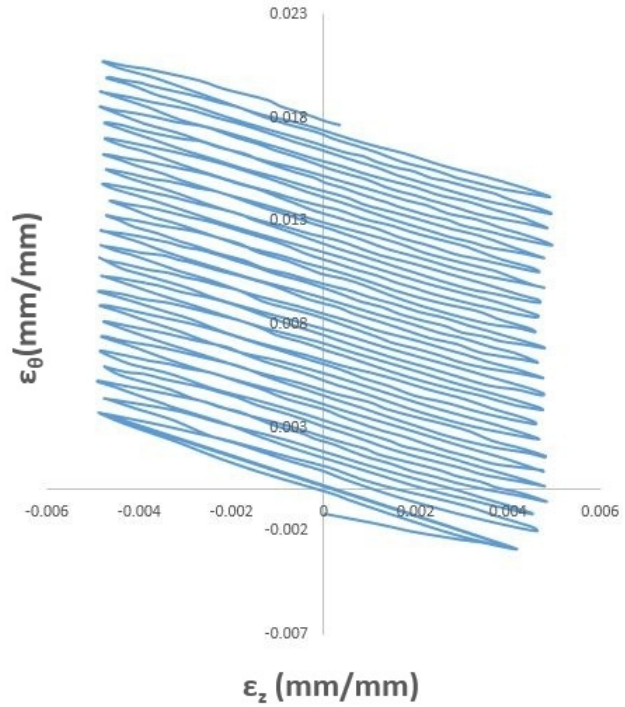

Figure 5.103: O-W model with $p = 4.7MPa$ and $(\epsilon_z)_a = 0.005mm/mm$

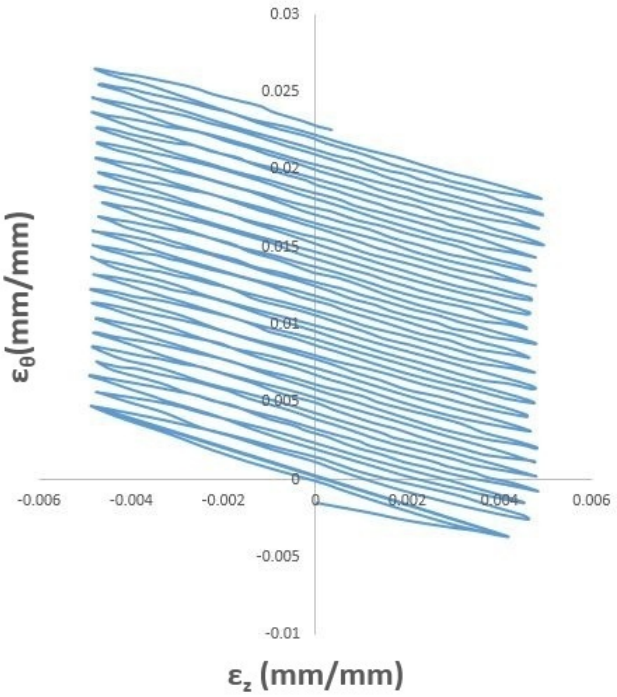

Figure 5.104: O-W model with $p = 6MPa$ and $(\epsilon_z)_a = 0.005mm/mm$

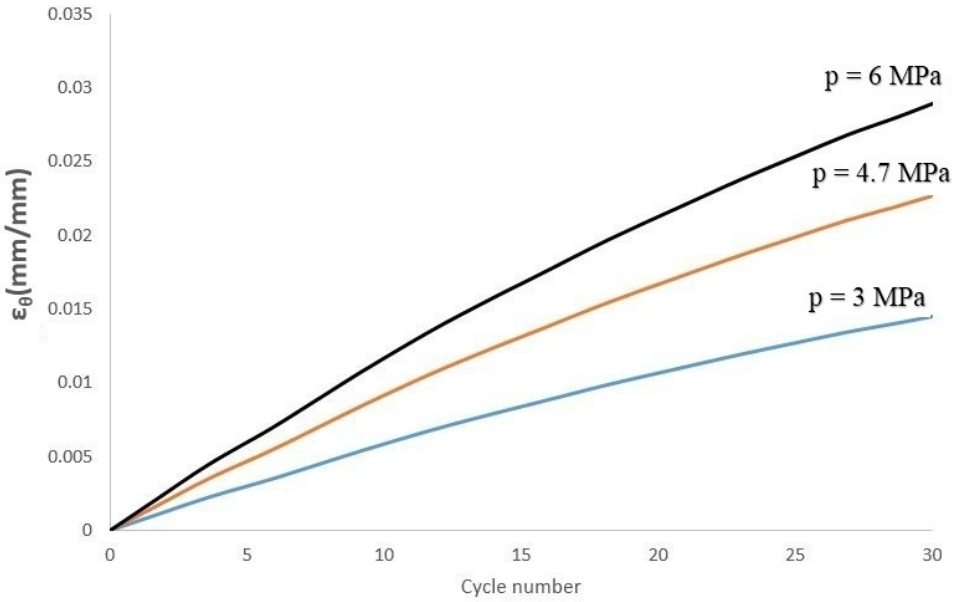

Figure 5.105: O-W model with different internal pressures and constant alternating strain $(\epsilon_z)_a = 0.005mm/mm$

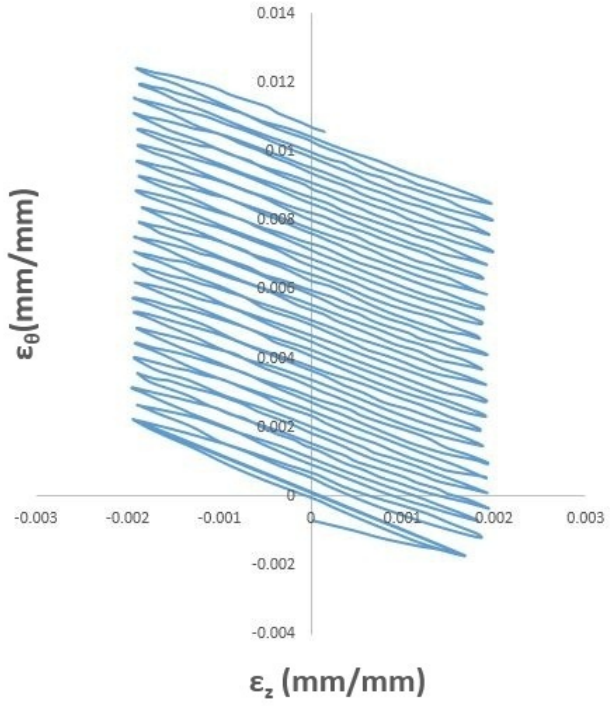

Figure 5.106: O-W model with $p = 4.7MPa$ and $(\epsilon_z)_a = 0.002$

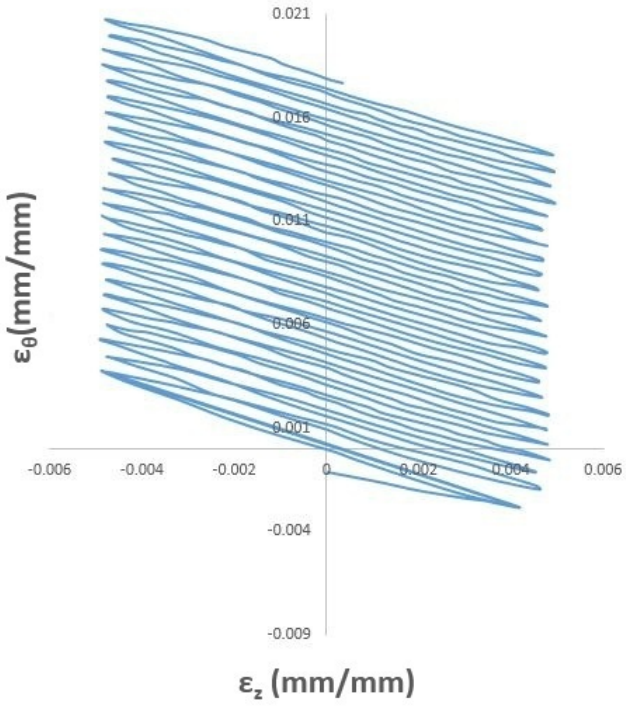

Figure 5.107: O-W model with $p = 4.7MPa$ and $(\epsilon_z)_a = 0.005$

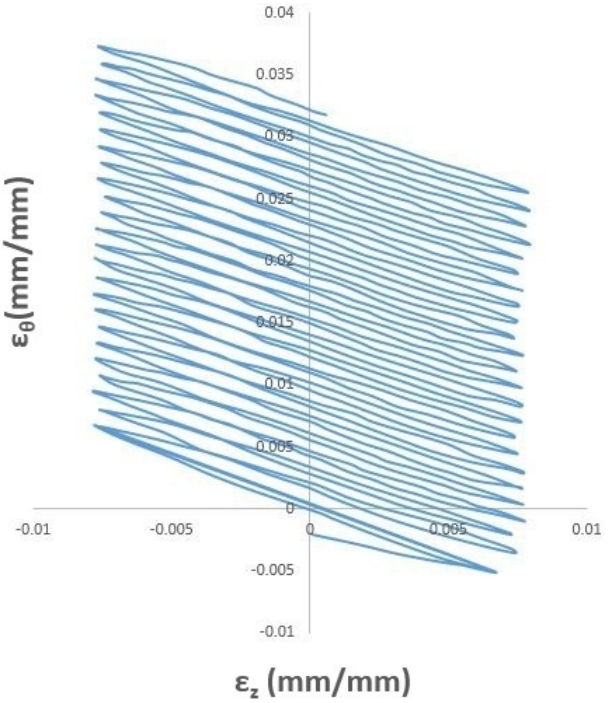

Figure 5.108: O-W model with $p = 4.7MPa$ and $(\epsilon_z)_a = 0.008$

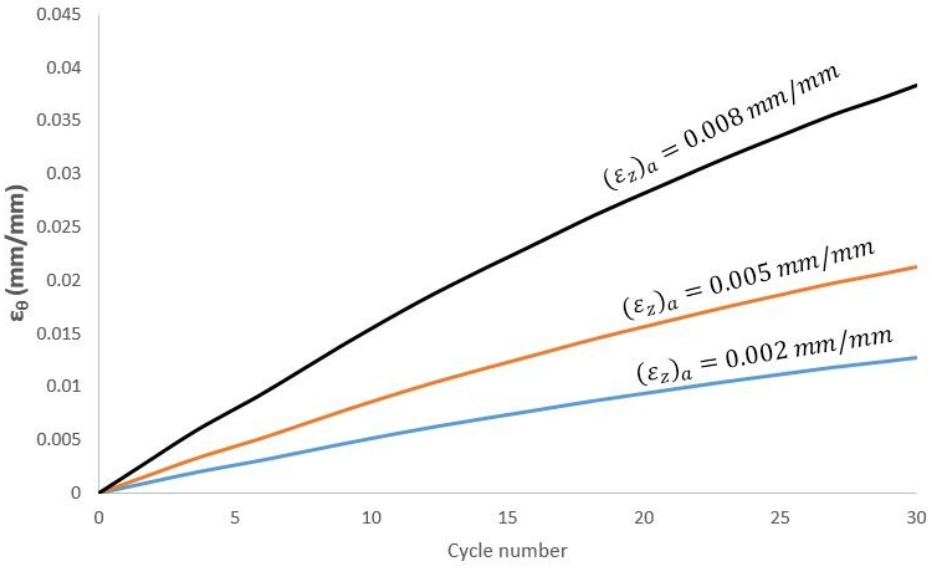

Figure 5.109: O-W model with different alternating strains and $p = 4.7MPa$

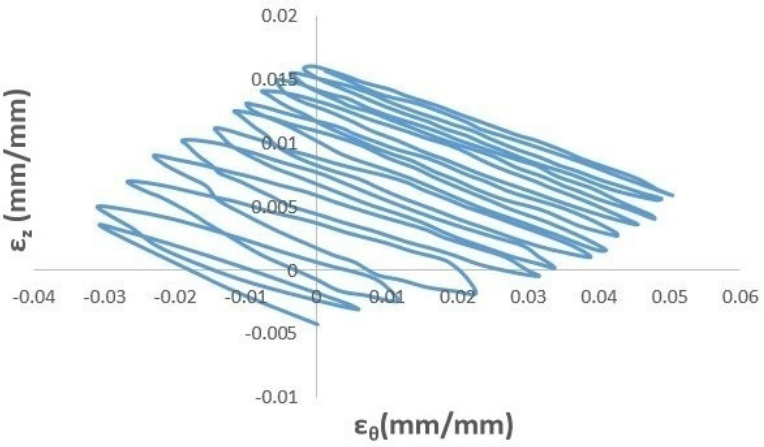

Figure 5.110: O-W model with $p = 2.5MPa$ and $\sigma_a = 240MPa, \sigma_m = 40MPa$

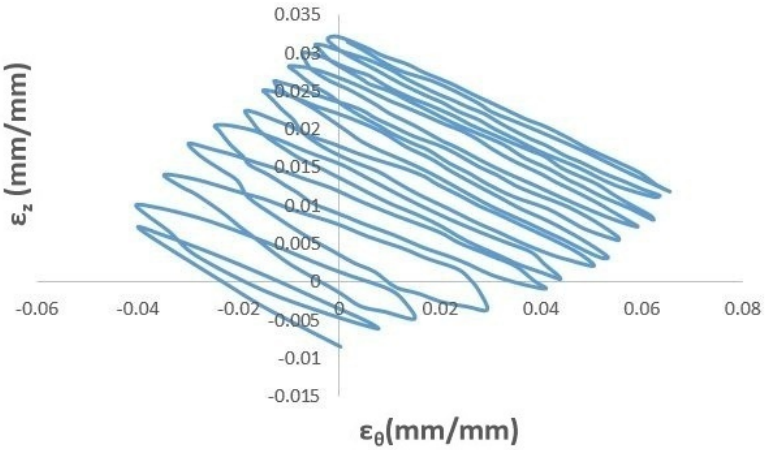

Figure 5.111: O-W model with $p = 4MPa$ and $\sigma_a = 240MPa, \sigma_m = 40MPa$

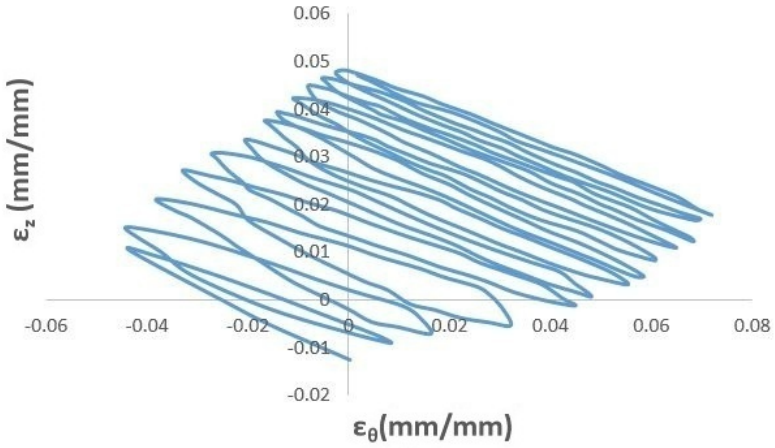

Figure 5.112: O-W model with $p = 5.796MPa$ and $\sigma_a = 240MPa, \sigma_m = 40MPa$

5.2.2 Comparison of the Results of Different Kinematic Hardening Models

Finally, a comparison of kinematic hardening models with experimental data in [18] is given in Figure 5.113 for 4.7 MPa internal pressure and 0.005 mm/mm alternating strain.

Without experimental data, comparison of the models for biaxial ratcheting with internal pressures of 3MPa and 6MPa and strain amplitude of 0.005 are given in Figure 5.114 and Figure 5.115. The comparison of models with 4.7MPa internal pressure and strain amplitude of 0.002 mm/mm and 0.008 mm/mm are given in Figure 5.116 and Figure 5.117.

It is seen that increasing internal pressure and strain amplitudes increases the ratcheting strain for all of the models.

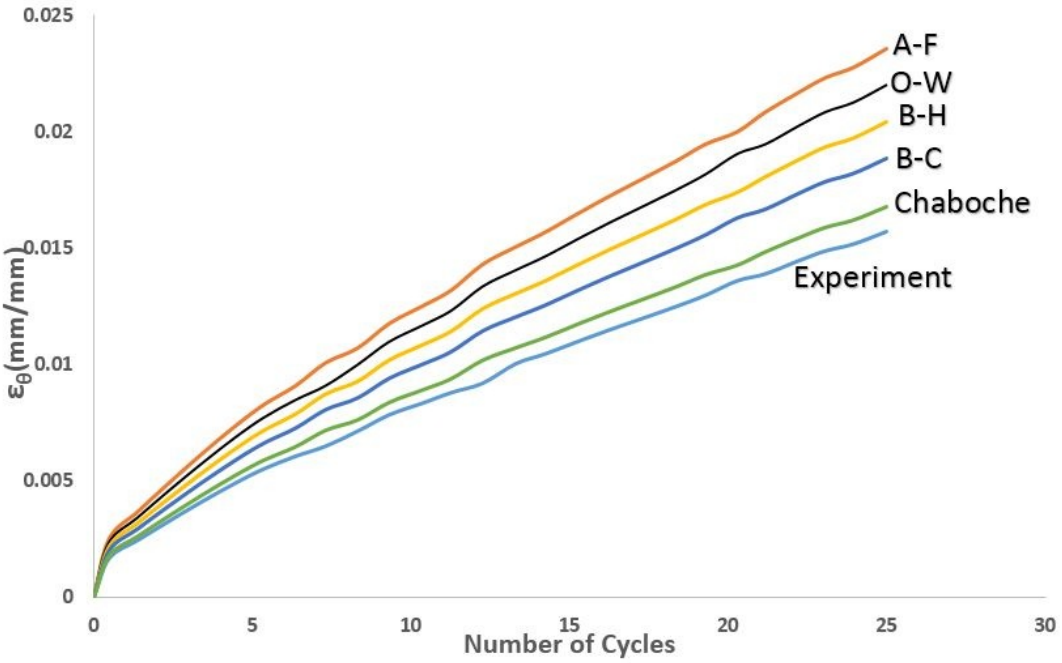

Figure 5.113: Comparison of experimental values and ratcheting results of kinematic hardening models for $p = 4.7MPa$ and $(\epsilon_z)_a = 0.005mm/mm$

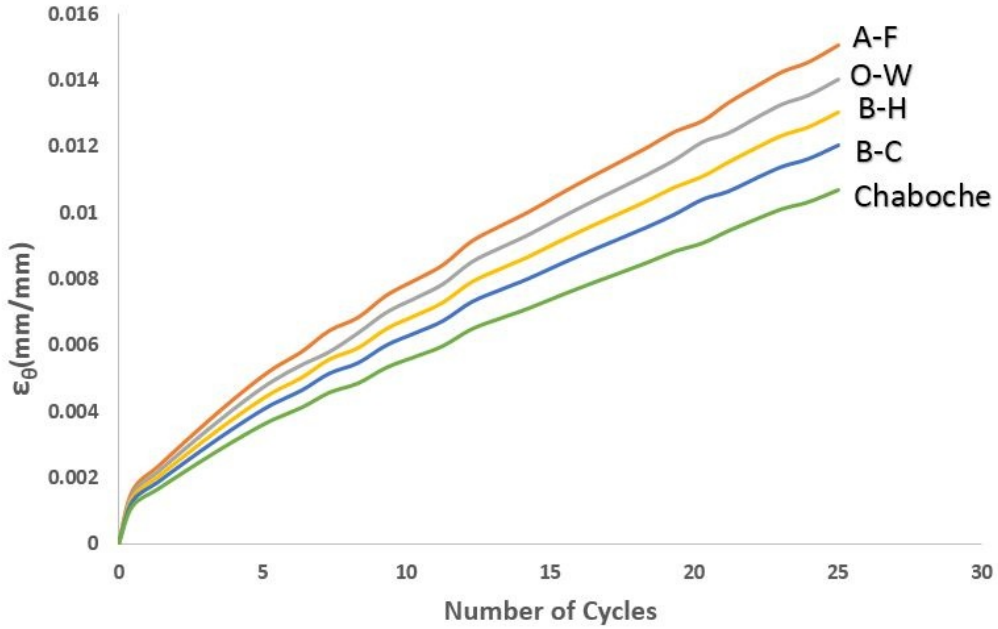

Figure 5.114: Comparison of ratcheting results of kinematic hardening models for $p = 3MPa$ and $(\epsilon_z)_a = 0.005mm/mm$

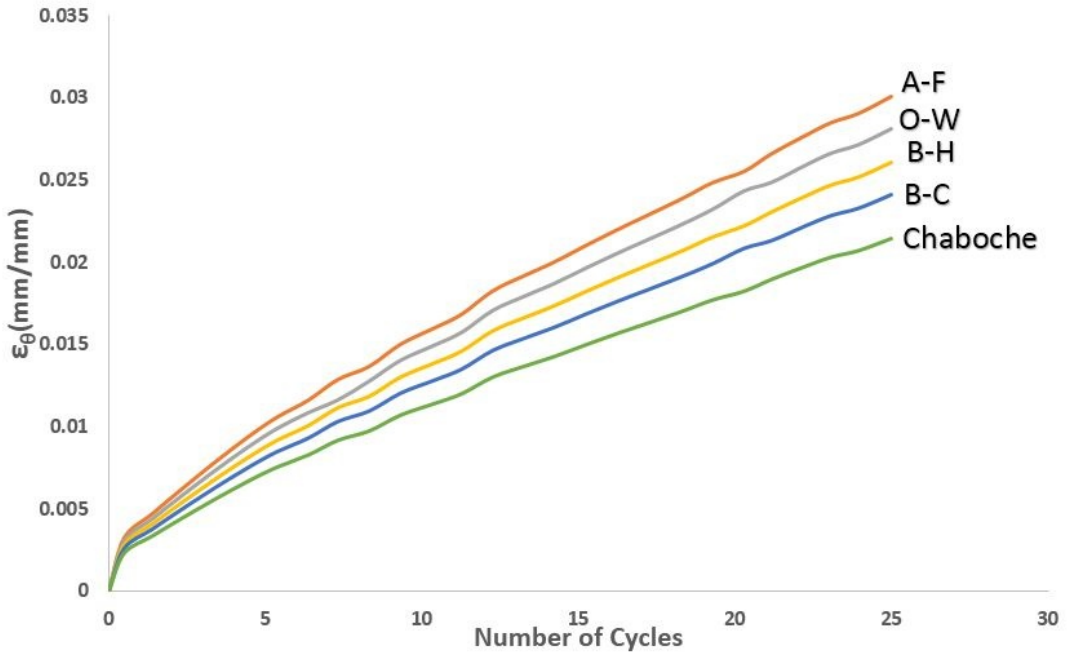

Figure 5.115: Comparison of ratcheting results of kinematic hardening models for $p = 6MPa$ and $(\epsilon_z)_a = 0.005mm/mm$

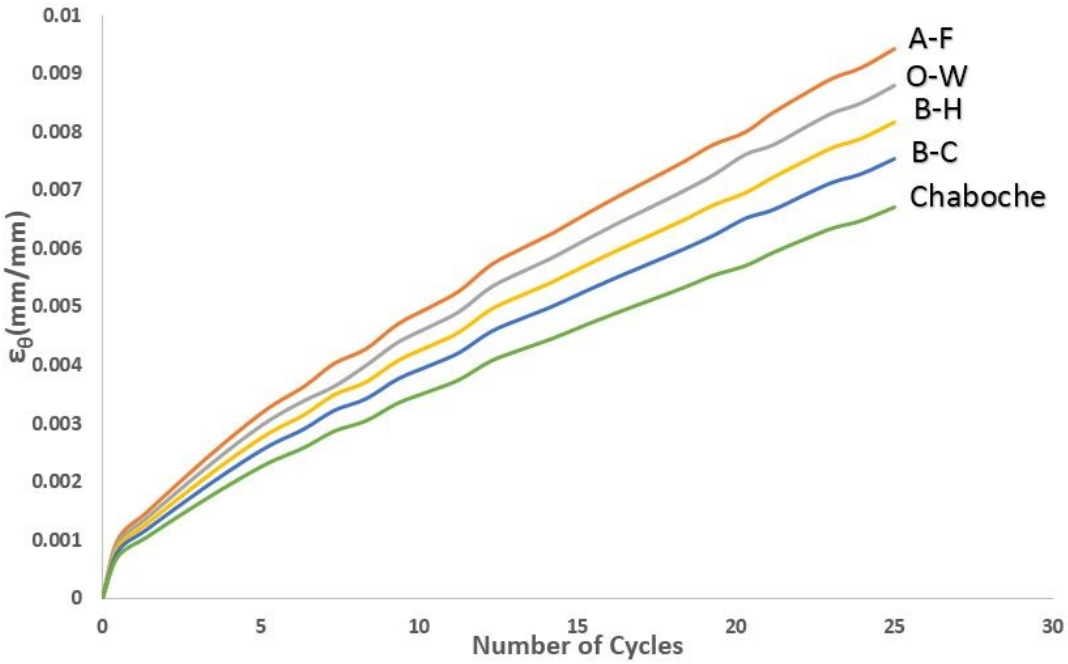

Figure 5.116: Comparison of ratcheting results of kinematic hardening models for $p = 4.7MPa$ and $(\epsilon_z)_a = 0.002mm/mm$

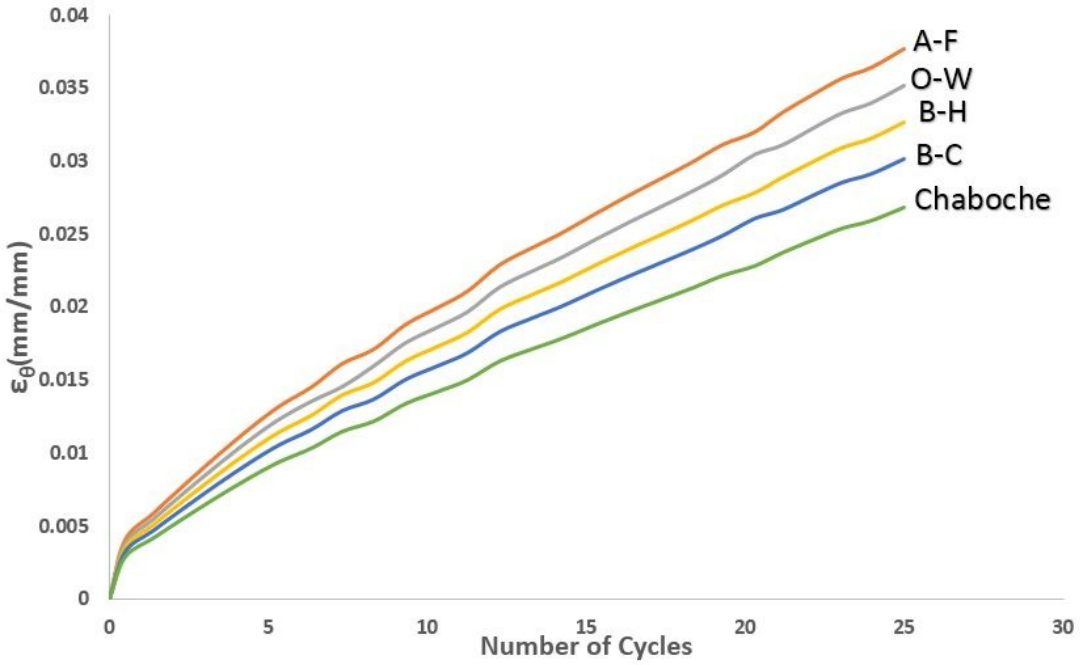

Figure 5.117: Comparison of ratcheting results of kinematic hardening models for $p = 4.7MPa$ and $(\epsilon_z)_a = 0.008mm/mm$

In biaxial loading, it was observed that the closed hysteresis loops in the stress strain diagram of Prager model were present for all directions of loading. Plastic strain sticks in a constant value. Thefore, Prager model did not give any amount of strain accumulation.

A-F model had the largest estimation to biaxial ratcheting. This is an expected result since there are no term that takes the effect of yield surface normal into account although the surface normal changes in each cycle. Since there is no consideration about multidirectional movement of yield surface, it is a similar analysis with uniaxial loading. The only term that includes the direction concept is the first one which is the linear proposal of Prager model. Therefore, its contribution to A-F model to adapt from uniaxial loading to biaxial loading is ineffective. As a result, A-F model is not eligible for simulating biaxial ratcheting.

B-C model's results deviated from A-F model unlike the case in uniaxial loading since the surface normal is not the same in every load cycle. Over prediction of A-F model has been decreased by this model. However, B-C model did not give the smallest

amount of ratcheting. Overprediction was still existing. Therefore, additional models were proposed for simulation of cyclic loading. One of these models is the first version of B-H model. However, that model did also not give reasonable results.

In the Chaboche's model the accumulations have been decreased in the simulations significantly. As in the uniaxial case, in biaxial loading, this model behaves more stable since the accumulation rates are lower than the others. Chaboche model has given the least amount of ratcheting among all of the other tried models.

The Bari-Hassan model in which the Dolebelle parameter was used and detected to give a value between A-F and Chaboche model at the end of the analyses.

The good performance of Ohno-Wang model in uniaxial ratcheting did not hold for biaxial ratcheting. After A-F model, this model is the second one estimating the highest amount of ratcheting in tangential direction. Hence, although it suits the uniaxial cyclic loading cases, its use in biaxial loading is poor.

5.3 Hill48 Yield Criterion

In this part, analysis of ratcheting using anisotropic material assumption with Hill48 yield criterion is performed. Figure 5.118 - Figure 5.120 show ratcheting of A-F, Chaboche and O-W models with 4.7 MPa internal pressure and 0.005 mm/mm axial alternating strain.

5.3.1 Armstrong-Frederick Model

In Figure 5.118, result of A-F hardening model with Hill yield criterion is presented.

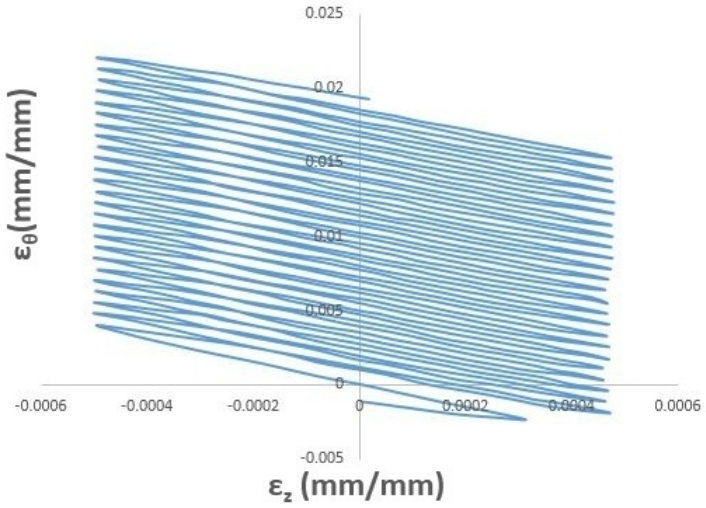

Figure 5.118: A-F model with $p = 4.7MPa$ and $(\epsilon_z)_a = 0.005mm/mm$

5.3.2 Chaboche Model

Figure 5.119 shows result of Chaboche hardening model with Hill yield criterion.

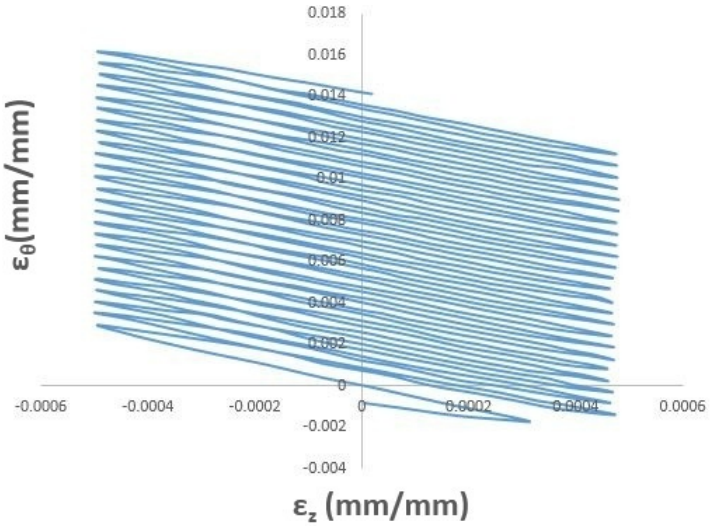

Figure 5.119: Chaboche model with $= 4.7MPa$ and $(\epsilon_z)_a = 0.005mm/mm$

5.3.3 Ohno-Wang Model

In Figure 5.120, result of O-W hardening model with Hill yield criterion is given.

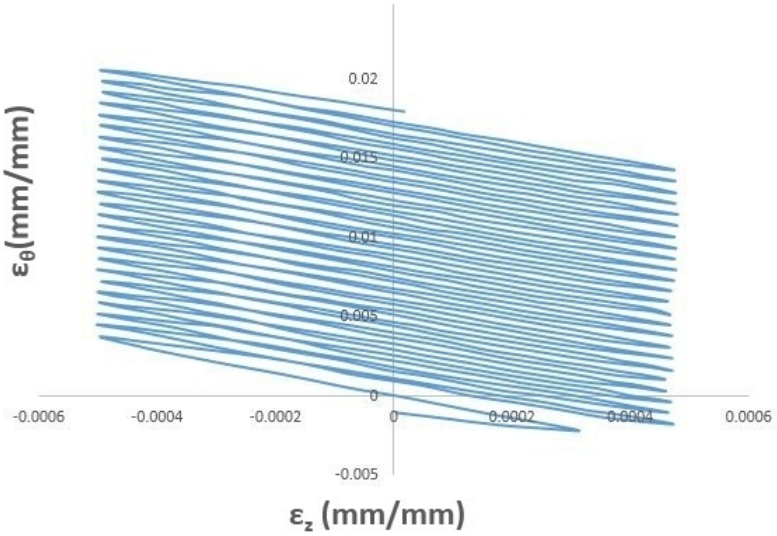

Figure 5.120: O-W model with $p = 4.7MPa$ and $(\epsilon_z)_a = 0.005mm/mm$

5.3.4 Comparison of Different Kinematic Hardening Models

Figure 5.121 presents time strain accumulation behaviors of Prager, A-F, Chaboche and O-W models with 4.7 MPa internal stress and 0.005 mm/mm alternating strain. It is observed that Prager model did not give any ratcheting in conjunction with Hill's yield criterion also. The order of kinematic hardening models remained same for Hill's yield criterion compared to von Mises criterion. A-F model had the largest estimation. Chaboche model has given the lowest amount of ratcheting. Ratcheting rates are close to the obtained by constitutive models with von-Mises criterion.

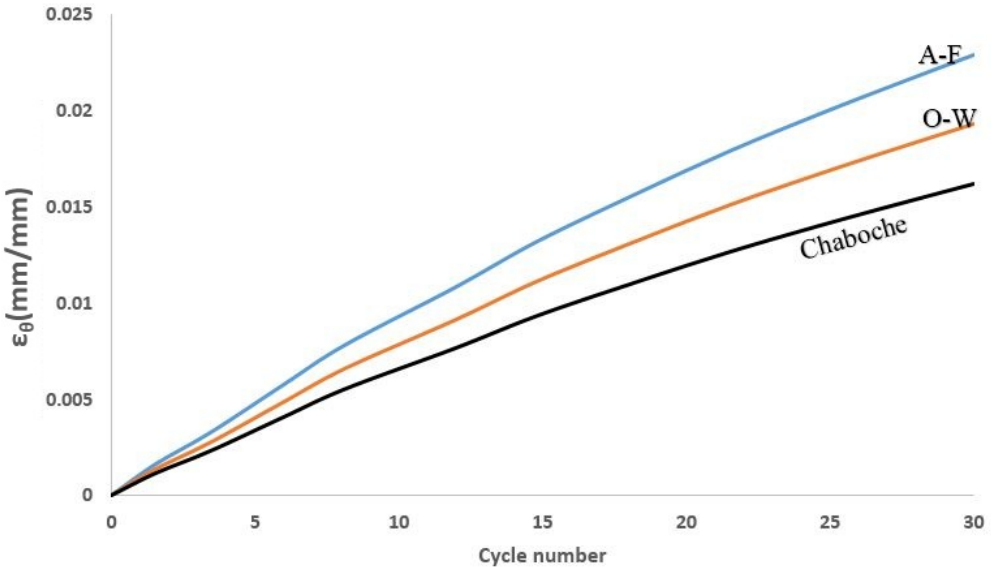

Figure 5.121: Three models with $p = 4.7MPa$ and $(\epsilon_z)_a = 0.005mm/mm$

5.4 Aretz Yield Criterion

The ratcheting results of constitutive models using A-F, Chaboche and O-W models together with Aretz yield criterion are presented in this section. Figure 5.122 - Figure 5.124 show ratcheting of A-F, Chaboche and O-W models with 4.7 MPa internal pressure and 0.005 mm/mm alternating axial strain.

5.4.1 Armstrong-Frederick Model

In Figure 5.122, result of A-F hardening model with Aretz yield criterion is presented.

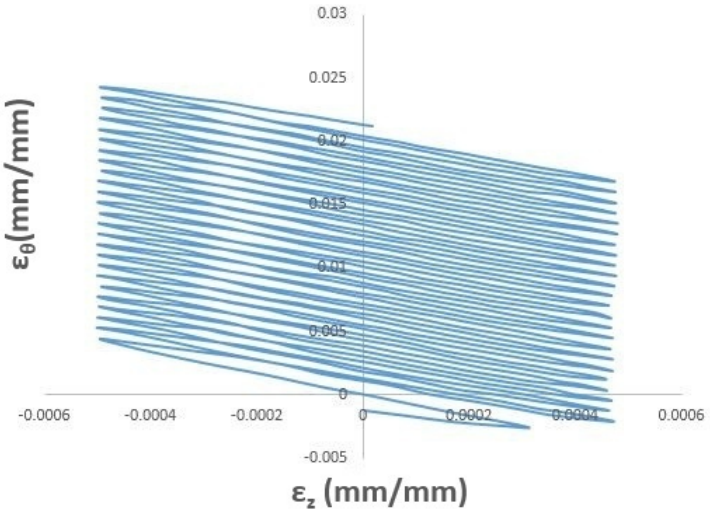

Figure 5.122: A-F model with $p = 4.7MPa$ and $(\epsilon_z)_a = 0.005mm/mm$

5.4.2 Chaboche Model

Figure 5.123 shows the result of Chaboche hardening model with Aretz yield criterion.

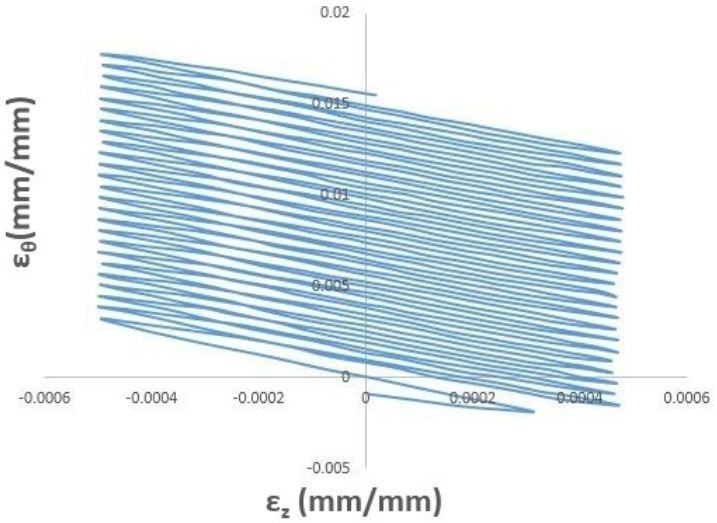

Figure 5.123: Chaboche model with $p = 4.7MPa$ and $(\epsilon_z)_a = 0.005mm/mm$

5.4.3 Ohno-Wang Model

In Figure 5.124, results of O-W hardening model with Aretz yield criterion is given.

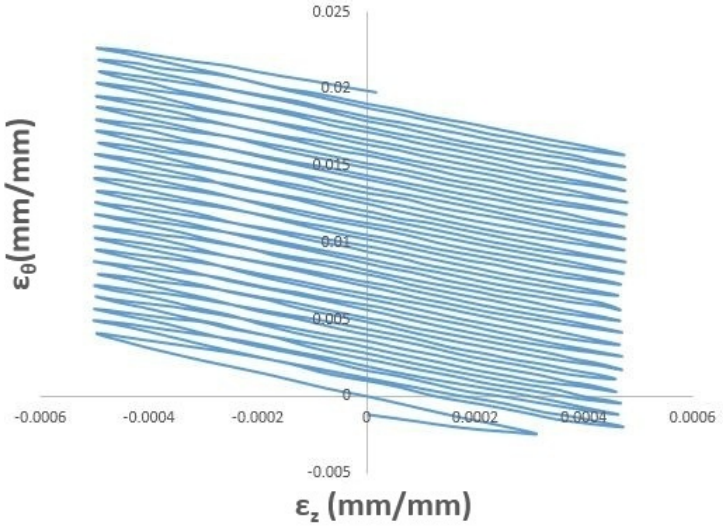

Figure 5.124: O-W model with $p = 4.7MPa$ and $(\epsilon_z)_a = 0.005mm/mm$

5.4.4 Comparison of Different Kinematic Hardening Models

Figure 5.125 presents cycle number strain behaviors of three models in 4.7 MPa internal stress and 0.005 mm/mm alternating strain. In Figure 5.125, results of different different kinematic hardening models with Aretz yield criterion are compared. It is observed that A-F had the largest amount of ratcheting while Chaboche had the lowest amount.

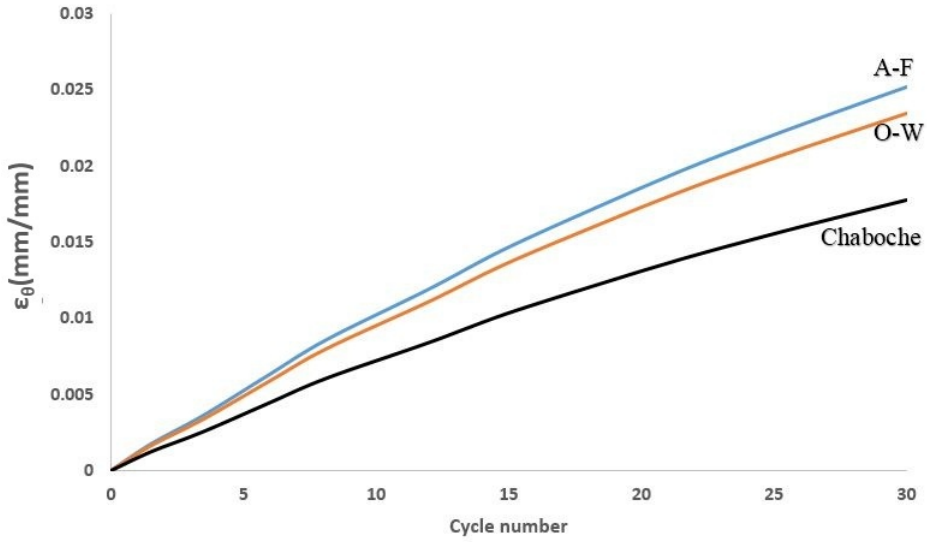

Figure 5.125: Three models with $p = 4.7MPa$ and $(\epsilon_z)_a = 0.005mm/mm$

5.5 Comparison of Ratcheting for Using Different Yield Criteria

In this section, a comparison of three yield criteria von Mises, Hill48 and Aretz for A-F model is presented. Figure 5.126 - Figure 5.128 show the results of three yield criteria obtained by using A-F, Chaboche and O-W models.

It is seen that higher ratcheting is observed for Aretz criterion where the least values are obtained by von Mises criterion for all kinematic hardening models.

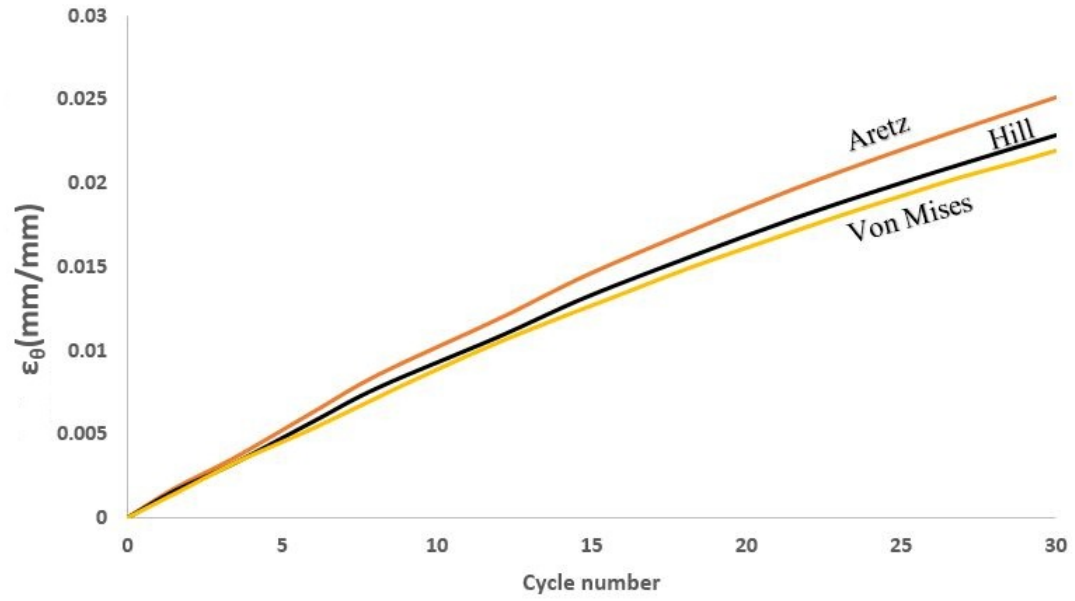

Figure 5.126: Comparison of three yield criteria for A-F model for $p = 4.7MPa$ and $(\epsilon_z)_a = 0.005mm/mm$

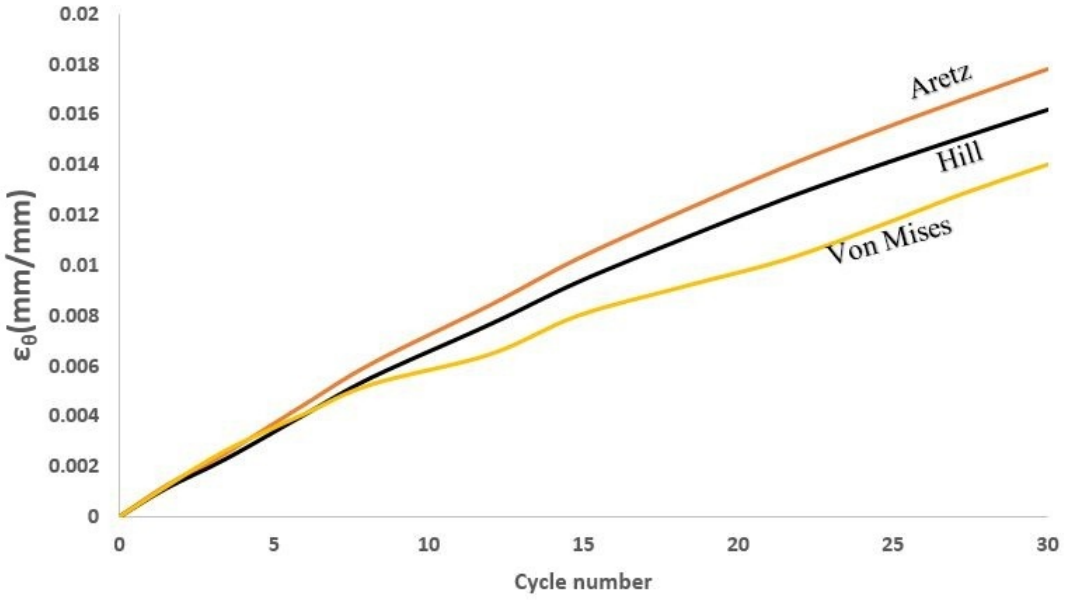

Figure 5.127: Comparison of three yield criteria for Chaboche model for $p = 4.7MPa$ and $(\epsilon_z)_a = 0.005mm/mm$

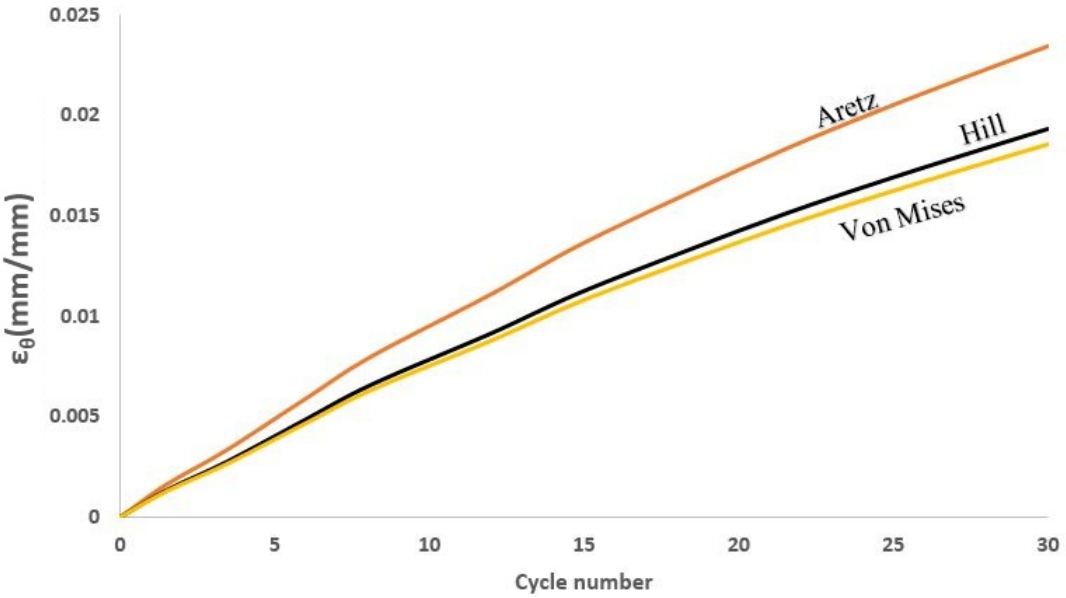

Figure 5.128: Comparison of three yield criteria for O-W model in for $p = 4.7MPa$ and $(\epsilon_z)_a = 0.005mm/mm$

CHAPTER 6

CONCLUSION AND FUTURE WORK

6.1 Conclusion

In this thesis, ratcheting responses of isotropic and anisotropic materials to both uniaxial and biaxial loading were investigated. For this purpose, symmetric and unsymmetric stress and strain cycles were applied. Six different kinematic hardening models and three different yield criteria were used. Following conclusions have been acquired from the current study:

1. Prager model does not give strain accumulation for uniaxial and biaxial loading. It is not appropriate to simulate cyclic strain accumulation.

2. In uniaxial loading, the order of the ratcheting from highest to lowest is as follows: Bari-Hassan, Armstrong-Frederick and Burlet-Cailletaud, Chaboche, Ohno-Wang models for all cases.

3. Burlet-Cailletaud model gives the same result with Armstrong-Frederick model for uniaxial loading since the unit inner product of surface normal on the radial evanescence term.

4. In uniaxial loading, highest amount of ratcheting is obtained in Bari-Hassan model. The possible reason is the parameter determination of this model which was developed to get a value which balances the Chaboche and Armstrong-Frederick models.

5. Increasing mean stress and stress amplitude increases the ratcheting amount for all of the models used in uniaxial loading. However, accumulation rate, i.e,

the plastic strain increase in each cycle, is different. The largest ratcheting increase is obtained by Armstrong-Frederick model while the smallest ratcheting increase is observed in Chaboche model.

6. Chaboche and Ohno-Wang model's performances are acceptable for uniaxial loading. Therefore, these two can be used to simulate uniaxial ratcheting of materials in cyclic loading.

7. In biaxial loading, from highest ratcheting to lowest order is as follows: Armstrong-Frederick, Ohno-Wang, Bari-Hassan, Burlet-Cailletaud and Chaboche for all cases.

8. For biaxial case studied in this thesis, Chaboche model gives the closest results to the experiments with a slight over estimation. The other models are significantly above the desired values.

9. For different mean and alternating stresses, analyses give similar results as the total value of mean and alternating stresses are taken into account.

10. Introduction of Aretz yield function has increased the ratcheting. This is most probably because of the decrease in yield strength of longitudinal direction. Since the radius of yield surface decreased, accumulated plastic strain has been increased in return algorithm. The analyses results of constitutive models with obtained with Hill's yield criterion are observed to be slightly higher than the ones obtained by using von-Mises criterion.

6.2 Future Work

As a first future work, a model that predicts both uniaxial and multiaxial cases adequately can be developed. Another future work may include micro deformations of the materials because there are few studies that concern the effect of anisotropy and micro structural behaviors on ratcheting. In conclusion, this thesis can be a door to find a model that gives correct amount of ratcheting both uniaxial and multiaxial conditions for both isotropic and anisotropic materials.

REFERENCES

[1] M. Abdel-Karim and N. Ohno. Kinematic hardening model suitable for ratchetting with steady-state. *International Journal of Plasticity*, 16(3):225–240, 2000.

[2] P. J. Armstrong. A mathematical representation of the multiaxial bauschinger effect. *CEBG Report RD/B/N, 731*, 1966.

[3] S. Bari and T. Hassan. Anatomy of coupled constitutive models for ratcheting simulation. *International Journal of Plasticity*, 16(3):381–409, 2000.

[4] S. Bari and T. Hassan. Kinematic hardening rules in uncoupled modeling for multiaxial ratcheting simulation. *International Journal of Plasticity*, 17(7):885–905, 2001.

[5] S. Bari and T. Hassan. An advancement in cyclic plasticity modeling for multiaxial ratcheting simulation. *International Journal of Plasticity*, 18(7):873–894, 2002.

[6] H. Burlet and G. Cailletaud. Modeling of cyclic plasticity in finite element codes. *Proc. of Constitutive Laws for Engineering Materials: Theory and Applications, Desai et al., Elsevier, Tucson, AZ*, pages 1157–1164, 1987.

[7] J. Chaboche and D. Nouailhas. Constitutive modeling of ratchetting effects—part i: experimental facts and properties of the classical models. *Journal of Engineering Materials and Technology*, 111(4):384–392, 1989.

[8] X. Chen and R. Jiao. Modified kinematic hardening rule for multiaxial ratcheting prediction. *International Journal of Plasticity*, 20(4):871–898, 2004.

[9] X. Chen, R. Jiao, and K. Kim. Simulation of ratcheting strain to a high number of cycles under biaxial loading. *International journal of solids and structures*, 40(26):7449–7461, 2003.

[10] X. Chen, R. Jiao, and K. S. Kim. On the ohno–wang kinematic hardening rules for multiaxial ratcheting modeling of medium carbon steel. *International Journal of Plasticity*, 21(1):161–184, 2005.

[11] W. Chung, J. Cho, and T. Belytschko. On the dynamic effects of explicit fem in sheet metal forming analysis. *Engineering Computations*, 15(6):750–776, 1998.

[12] E. Corona, T. Hassan, and S. Kyriakides. On the performance of kinematic hardening rules in predicting a class of biaxial ratcheting histories. *International Journal of Plasticity*, 12(1):117–145, 1996.

[13] Y. Dafalias and E. Popov. A model of nonlinearly hardening materials for complex loading. *Acta mechanica*, 21(3):173–192, 1975.

[14] P. Delobelle, P. Robinet, and L. Bocher. Experimental study and phenomenological modelization of ratchet under uniaxial and biaxial loading on an austenitic stainless steel. *International Journal of Plasticity*, 11(4):295–330, 1995.

[15] C. Gupta, J. Chakravartty, G. Reddy, and S. Banerjee. Uniaxial cyclic deformation behaviour of sa 333 gr 6 piping steel at room temperature. *International journal of pressure vessels and piping*, 82(6):459–469, 2005.

[16] R. Halama, J. Sedlák, and M. Šofer. Phenomenological modelling of cyclic plasticity. In *Numerical Modelling*. InTech, 2012.

[17] F. Harewood and P. McHugh. Comparison of the implicit and explicit finite element methods using crystal plasticity. *Computational Materials Science*, 39(2):481–494, 2007.

[18] T. Hassan, E. Corona, and S. Kyriakides. Ratcheting in cyclic plasticity, part ii: multiaxial behavior. *International journal of plasticity*, 8(2):117–146, 1992.

[19] T. Hassan and S. Kyriakides. Ratcheting of cyclically hardening and softening materials: I. uniaxial behavior. *International Journal of Plasticity*, 10(2):149–184, 1994.

[20] T. Hassan, L. Taleb, and S. Krishna. Influence of non-proportional loading on ratcheting responses and simulations by two recent cyclic plasticity models. *International Journal of Plasticity*, 24(10):1863–1889, 2008.

[21] T. Hassan, Y. Zhu, and V. C. Matzen. Improved ratcheting analysis of piping components. *International journal of pressure vessels and piping*, 75(8):643–652, 1998.

[22] T. J. Hughes and W. Liu. Implicit-explicit finite elements in transient analysis: stability theory. *Journal of applied Mechanics*, 45(2):371–374, 1978.

[23] Y. Jiang and H. Sehitoglu. Modeling of cyclic ratchetting plasticity, part i: development of constitutive relations. *Journal of Applied Mechanics*, 63(3):720–725, 1996.

[24] G. Kang and Q. Kan. Constitutive modeling for uniaxial time-dependent ratcheting of ss304 stainless steel. *Mechanics of Materials*, 39(5):488–499, 2007.

[25] S. Kulkarni, Y. Desai, T. Kant, G. Reddy, Y. Parulekar, and K. Vaze. Uniaxial and biaxial ratchetting study of sa333 gr. 6 steel at room temperature. *International journal of pressure vessels and piping*, 80(3):179–185, 2003.

[26] H. Mahbadi and M. Eslami. Cyclic loading of beams based on the prager and frederick–armstrong kinematic hardening models. *International Journal of Mechanical Sciences*, 44(5):859–879, 2002.

[27] H. Mahbadi and M. Eslami. Cyclic loading of thick vessels based on the prager and armstrong–frederick kinematic hardening models. *International Journal of Pressure Vessels and Piping*, 83(6):409–419, 2006.

[28] N. Ohno and J.-D. Wang. Kinematic hardening rules with critical state of dynamic recovery, part i: formulation and basic features for ratchetting behavior. *International journal of plasticity*, 9(3):375–390, 1993.

[29] L. Olovsson, K. Simonsson, and M. Unosson. Selective mass scaling for explicit finite element analyses. *International Journal for Numerical Methods in Engineering*, 63(10):1436–1445, 2005.

[30] L. Olovsson, M. Unosson, and K. Simonsson. Selective mass scaling for thin walled structures modeled with tri-linear solid elements. *Computational Mechanics*, 34(2):134–136, 2004.

[31] L. Portier, S. Calloch, D. Marquis, and P. Geyer. Ratchetting under tension–torsion loadings: experiments and modelling. *International Journal of Plasticity*, 16(3):303–335, 2000.

[32] B. Postberg and E. Weiß. Simulation of ratcheting of aisi 316l (n) steel under nonproportional uniaxial loading and high number of load cycles using the ohno and wang nonlinear kinematic material model. *International journal of pressure vessels and piping*, 77(5):207–213, 2000.

[33] W. Prager. A new methods of analyzing stresses and strains in work hardening plastic solids. *J. Appl. Mech.(ASME)*, 23:493–496, 1956.

[34] S. M. Rahman, T. Hassan, and E. Corona. Evaluation of cyclic plasticity models in ratcheting simulation of straight pipes under cyclic bending and steady internal pressure. *International Journal of Plasticity*, 24(10):1756–1791, 2008.

[35] M. Ruggles and E. Krempl. The influence of test temperature on the ratchetting behavior of type 304 stainless steel. *J. Eng. Mater. Technol.(Trans. ASME)*, 111(4):378–383, 1989.

[36] E. Q. Sun. Shear locking and hourglassing in msc nastran, abaqus, and ansys. In *Msc software users meeting*, 2006.

[37] J. Sun, K. Lee, and H. Lee. Comparison of implicit and explicit finite element methods for dynamic problems. *Journal of Materials Processing Technology*, 105(1):110–118, 2000.

[38] N. Tseng and G. Lee. Simple plasticity model of two-surface type. *Journal of Engineering Mechanics*, 109(3):795–810, 1983.

[39] M. Yaguchi and Y. Takahashi. Ratchetting of viscoplastic material with cyclic softening, part 1: experiments on modified 9cr–1mo steel. *International Journal of Plasticity*, 21(1):43–65, 2005.

[40] F. Yoshida. A constitutive model of cyclic plasticity. *International Journal of Plasticity*, 16(3):359–380, 2000.

[41] F. YOSHIDA, S. YAMAMOTO, M. ITOH, and M. OHMORI. Bi-axial strain accumulations in mechanical ratcheting. *Bulletin of JSME*, 27(232):2100–2106, 1984.